

Electronic Thesis and Dissertation Repository

2-10-2020 3:00 PM

Progressive Failure of Transmission Line Towers under Different Tornado Wind Fields

Wesam AbdElhamid Mohamed, *The University of Western Ontario*

Supervisor: El Damatty, Ashraf, *The University of Western Ontario*

Co-Supervisor: El Ansary, Ayman, *The University of Western Ontario*

A thesis submitted in partial fulfillment of the requirements for the Master of Engineering Science degree in Civil and Environmental Engineering

© Wesam AbdElhamid Mohamed 2020

Follow this and additional works at: <https://ir.lib.uwo.ca/etd>



Part of the [Civil Engineering Commons](#), and the [Structural Engineering Commons](#)

Recommended Citation

AbdElhamid Mohamed, Wesam, "Progressive Failure of Transmission Line Towers under Different Tornado Wind Fields" (2020). *Electronic Thesis and Dissertation Repository*. 6850.
<https://ir.lib.uwo.ca/etd/6850>

This Dissertation/Thesis is brought to you for free and open access by Scholarship@Western. It has been accepted for inclusion in Electronic Thesis and Dissertation Repository by an authorized administrator of Scholarship@Western. For more information, please contact wlsadmin@uwo.ca.

Abstract

High-intensity wind events (downbursts and tornadoes) cause the majority of weather-related transmission line (TL) failures, which detrimentally affect the society. This study investigates the progressive failures of single TL towers and TL systems under different F2 tornadoes. Different tornado wind fields are incorporated in a fluid-structure software developed at Western University. Progressive failure analysis is then conducted for four towers under the most critical tornado configurations identified from extensive parametric studies. Moreover, the cost associated with designing TLs to sustain F2 tornadoes is investigated by strengthening the TL towers. Finally, the progressive failure within self-supported TL systems under different tornadoes, and the effect of changing the insulator length and the TL span on the propagation of failure are examined. To summarize, this thesis compares the progressive failures of TLs under different F2 tornado wind fields. It also presents different techniques to enhance the resilience of TL systems under tornadoes.

Keywords

Transmission lines, high-intensity wind (HIW), tornadoes, progressive failure, strengthening

Summary for Lay Audience

In Canada, tornadoes occur in almost all southern regions of the country, especially Southwestern Ontario which experiences the highest rate of tornado incidences. Tornadoes are speedily rotating columns of air that extend from the surface of the Earth to the cumulonimbus clouds. Tornadoes are categorized by the Fujita scale. The Fujita scale classifies tornadoes into five categories (F0; least damaging to F5; most damaging) based on the different characteristics of the tornado. This study is motivated by many failure incidences observed in Canada and worldwide of transmission line (TL) systems during tornadoes and by the lack of appropriate design guidelines accounting for high-intensity wind events like tornadoes. The current study is part of a research program initiated at Western University, a few years ago, that focuses on investigating the reasons of failure of TLs under high-intensity wind events and how to improve current design provisions to have more resilient TLs under such extreme wind events. The main objectives of the current study are to investigate the propagation of failure of TL systems under different tornadoes and to examine how changing different components of the TL system affects the failure. The results drawn from the study show that TL towers collapse differently under different tornadoes and that some components of the TL systems significantly affect the resilience of TLs and can be used to mitigate the losses due to tornadoes. To summarize, the thesis presents different approaches to improve the resilience of TLs under F2 tornadoes.

Co-Authorship Statement

This thesis has been presented in accordance with the Integrated-Article format thesis regulations stipulated by the School of Graduate and Postdoctoral Studies at the University of Western Ontario. Statements of the co-authorship of individual chapters are as follows:

Chapter 2: Progressive Failure of a Single Transmission Line Tower under Different Tornado Wind Fields

Incorporating the tornado wind fields into the fluid-structure software was done by Wesam AbdElhamid Mohamed under the supervision of Dr. Ashraf El Damatty. Numerical simulations and analysis of the results were conducted by Wesam AbdElhamid Mohamed under the supervision of Dr. Ashraf El Damatty and Dr. Ayman El Ansary.

Drafts of Chapter 2 were written by Wesam AbdElhamid Mohamed, and modifications were done under the supervision of Dr. Ayman El Ansary and Dr. Ashraf El Damatty.

Chapter 3: Progressive Failure of Self-supported Transmission Line Towers under Different Tornado Wind Fields

Extending the fluid-structure software to include the progressive failure within the TL was done by Ahmed Shehata under the supervision of Dr. Ashraf El Damatty. Incorporating the tornado wind fields into the extended version of the fluid-structure software was done by Wesam AbdElhamid Mohamed under the supervision of Dr. Ashraf El Damatty. Numerical simulations and analysis of the results were conducted by Wesam AbdElhamid Mohamed under the supervision of Dr. Ashraf El Damatty and Dr. Ayman El Ansary.

Drafts of Chapter 3 were written by Wesam AbdElhamid Mohamed, and modifications were done under the supervision of Dr. Ayman El Ansary and Dr. Ashraf El Damatty.

Table of Contents

Abstract.....	ii
Summary for Lay Audience.....	iii
Co-Authorship Statement.....	iv
Table of Contents.....	v
List of Tables.....	viii
List of Figures.....	ix
Chapter 1	1
1 Introduction.....	1
1.1 Background.....	1
1.2 Literature.....	4
1.2.1 Tornado Wind Fields.....	4
1.2.2 Behaviour and failure analysis of transmission lines under tornadoes.....	5
1.3 Research gaps.....	8
1.4 Thesis objective.....	9
1.5 Methodology.....	10
1.6 Thesis organization.....	12
1.6.1 Progressive Failure of a Single Transmission Line Tower under Different Tornado Wind Fields.....	12
1.6.2 Progressive Failure of Self-supported Transmission Line Towers under Different Tornado Wind Fields.....	12
1.7 References.....	13
Chapter 2	17
2 Progressive Failure of a Single Transmission Line Tower under Different Tornado Wind Fields.....	17
2.1 Introduction.....	17

2.2	Description of the Numerical Model	20
2.2.1	Description of Tornado Wind Fields	20
2.2.2	Description of the Finite Element Model.....	21
2.2.3	Description of the Considered Towers	22
2.3	Parametric Study.....	25
2.3.1	Parametric Study Results	26
2.4	Progressive Failure Analysis.....	28
2.4.1	Verification of Numerical Model.....	30
2.4.2	Progressive Failure Analysis Results.....	31
2.5	Strengthening of Towers.....	51
2.6	Conclusion	56
2.7	References.....	57
Chapter 3	61
3	Progressive Failure of Self-supported Transmission Line Towers under Different Tornado Wind Fields.....	61
3.1	Introduction.....	61
3.2	Description of the Numerical Model	65
3.2.1	Description of Tornado Wind Fields	65
3.2.2	Description of the Considered Towers	66
3.2.3	Description of the Finite Element Model.....	69
3.3	Parametric Study.....	70
3.3.1	Parametric Study Results	71
3.4	Progressive Failure Analysis.....	72
3.4.1	Verification of Numerical Model.....	76
3.4.2	Progressive Failure Analysis Results.....	79
3.5	Effect of insulator length on the propagation of failure within the TL system... 115	

3.6 Effect of Span length on the propagation of failure within the TL system.....	118
3.7 Conclusion	122
3.8 References.....	124
Chapter 4	128
4 Conclusions and Future Work.....	128
4.1 Conclusions.....	128
4.2 Main contributions	131
4.3 Recommendations for future work	132
Curriculum Vitae	133

List of Tables

Table 1-1: Ranges of wind speed, path length, and path-width from the Fujita-Pearson scales [7].	4
Table 2-1: Properties of TLs.	23
Table 2-2: Results of the parametric study.	26
Table 2-3: Summary of the verification study.	30
Table 2-4: Summary of the progressive failure analysis results.	48
Table 2-5: Summary of the strengthening attempts for G1 tower.	54
Table 2-6: Comparison between the highest capacity ratio, λ , before and after strengthening of the transmission line towers.....	55
Table 3-1: Ranges of wind speed, path length, and pathwidth from the Fujita-Pearson scales [6].	62
Table 3-2: Properties of TL.....	68
Table 3-3: Results of the parametric study.	71
Table 3-4: Properties of TLs used in the verification.	77
Table 3-5: Summary of the verification study.	79
Table 3-6: Summary of the progressive failure analysis results for S2 TL under the Stockton 2005 tornado wind field.....	113
Table 3-7: Summary of the progressive failure analysis results for S2 TL under Hangan’s tornado wind field.	114
Table 3-8: Ground wires and conductors’ sag used in the parametric study.	118

List of Figures

Figure 1-1: Components of TL systems (https://tinyurl.com/y3lup5q7 & https://tinyurl.com/y54ajvhv).....	2
Figure 1-2: Transmission line systems (https://tinyurl.com/r8p5ya2).....	3
Figure 1-3: (A) Failure of one TL tower within the line. (B) Close-up image of a failed transmission line tower within a TL. “Manitoba Hydro, 2019”.	7
Figure 2-1: Vertical profiles of tangential velocity component of Stockton [22] and Hangan’s [3, 30] tornado wind fields for radial distances, r , from tornado center.	21
Figure 2-2: Schematic illustrating studied TL towers. (A) G1; (B) G2; (C) S1; and (D) S2 TLs.	23
Figure 2-3: Detailed Drawing for G1 [31]......	24
Figure 2-4: Critical tornado configurations parameters (R and θ) relative to the tower of interest.....	25
Figure 2-5: Flow chart outlining the progressive failure analysis for each critical tornado configuration.	28
Figure 2-6: Sensitivity analysis to determine the loading increment.....	29
Figure 2-7: Progressive failure of G1 tower in the first scenario, $\lambda = 4$. (A,B) 25%; (C) 32.5%; (D) 67.5%; and (E) 70%.....	31
Figure 2-8: Progressive failure of G2 tower. (A) 10%; (B) 12.5%; (C) 15%; (D) 17.5%; (E) 20%; (F) 22.5%; (G) 25%; (H) 27.5%; (I) 30%; (J) 32.5%; (K) 35%; and (L) 37.5%.	34
Figure 2-9: Progressive failure of S1 tower. (A) 7.5%; (B) 20%; and (C) 22.5%.....	34

Figure 2-10: Progressive failure of S2 tower in first critical scenario, $\lambda = 11$. (A) 10%; (B) 17.5%; (C) 40%; (D) 42.5%; and (E) 45%.....	36
Figure 2-11: Progressive failure of S2 tower in the fourth critical scenario, $\lambda = 9.4$. (A) 10%; (B) 12.5%; (C) 17.5%; (D) 32.5%; (E) 40%; and (F) 42.5%.....	36
Figure 2-12: Progressive failure of G1 tower in the first scenario. (A, B) 25%; (C) 30%; (D) 50%; (E,F) 60%; (G,H) 62.5%; (I) 65%; and (J) 67.5%.....	38
Figure 2-13: Progressive failure of G2 tower in the first scenario. (A) 10%; (B) 12.5%; (C) 15%; (D) 17.5%; (E) 20%; (F) 22.5%; (G) 25%; (H) 27.5%; (I) 30%; (J) 32.5%; (K) 35%; and (L) 37.5%.....	41
Figure 2-14: Progressive failure of G2 tower in the fourth scenario. (A) 15%; (B) 17.5%; (C) 20%; (D) 22.5%; (E) 25%; (F) 27.5%; (G) 30%; and (H) 32.5%.....	43
Figure 2-15: Progressive failure of S1 tower in the first scenario. (A) 7.5%; (B) 15%; (C) 17.5%; (D) 20%; and (E) 22.5%.....	44
Figure 2-16: Progressive failure of S2 tower in the first scenario. (A) 10%; (B) 12.5%; (C) 15%; (D) 32.5%; (E) 35%; (F) 37.5%; and (G) 40%.....	45
Figure 2-17: Progressive failure of S2 tower in the second scenario. (A) 10%; (B) 12.5%; (C) 15%; (D) 22.5%; (E) 25%; (F) 32.5%; and (G,H) 35%.....	47
Figure 2-18: Flow chart describing the tower strengthening procedure.....	52
Figure 2-19: Progressive failure of G1 tower after attempting four iterations of strengthening. (A) 72.5%; (B) 75%; (C) 77.5%.....	53
Figure 3-1: (A) Failure of one transmission line tower within the line. (B) Close-up image of a failed transmission line tower within a TL. “Manitoba Hydro, 2019”.....	64
Figure 3-2: Vertical profiles of tangential velocity component of Stockton [24] and Hangan’s [3, 30] tornado wind fields for radial distances, r , from tornado center.....	66

Figure 3-3: Schematic of the SL transmission line.....	67
Figure 3-4: Schematic illustrating studied S2 TL towers.	68
Figure 3-5: Critical tornado configurations parameters (R and θ) relative to the tower of interest.....	70
Figure 3-6: Post failure geometry [32].....	73
Figure 3-7: Flow chart outlining the progressive failure analysis for each critical tornado configuration.....	75
Figure 3-8: Sensitivity analysis to determine the loading increment.....	76
Figure 3-9: Schematic illustrating studied TL towers used in the verification. (A) G1; (B) G2 transmission line.	77
Figure 3-10: Detailed Drawing for G1 [35].....	78
Figure 3-11: Progressive failure of S2 tower in first critical scenario, $\lambda = 11$. (A) 10%; (B) 12.5%; (C) 15%; (D) 17.5%; (E) 20%; (F) 25%; (G) 27.5%; (H) 32.5%; (I) 35%; (J) 37.5%; (K) 40%; (L) 50%; (M) 52.5%; (N,O) 55%; (P) 57.5%; (Q) 60%; (R) 67.5%; (S,T) 70; and (U) 72.5%.	86
Figure 3-12: Progressive failure of S2 tower in second critical scenario, $\lambda = 9.4$. (A) 10%; (B) 12.5%; (C) 15%; (D) 17.5%; (E) 22.5%; (F) 25%; (G) 27.5%; (H) 30%; (I) 32.5%; (J) 35%; (K) 37.5%; and (L,M) 40%.	90
Figure 3-13: S2NL third mode. (A) 12.5%; (B) 32.5%; (C) 35%; (D) 37.5%; (E) 40%; (F) 62.5%; (G) 65%; (H) 67.5%; and (I) 70%.	93
Figure 3-14: S2NL fourth mode. (A) 10%; (B) 12.5%; (C) 32.5%; (D) 35%; (E) 37.5%; (F) 40%; and (G) 42.5%.	96
Figure 3-15: S2NL fifth mode. (A) 10%; (B) 12.5%; (C) 35%; (D) 37.5%; (E) 40%; (F) 42.5%; and (G) 45%.	99

Figure 3-16: S2L first failure mode. (A) 10%; (B) 20%; (C) 40%; (D) 42.5%; (E) 45%; (F) 47.5%; (G) 92.5%; (H) 95%; and (I) 97.5%	102
Figure 3-17: S2L second failure mode. (A) 10%; (B) 40%; (C) 42.5%; and (D) 45%..	104
Figure 3-18: S2L third failure mode. (A) 10%; (B) 40%; (C) 42.5%; (D) 45%; (E) 47.5%; (F) 50%; (G) 52.5%; and (H) 55%.....	106
Figure 3-19: S2L fourth failure mode. (A) 10%; (B) 40%; (C) 42.5%; (D) 45%; (E) 60%; (F) 62.5%; (G) 65%; and (H) 67.5%.....	109
Figure 3-20: S2L fifth failure mode. (A) 10%; (B) 12.5%; (C) 40%; (D) 42.5%; (E) 45%; and (F) 47.5%.....	111
Figure 3-21: Effect of insulator length on the failure load of the transmission line. [(A) Critical scenario: $R = 120$ m, $\theta = 225^\circ$; (B) Critical scenario: $R = 120$ m, $\theta = 285^\circ$]....	116
Figure 3-22: Effect of insulator length on the peak capacity ratio, λ , of the transmission line. [(A) Critical scenario: $R = 120$ m, $\theta = 225^\circ$; (B) Critical scenario: $R = 120$ m, $\theta = 285^\circ$]......	117
Figure 3-23: Effect of span on the failure load of the transmission line. (A) Critical scenario: $R = 120$ m, $\theta = 225^\circ$; (B) Critical scenario: $R = 120$ m, $\theta = 45^\circ$. [<i>Sc = Scenario; Tow = Tower</i>].	119
Figure 3-24: Effect of span on the tornado wind speed at failure of the transmission line towers. (A) Critical scenario: $R = 120$ m, $\theta = 225^\circ$; (B) Critical scenario: $R = 120$ m, $\theta = 45^\circ$. [<i>Sc = Scenario; Tow = Tower</i>].	120
Figure 3-25: Effect of insulator length on the peak capacity ratio, λ , of the transmission line under two critical scenarios: $R = 120$ m, $\theta = 225^\circ$ (Sc1) and $R = 120$ m, $\theta = 45^\circ$ (Sc2). [<i>Sc = Scenario</i>].	121

Chapter 1

1 Introduction

1.1 Background

Communities around the world rely heavily on electricity as a source of fuel. The continuous supply of electricity has become a necessity for all day to day operations of the society. The infrastructure system to deliver electricity includes the power source, the outlet, and the power grids. The infrastructure system should ensure the availability of a constant supply of electricity with minimal disturbance. Electrical power grids play an essential role in delivering electricity to power the outlets. The main element in an electrical power network is the Transmission Lines (TLs). Outages of power due to TL tower failures can cause substantial effects on both the economy and society.

As shown in Figure 1-1, TL systems are composed of different components: towers, conductors, ground wires, insulators, dampers, and spacers. The conductors transfer electricity from the producer to the end-users. They are connected to the towers through insulators, which are connected to the cross arms of the towers. The towers support the system of conductors at different spacing, called span.

In 2013, The White House in Washington has estimated the occurrence of at least 600 power outages due to severe weather resulting in an annual average of economic loss ranging between \$18-\$33 billion [1]. As shown in Figure 1-2, the TLs can extend for thousands of kilometers. Hence, the probability of exposure of TLs to local High-intensity Wind (HIW) events is high. Investigations of TL failures show that most of the TL failures around the world are caused by HIW events, such as downbursts and tornadoes [2, 3]. However, this study focuses mainly on tornadoes.

In Canada, southern regions experience numerous tornado events, with an average of an F3 tornado occurring every five years in Southwestern Ontario [4]. Moreover, most weather-related TL failures in Ontario Hydro were caused by tornadoes due to the significant probability of a tornado crossing a TL according to Ishac and White [2]. Additionally, 92% of the TL failures related to tornadoes in Southwestern Ontario were

reported to be caused by F2 tornadoes or less on the Fujita scale [4]. Despite these alarming statistics, HIW events are not considered in practice manuals and design guidelines. Instead, conventional boundary layer wind profiles associated with synoptic wind are used to develop the design loads in the design guidelines. This is problematic due to the locality of HIW events, as well as the difference in wind profiles, associated with those events.

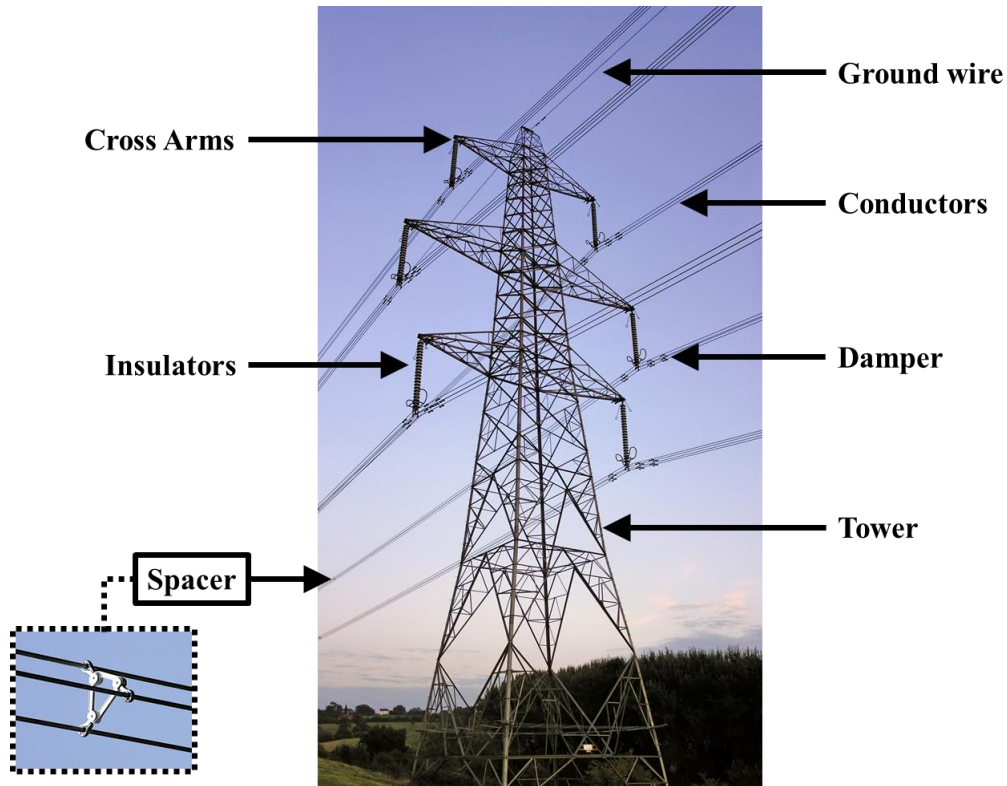


Figure 1-1: Components of TL systems (<https://tinyurl.com/y3lup5q7> & <https://tinyurl.com/y54ajvhv>).



Figure 1-2: Transmission line systems (<https://tinyurl.com/r8p5ya2>).

1.2 Literature

Many previous studies available in the body of the literature investigated the behaviour of TLs under HIW events, both downbursts and tornadoes. However, the literature review in this thesis will only focus on tornado wind fields as this is the main scope of the current study.

1.2.1 Tornado Wind Fields

Tornadoes are defined by Fujita [5] as “highly convergent swirling wind affecting a relative narrow path”. Tornadoes were classified by Fujita in 1971 into seven categories according to the tornado wind speed and the related structural damage based on the damage surveys [6]. Fujita and Pearson [7] developed the Fujita-Pearson scale in 1973 to classify tornadoes into seven main categories based on tornado wind speed, path length and width as shown in Table 1-1.

Table 1-1: Ranges of wind speed, path length, and path-width from the Fujita-Pearson scales [7].

Scale	Fujita scale wind speed (mph)	Pearson path length (miles)	Pearson path width (yards)
0	40-72	0.3-0.9	6-17
1	73-112	1.0-3.1	18-55
2	113-157	3.2-9.9	56-175
3	158-506	10-31	176-556
4	207-260	32-99	0-0.9 miles
5	261-318	100-315	1.0-3.1 miles
6	319-380	316-999	3.3-9.9 miles

Tornadoes have more localized occurrences with narrow path widths and high values of vertical wind component. Hence, it is important to understand the characteristics of tornado wind fields. Although some field measurements for tornadoes are reported in the literature [8, 9], the recorded data is still lacking for the zone near to the ground surface. This is the

zone of interest for structural engineers since it covers all structures. Thus, it was essential to develop some laboratory simulations such as those done by Sarkar et al. [8], Wan and Chang [10], Ward [11], Davies-Jones [12], Church et al. [13], Church et al. [14], Baker and Church [15], and Rotunno [16], as well as numerical simulations conducted by Hangan and Kim [3], Lewellen [17], Lewellen et al. [18], Lewellen et al. [19], Lewellen and Lewellen [20], Xia et al. [21], Selvam and Millett [22], Gairola and Bitsuamlak [23], and El Damatty et al. [24].

1.2.2 Behaviour and failure analysis of transmission lines under tornadoes

An extensive research program started at Western University after the failure of TLs in Winnipeg, Canada during a microburst event in 1996. The goal of the project was to investigate the behaviour of TLs under HIW events. Failure of self-supported TL towers due to tornadoes and downbursts has been examined by Savory et al. [25]. However, the modelling of the conductors and the vertical velocity component of the tornado wind field were not included in this study. This is specifically problematic, given how significant their effect on the nature of the problem

One of the major outcomes of the project at Western University is the development of an in-house fluid-structure software [26] that can assess the response and failure of TL towers under downbursts [26, 27]. Using the results of the Computational Fluid Dynamics (CFD) simulations conducted by Hangan and Kim [3], this software was extended in 2010 to incorporate the tornado wind fields. By then, the software could be utilized to assess the failure of TLs under tornadoes [28]. Later, this model was further extended to include geometric nonlinearity of the tower members [29]. The software was then utilized to investigate the failure modes of two guyed TL towers under two critical tornado configurations [30]. The critical configurations of the tornado wind fields were identified from parametric studies conducted in previous investigations [28, 29].

In order to accurately estimate the stiffness of the system and the conductors' reactions, Shehata et al. [26] recommended considering at least six spans of the TL system in the analysis. To analyze the conductors and calculate their reactions due to tornado loading, non-linear finite element cable elements were used by Hamada and El Damatty [31].

However, this technique is time-consuming, especially when conducting parametric studies. Therefore, to address this problem, Aboshosha and El Damatty [32] developed a novel technique to calculate the reactions of the conductors. The semi-closed form solution, which is used in this technique, calculates the conductors' reactions of a multi-spanned TL system under tornado loads. The semi-closed form technique requires significantly less computational time compared to non-linear finite element methods. Aboshosha and El Damatty [32] reported that the proposed technique can be up to 185 times faster than using Finite Element Analysis, where a case study shows that a parametric study requires 18 minutes to be conducted using this technique, while it needs approximately 45 hours to be conducted using Finite Element Analysis.

The progressive failure analysis conducted by Hamada and El Damatty [30] shows the progression of failure within single guyed TL towers under tornadoes using one tornado wind field. Considering one tower in the progressive failure analysis does not address the knowledge gap of how failure propagates within TL systems. As shown in Figure 1-3, some of the damage surveying observations show that towers may collapse without causing a domino effect failure for the entire TL. These observations motivated researchers to investigate the progressive failure of the TL system as a system composed of multiple TL towers and conductors. Shehata and El Damatty [33] extended the fluid-structure software developed at Western University to capture the incremental deformation and the post-failure geometry of the collapsed segment of the tower. The post-failure geometry is then used in calculating the conductors' forces to the adjacent towers within the line. This novel technique utilizes the 3D extensible catenary approach developed by Shehata and El Damatty [34] to calculate the conductors' reactions. This is important to predict how the failure of a TL tower within the unit will influence the adjacent towers since TLs are built to function as a unit.



Figure 1-3: (A) Failure of one TL tower within the line. (B) Close-up image of a failed transmission line tower within a TL. “Manitoba Hydro, 2019”.

1.3 Research gaps

To the best of the author's knowledge, no studies were previously conducted to investigate the progressive failure of guyed and self-supported TL towers under different tornado wind fields. Moreover, the available literature considered only the progressive failure of single TL towers without investigating the TL as a system. Very few to none focused on assessing the progression of failure within the TL system under different tornado wind fields. Furthermore, the effect of the insulator length on the propagation of failure within the TL system and the effect of the variation in the span on the propagation of failure have never been studied before.

1.4 Thesis objective

The current study investigates the progressive failure of guyed and self-supported TLs under different tornado wind fields. The objectives are as follows:

1. Study the progressive failure of a single TL tower under different tornado wind fields.
2. Assess the economic implications for designing TL towers that can sustain F2 tornadoes.
3. Study the progressive failure of a TL system under different tornado wind fields.
4. Assess the effect of changing the insulator length and TL span on the propagation of failure of the TL towers.

1.5 Methodology

Two tornado wind fields are incorporated in the fluid-structure program developed at Western University [27, 28, 33]. The tornado wind fields are obtained from CFD simulations conducted by Hangan and Kim [3] and El Damatty et al. [24]. The software is then verified by comparing the results obtained with the findings of Hamada and El Damatty [29].

The program is then used to conduct extensive parametric studies to identify the critical tornado configurations for the guyed and self-supported TL towers under each of the two tornado wind fields incorporated in this study. The parametric studies are based on varying the location of the tornado relative to the tower where non-linear analysis of the TL systems under F2 tornado loads is conducted for each configuration. The most critical configurations are sorted according to the highest peak demand-to-capacity ratio within all the tower members. The demand-to-capacity ratio is the ratio of the internal forces of structural members to the capacities of the members. The capacities of the structural members are calculated based on ASCE 10-15 [35].

The extended version of the numerical model is verified by comparing the critical configurations to those presented by Hamada and El Damatty [29]. Accordingly, these critical tornado configurations are considered in a non-linear finite element analysis to identify failure modes of the investigated single towers and then compare them to those reported by Hamada and El Damatty [30].

The software is then used to examine the progressive failure of two guyed and two self-supported TL towers. The towers are designed and constructed to resist synoptic wind loading as per the design guidelines. Furthermore, for cases where towers suffered from failure prior to reaching the full F2 tornado load, a strengthening is proposed to increase the resiliency of the tower to resist the full load where the associated percentage of increase in tower weight is reported.

Finally, the software is used to examine the progressive failure of self-supported TL systems under different tornado wind fields. The examined system is composed of seven towers and eight spans. The effect of changing the insulator length and the span of the TL

system on the propagation of failure within the towers in the TL system is then evaluated.

1.6 Thesis organization

This thesis is presented in an Integrated-Article format. Chapter 1 presents a review of the literature related to investigating the tornado wind fields and the response of TLs under tornado wind loading. The objectives presented in Section 1.1 are achieved and presented in the following chapters.

1.6.1 Progressive Failure of a Single Transmission Line Tower under Different Tornado Wind Fields

In this chapter, the progressive failure of single guyed and self-supported TL towers under different tornado wind fields is examined. This is achieved by incorporating the tornado wind fields in a fluid-structure software that has been developed at Western University. The software is then used to conduct a progressive failure analysis for two guyed and two self-supported TL towers under the most critical tornado configurations identified through an extensive parametric study. The study then provides an insight into the cost associated with designing TL towers that can sustain F2 tornado loads. This is achieved by strengthening the investigated towers.

1.6.2 Progressive Failure of Self-supported Transmission Line Towers under Different Tornado Wind Fields

In this chapter, the progressive failure of the TL system is investigated. This is achieved by incorporating the tornado wind fields in an extended version of the fluid-structure software that has been developed at Western University. The extended version of the software is a unique numerical tool that predicts the post-failure geometry of the failed segment of the tower and uses it to calculate the conductors' forces transmitted to the adjacent towers. Hence, the progressive failure of the entire TL system as a unit can be examined. The effect of changing the insulator length and the span of the TL on the propagation of failure within the TL system is then investigated.

1.7 References

- [1] E. O. of the President, “White House 2013 - Grid Resiliency and Economic Benefit,” 2013.
- [2] H. B. Ishac, M.F.; White, “Effect of tornado loads on transmission lines,” in *IEEE Transactions on Power Delivery*, 1995, p. Volume: 10; Issue: 1; pages: 445-451.
- [3] H. Hangan and J. D. Kim, “Swirl ratio effects on tornado vortices in relation to the Fujita scale,” *Wind Struct.*, vol. 11, pp. 291–302, Aug. 2008, doi: 10.12989/was.2008.11.4.291.
- [4] M. J. Newark, “Canadian tornadoes, 1950–1979,” *Atmos. - Ocean*, vol. 22, no. 3, pp. 343–353, 1984, doi: 10.1080/07055900.1984.9649203.
- [5] T. T. Fujita, “Tornadoes and Downbursts in the Context of Generalized Planetary Scales,” *Journal of the Atmospheric Sciences*, vol. 38, no. 8. pp. 1511–1534, 1981, doi: 10.1175/1520-0469(1981)038<1511:TADITC>2.0.CO;2.
- [6] T. T. Fujita, “Proposed Characterization of Tornadoes and Hurricanes by Area and Intensity,” *SMRP, Univ. Chicago*, vol. 91, p. 42, 1971.
- [7] Fujita and D. Pearson, “Results of FPP classification of 1971 and 1972 tornadoes,” *Am. Meteorol. Soc.*, pp. 142–145, 1973.
- [8] J. Sarkar, P., Haan, F., Gallus, Jr., W., Le, K. and Wurman, “Velocity measurements in a laboratory tornado simulator and their comparison with numerical and full-scale data,” in *37th Joint Meeting Panel on Wind and Seismic Effects*.
- [9] W. C. Lee and J. Wurman, “Diagnosed three-dimensional axisymmetric structure of the Mulhall tornado on 3 May 1999,” *J. Atmos. Sci.*, vol. 62, no. 7 II, pp. 2373–2393, 2005, doi: 10.1175/JAS3489.1.
- [10] C. A. Wan and C. C. Chang, “Measurement of the Velocity Field in a Simulated

Tornado-Like Vortex Using a Three-Dimensional Velocity Probe,” *Journal of the Atmospheric Sciences*, vol. 29, no. 1. pp. 116–127, 1972, doi: 10.1175/1520-0469(1972)029<0116:motvfi>2.0.co;2.

- [11] N. B. Ward, “The exploration of certain features of tornado dynamics using a laboratory model,” *J. Atmos. Sci.*, vol. 29, pp. 1194–1204, 1972.
- [12] R. P. Davies-Jones, “The Dependence of Core Radius on Swirl Ratio in a Tornado Simulator,” *Journal of the Atmospheric Sciences*, vol. 30, no. 7. pp. 1427–1430, 1973, doi: 10.1175/1520-0469(1973)030<1427:tdocro>2.0.co;2.
- [13] C. R. Church, J. T. Snow, and E. M. Agee, “Tornado Vortex Simulation at Purdue University,” *Bull. Am. Meteorol. Soc.*, vol. 58, no. 9, pp. 900–908, 1977, doi: 10.1175/1520-0477(1977)058<0900:tvsapu>2.0.co;2.
- [14] E. M. Church, C. R., Snow, J. T., Baker, G. L. and Agee, “Characteristics of tornado-like vortices as a function of swirl ratio: A laboratory investigation,” *J. Atmos Sci.*, vol. 36, pp. 1755–1776, 1979.
- [15] G. L. Baker and C. R. Church, “Measurements of the core radii and peak velocities in modeled atmospheric vortices,” *J. Atmos. Sci.*, vol. 36, no. 12, Dec. 1979. pp. 2413–2424, 1979.
- [16] R. Rotunno, “A study in tornado like vortex dynamics,” *J. Atmos. Sci.*, vol. 36, no. 1, Jan. 1979. pp. 140–155, 1979.
- [17] W. S. Lewellen, “A solution for three-dimensional vortex flows with strong circulation,” *J. Fluid Mech.*, vol. 14, no. 3, pp. 420–432, 1962, doi: 10.1017/S0022112062001330.
- [18] W. S. Lewellen, D. C. Lewellen, and R. I. Sykes, “Large-Eddy simulation of a tornado’s interaction with the surface,” *J. Atmos. Sci.*, vol. 54, no. 5, pp. 581–605, 1997, doi: 10.1175/1520-0469(1997)054<0581:LESOAT>2.0.CO;2.
- [19] D. C. Lewellen, W. S. Lewellen, and J. Xia, “The influence of a local swirl ratio

- on tornado intensification near the surface,” *J. Atmos. Sci.*, vol. 57, no. 4, pp. 527–544, 2000, doi: 10.1175/1520-0469(2000)057<0527:TIOALS>2.0.CO;2.
- [20] D. C. Lewellen and W. S. Lewellen, “Near-surface intensification of tornado vortices,” *J. Atmos. Sci.*, vol. 64, no. 7, pp. 2176–2194, 2007, doi: 10.1175/JAS3965.1.
- [21] J. Xia, W. S. Lewellen, and D. C. Lewellen, “Influence of Mach number on Tornado corner flow dynamics,” *J. Atmos. Sci.*, vol. 60, no. 22, pp. 2820–2825, 2003, doi: 10.1175/1520-0469(2003)060<2820:IOMNOT>2.0.CO;2.
- [22] R. P. Selvam and P. C. Millett, “Computer modeling of tornado forces on buildings,” *Wind Struct. An Int. J.*, vol. 6, no. 3, pp. 209–220, 2003, doi: 10.12989/was.2003.6.3.209.
- [23] A. Gairola and G. Bitsuamlak, “Numerical tornado modeling for common interpretation of experimental simulators,” *J. Wind Eng. Ind. Aerodyn.*, vol. 186, no. November 2017, pp. 32–48, 2019, doi: 10.1016/j.jweia.2018.12.013.
- [24] A. El Damatty, N. Ezami, and A. Hamada, “Case Study for Behaviour of Transmission Line Structures under Full-Scale Flow Field of Stockton, Kansas, 2005 Tornado,” in *Electrical Transmission and Substation Structures 2018*, 2018, pp. 257–268.
- [25] E. Savory, G. A. R. Parke, M. Zeinoddini, N. Toy, and P. Disney, “Modeling of tornado and microburst induced wind loading and failure of a lattice transmission tower,” vol. 23, pp. 365–375, 2001.
- [26] A. Y. Shehata, A. A. El Damatty, and E. Savory, “Finite element modeling of transmission line under downburst wind loading,” *Finite Elem. Anal. Des.*, vol. 42, no. 1, pp. 71–89, 2005, doi: 10.1016/j.finel.2005.05.005.
- [27] A. Y. Shehata and A. El Damatty, “Failure analysis of a transmission tower during a microburst,” *Wind Struct.*, vol. 11, Jun. 2008, doi: 10.12989/was.2008.11.3.193.

- [28] A. Hamada, A. A. E. Damatty, H. Hangan, and A. Y. Shehata, “Finite element modelling of transmission line structures under tornado wind loading,” *Wind Struct. An Int. J.*, vol. 13, no. 5, pp. 451–469, 2010, doi: 10.12989/was.2010.13.5.451.
- [29] A. Hamada and A. A. El Damatty, “Behaviour of guyed transmission line structures under tornado wind loading,” *Comput. Struct.*, vol. 89, no. 11–12, pp. 986–1003, 2011, doi: 10.1016/j.compstruc.2011.01.015.
- [30] A. Hamada and A. El Damatty, “Failure analysis of guyed transmission lines during F2 tornado event,” *Eng. Struct.*, vol. 85, Feb. 2015, doi: 10.1016/j.engstruct.2014.11.045.
- [31] A. Hamada and A. A. El Damatty, “Nonlinear Formulation of Four-Nodded Cable Element and Application to Transmission Lines under Tornadoes Nonlinear formulation of four-nodded cable element and application to transmission lines under tornadoes,” in *2014 International Conference on Advances in Wind and Structures (AWAS14) - ACEM14*, 2014, no. February 2016.
- [32] H. Aboshosha and A. El Damatty, “Effective technique to analyze transmission line conductors under high intensity winds,” *Wind Struct. An Int. J.*, vol. 18, no. 3, pp. 235–252, 2014, doi: 10.12989/was.2014.18.3.235.
- [33] A. Shehata and A. El Damatty, “Nonlinear Analysis of Transmission Lines under Downbursts,” in *The 15th International Conference on Wind Engineering (ICWE15)*, 2019.
- [34] A. Shehata and A. El Damatty, “Extensible Catenary Approach in Analyzing Transmission Line ’ s Conductors under Downbursts .,” *Manuscr. Prep.*
- [35] *Design of Latticed Steel Transmission Structures (10-15)*. American Society of Civil Engineers, 2015.

Chapter 2

2 Progressive Failure of a Single Transmission Line Tower under Different Tornado Wind Fields

2.1 Introduction

Electricity is a necessity in today's lifestyle as it is a source of fuel to perform daily tasks. The main element in an electrical power network is the transmission lines (TLs). TLs consist of two main elements as follows; conductors that transfer the electricity from the source of production to end-users, and the towers that support these conductors. Outages of power due to TL tower failures can cause social and economic disasters. Investigations of TL failures around the world have recorded that they are mostly from High-Intensity Wind (HIW) events, such as downbursts and tornadoes [1, 2].

A previous report states that power outages in the United States due to severe weather resulted in significant economic loss [3]. Many previous studies available in the body of the literature, studied the behaviour of TLs under downbursts. However, the literature review will focus on tornadoes as the main scope of the current study. Tornadoes are defined by Fujita [4] as "highly convergent swirling wind affecting a relative narrow path". In Canada, southern regions experience numerous tornado events, with an average of an F3 tornado occurring every five years in Southwestern Ontario [5]. Additionally, 92% of the tornadoes that cause TL failures in Southwestern Ontario were reported to be F2 or less on the Fujita scale [5]. Ishac and White [1] reported that most weather-related TL failures in Ontario Hydro are caused by tornadoes because of the significant probability of a tornado crossing a TL. Yet, design guidelines do not consider HIW events. Instead, synoptic winds are used to develop the design loads in the design guidelines. This is concerning because of the locality of HIW events, as well as the difference in wind profiles associated with those events. So, it is crucial to consider HIW profiles in investigating weather-related TL failures in order to be able to understand the failure mechanisms of TLs under HIW events and develop damage mitigation measures. As tornadoes have more localized occurrences with narrow path widths and high values of vertical wind component,

characteristics of tornado wind fields have to be investigated. Although some field measurements for tornadoes are reported in the literature [6, 7], the recorded data is still lacking for the zone near to the ground surface. This is the zone of interest for structural engineers since it covers all the structures. Hence, developing laboratory simulations such as those done by Sarkar et al. [6], Wan and Chang [8], Ward [9], Davies-Jones [10], Church et al. [11], Church et al. [12], Baker and Church [13], and Rotunno [14] as well as numerical simulations conducted by Hangan and Kim [2], Lewellen [15], Lewellen et al. [16], Lewellen et al. [17], Lewellen and Lewellen [18], Xia et al. [19], Selvam and Millett [20], Gairola and Bitsuamlak [21], and El Damatty et al. [22] was of great interest.

After the collapse of transmission towers during a microburst event in Winnipeg, Canada in 1996, an extensive research program began at the University of Western Ontario, investigating the behaviour of TLs under HIW events. Savory et al. investigated the failure of self-supported towers under downbursts and tornadoes [23]. However, the study did not include the modelling of the conductors and the vertical velocity component of the tornado wind field. One of the significant outcomes of this project is the development of an in-house software [24] that can predict and assess the behaviour of TLs [25] as well as failure analysis of transmission towers under downbursts [26]. This software was extended in 2010 to incorporate the tornado wind field, obtained from Computational Fluid Dynamics (CFD) simulations conducted by Hangan and Kim [2], which allowed assessing the failure of TLs under tornadoes [27]. Later, this model was further extended to include geometric nonlinearity of the tower members [28], and this model was utilized to analyze two guyed transmission systems investigating their failure modes [29] under two critical tornado configurations that were identified from parametric studies conducted in previous studies [27, 28].

The current study builds on the findings reported by Hamada et al. [27] and Hamada and El Damatty [28], where another tornado wind field obtained from CFD simulations conducted by El Damatty et al. [22] is incorporated in the fluid-structure program. The program is then used to conduct a parametric study to identify the critical tornado configurations for the second tornado wind field, newly incorporated in this study. To verify this extended version of the numerical model the critical configurations are compared to those identified by Hamada and El Damatty [28]. Accordingly, these critical

tornado configurations are considered in a non-linear finite element analysis to identify failure modes of guyed and self-supported towers, and then compare them to those reported by Hamada and El Damatty [29]. Furthermore, for cases where towers suffered from failure prior to reaching the full F2 tornado load, strengthening is proposed to increase the ability of the tower to resist the full F2 tornado load and the associated percentage of increase in tower weight is reported. This study is considered the first of its kind to; i) investigate the progressive failure of single guyed and self-supported towers under different F2 tornado wind fields, ii) assess the performance of as-built towers, designed following current code provisions under the effect of normal wind, when exposed to different F2 tornado wind fields, iii) provide an insight to the cost associated with strengthening to enhance the resiliency of these towers to sustain the full F2 tornado load.

2.2 Description of the Numerical Model

The numerical simulations conducted in this study incorporate the tornado wind fields that were obtained from CFD simulations conducted by Hangan and Kim [2] and El Damatty et al. [22], and finite element models to simulate the TL system. The description of each component of the model is outlined in the following subsections.

2.2.1 Description of Tornado Wind Fields

A tornado wind field is represented by three velocity components: the tangential (V_{mt}), radial (V_{mr}), and axial (V_{ma}). The velocity components are each presented as a function of the cylindrical coordinates, r , θ_t , z , measured from the center of the tornado.

Two different tornado wind fields are considered in the current study to investigate the progressive failure of the towers. The first wind field is based on CFD simulations conducted by Hangan and Kim [2] using the commercial software FLUENT [30] to simulate tornado wind fields. The maximum scaled-up velocities of the three velocity components for this wind field [31] are: the maximum tangential velocity is 78 m/s at radius, $r = 96$ m and height, $z = 19$ m; the maximum radial velocity is 49 m/s at the radius, $r = 146$ m and height, $z = 6$ m; the maximum axial velocity is 37 m/s at the radius, $r = 171$ m and height, $z = 127$ m.

The second wind field is based on the CFD simulation for the Stockton, Kansas, 2005 tornado [22]. The maximum velocity of the three velocity components are: the maximum tangential velocity is 53 m/s at radius, $r = 205$ m and height, $z = 60$ m; the maximum radial velocity is 14 m/s at radius, $r = 241$ m and height, $z = 158$ m; the maximum axial velocity is 32.9 m/s at radius, $r = 287$ m and height, $z = 269$ m.

The vertical profiles of the tangential velocity component for both tornado wind fields are shown in Figure 2-1.

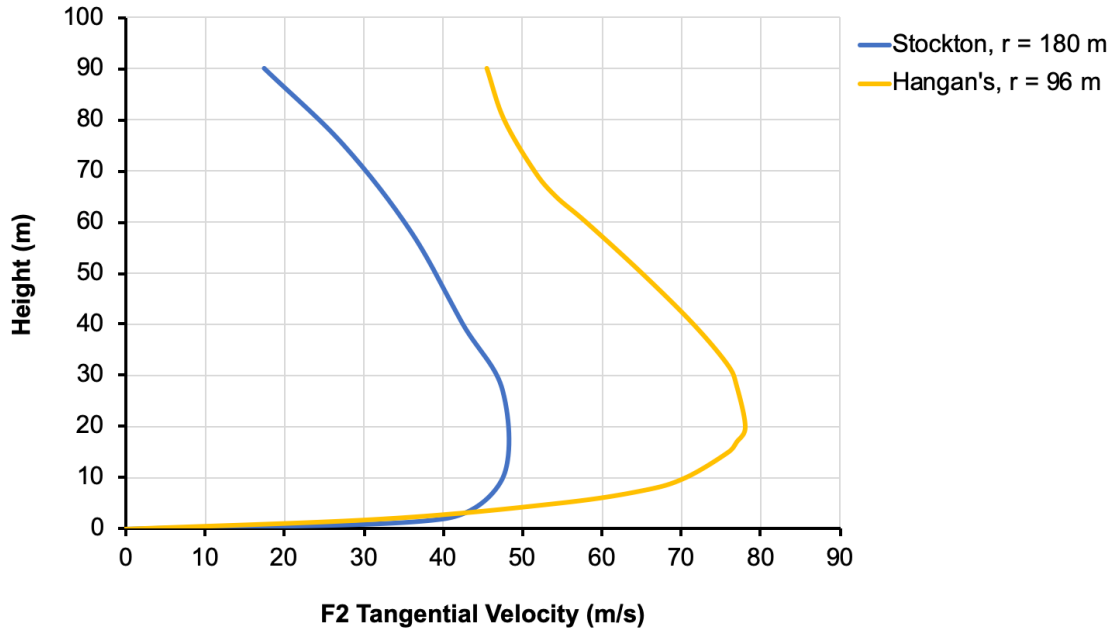


Figure 2-1: Vertical profiles of tangential velocity component of Stockton [22] and Hangan's [3, 30] tornado wind fields for radial distances, r , from tornado center.

In order to be able to predict the members' demand-to-capacity ratios and compare the progressive failure of the towers under different tornado wind fields, the velocity components of the simulated wind fields are scaled. Specifically, the procedure applied is based on scaling the maximum resultant of the radial and tangential components to match the maximum wind speed for F2 tornadoes on the Fujita scale which is 70 m/s [32].

2.2.2 Description of the Finite Element Model

Each line system of those discussed in the previous section is modelled considering six spans. The numerical model comprises five towers (the tower of interest and the two adjacent towers from each side) plus two hinged supports at both ends. The choice of this number of towers per line ensures that the simulation accurately reflects the appropriate stiffness of the system and the forces transferred from the conductors and ground wires to the tower of interest, as concluded by Shehata et al. [24]. The reactions of the conductors are calculated using the technique developed by Aboshosha and El Damatty [33]. The technique allows calculating the conductors' reactions of a multi-spanned TL system under

tornado loads using a semi-closed form solution. The semi-closed form technique requires significantly less computational time compared to non-linear finite element methods. Saving computational time is a crucial factor when conducting extensive parametric studies. To model the tower members, two noded three-dimensional frame elements are used. Rigid connections are assumed between the primary chord members to simulate the multi-bolted connections, while hinged connections are used to simulate the single-bolt connections between the diagonal and the primary chord members.

2.2.3 Description of the Considered Towers

A sample of four TLs is considered in the current study to investigate the progressive failure of the two most common types of TL towers (guyed and self-supported) under F2 tornadoes. The two guyed towers are labelled as G1 and G2, and the two self-supported towers are labelled S1 and S2, as shown in Figure 2-2.

For the guyed towers, the structure can be simplified as an overhanging beam with a base pin support and the guy's cross-arm supported by springs. While the structural system of the self-supported towers can be simplified as a cantilever beam fixed at the base.

The first guyed TL system, GL1, has a line span of 480 m. The guyed towers, G1, support two conductors, which are connected to the towers through 3.9 m insulators, and one ground-wire at the top of the tower at a height of 44.39 m. The conductors and ground-wire initial sags are 20 m and 13 m, respectively. The height of the guyed tower G1 is 44.39 m and is supported by four down guys attached to G1's cross-arms at a height of 38.23 m point (Figure 2-2A). On the other hand, the second guyed TL system, GL2, has a line span of 460 m. The guyed towers, G2, support two conductors, which are connected to the towers through 4.27 m insulators, and two ground-wires at the highest points of the tower at a height of 46.57 m. The conductors and ground-wire initial sags are 14 m and 16 m, respectively. The height of the guyed tower G2 is 46.57 m and is supported by four guys attached to G2's cross-arms (Figure 2-2B).

With respect to the self-supported TLs, the first self-supported TL system, SL1, has a line span of 213 m. The self-supported towers, S1, support six conductors, which are connected to the towers through 4.267 m insulators, and two ground-wires. The conductors and

ground-wires have initial sags of 3.9 m and 3 m, respectively. The height of the S1 tower is 54.65 m (Figure 2-2C). The second self-supported TL system, SL2, has a line span of 450 m. The self-supported towers, S2, support six conductors, which are connected to the towers through 2.438 m insulators, and two ground-wires. The conductors and ground-wires have initial sag of 19.5 m and 14 m, respectively. The height of the S2 tower is 51.81 m (Figure 2-2D). The physical parameters for conductors and ground-wires in GL1, GL2, SL1, and SL2 are outlined in Table 2-1. The investigated towers are designed to resist synoptic wind with design wind speeds shown in Table 2-1. A sample of the detailed drawings for the towers is provided for G1 in Figure 2-3.

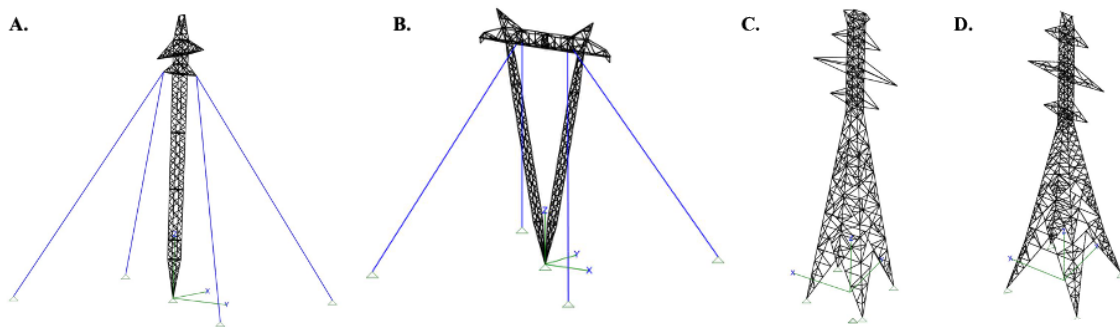


Figure 2-2: Schematic illustrating studied TL towers. (A) G1; (B) G2; (C) S1; and (D) S2 TLs.

Table 2-1: Properties of TLs.

Tower	G1	G2	S1	S2
Type	Guyed	Guyed	Self-supported	Self-supported
Tower Weight (kN)	34	78.2	96.8	78.1
Span (m)	480	460	213.36	450
Guy Diameter (m)	0.0165	0.0195	N/A	N/A
Tower Height (m)	44.39	46.57	54.65	51.81

Number of Conductors	2	3	6	6
Number of Ground Wires	1	2	2	2
Conductor Weight (N/m)	28.97	8.67	28.97	20.14
Ground Wire Weight (N/m)	3.9	5.45	10.4	3.823
Conductor Sag (m)	20	14	3.9	19.5
Ground Wire Sag (m)	13.54	16	3	14
Insulator Length (m)	3.9	4.27	4.267	2.438
Design Wind Speed (m/s)	32	36	45	34

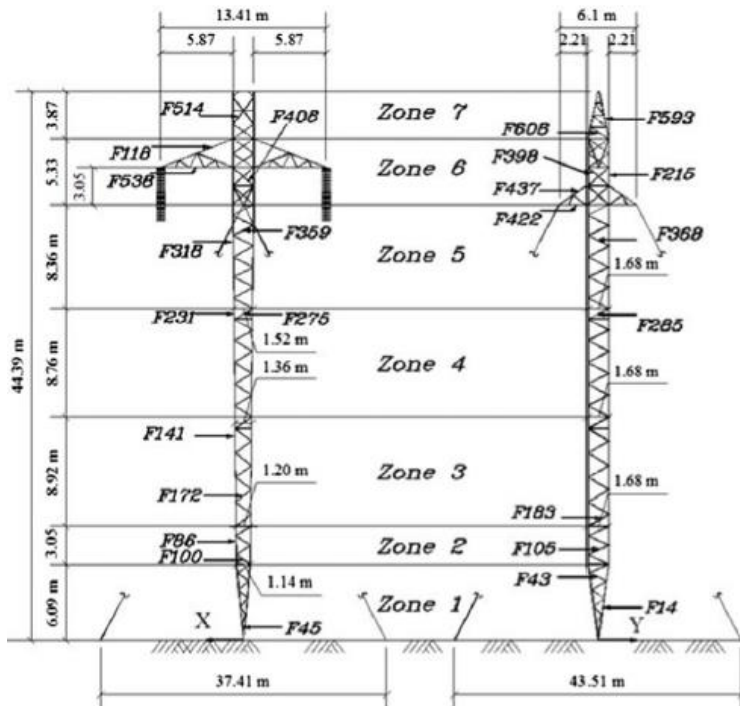


Figure 2-3: Detailed Drawing for G1 [31].

2.3 Parametric Study

The parametric study is based on the analysis of the towers under the full F2 tornado loads. The extensive parametric study considers different cases in which the location of the tornado changes relative to the tower. The variation of the tornado locations allows examining the effect of the localized nature of tornado events. This is achieved by covering a domain of polar coordinates (R, θ) , relative to the centre of the tower of interest, as shown in Figure 2-4. The Radius, R , ranges from 0 m to 500 m with an increment of 20 m (26 cases). The angle, θ , ranges from 0° to 345° with an increment of $\theta = 15^\circ$ (24 cases). This concludes a total of 624 cases to be investigated for each tower in this parametric study.

The parametric study allows identifying the critical tornado configurations that cause the failure of main members of a tower, based on the peak demand-to-capacity ratio (λ) recorded after non-linear analysis of the TL system under tornado wind loading. The demand-to-capacity ratio is the ratio of the internal forces of structural members to the capacities of the members. The capacity of the structural members is calculated based on ASCE 10-15 [34].

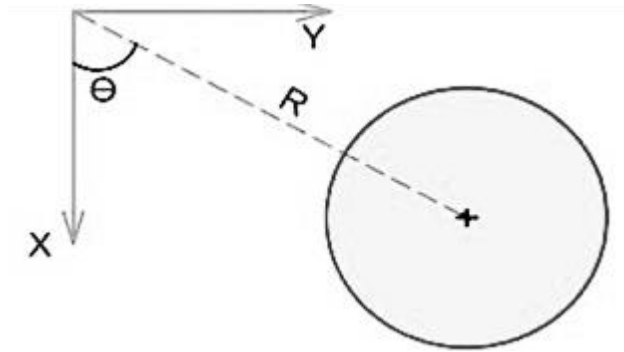


Figure 2-4: Critical tornado configurations parameters (R and θ) relative to the tower of interest.

2.3.1 Parametric Study Results

The results of the parametric study are summarized in Table 2-2. As shown in Table 2-2, the parametric study is conducted considering each of the four TL tower systems while considering two different tornado wind fields. The numerical models developed by Hangan and Kim [2], and El Damatty et al. [22] are integrated with the finite element model to investigate the critical tornado configuration for each tower system. Five critical scenarios for each of the tower systems are reported. These critical scenarios are ranked in a descending order based on the maximum demand-to-capacity ratio (λ) experienced within all the tower members. The most critical configuration for each tower under both tornado wind fields is determined based on the highest demand-to-capacity ratio within all the structural members of the tower as bolded in Table 2-2.

Table 2-2: Results of the parametric study.

Tower	Tornado Wind Field	Scenario	Critical configuration (R, θ)	λ
G1	Hangan and Kim [2]	1	120 m, 165°	4.3
		2	120 m, 0°	4.3
		3	120 m, 255°	2.1
		4	160 m, 60°	1.5
		5	180 m, 240°	1.5
	Stockton [22]	1	200 m, 0°	4.7
		2	200 m, 75°	2.1
		3	260 m, 60°	1.8
		4	280 m, 240°	1.7
		5	320 m, 240°	1.6
G2	Hangan and Kim [2]	1	100 m, 165°	11.4
		2	120 m, 165°	11.3
		3	120 m, 150°	8.9
		4	120 m, 255°	7.4
		5	100 m, 255°	6.0

S1	Stockton [22]	1	180 m, 0°	11.5
		2	200 m, 0°	11.4
		3	200 m, 345°	11.2
		4	200 m, 75°	7.5
		5	180 m, 90°	6.1
	Hangan and Kim [2]	1	160 m, 75°	12.6
		2	120 m, 255°	12.5
		3	120 m, 270°	9.8
		4	140 m, 90°	9.6
		5	120 m, 0°	9.0
Stockton [22]	1	220 m, 75°	14	
	2	200 m, 0°	9.6	
	3	220 m, 165°	9.2	
	4	200 m, 150°	6.9	
	5	220 m, 345°	6.7	
S2	Hangan and Kim [2]	1	120 m, 225°	11.0
		2	120 m, 45°	10.8
		3	120 m, 240°	9.8
		4	120 m, 285°	9.4
		5	160 m, 75°	9.3
	Stockton [22]	1	200 m, 30°	11.0
		2	260 m, 75°	10.5
		3	200 m, 210°	10.3
		4	240 m, 75°	9.9
		5	180 m, 75°	9.3

2.4 Progressive Failure Analysis

Based on the critical configurations identified in the parametric study, progressive failure analysis of the towers is investigated. For each of the identified critical tornado configuration, a non-linear analysis that involves geometric non-linearity is conducted. A non-linear analysis is conducted, where the tower is being solved at each increment of loading to identify the members that have reached the structural capacity. The identified members are then eliminated from the structural stiffness matrix in subsequent increments, where incrementally, deformed shape and the plastic hinge formation are detected. Once the structure cumulatively loses its overall stability, failure load and the associated failure mode are captured. Figure 2-5 summarizes the procedure followed to conduct the progressive failure analysis.

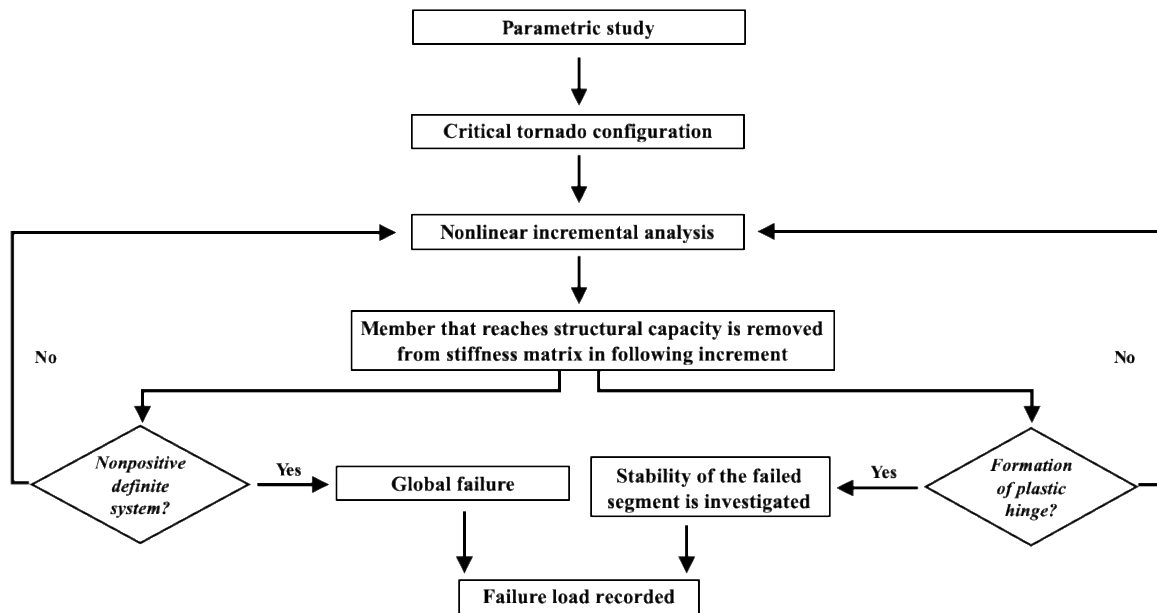
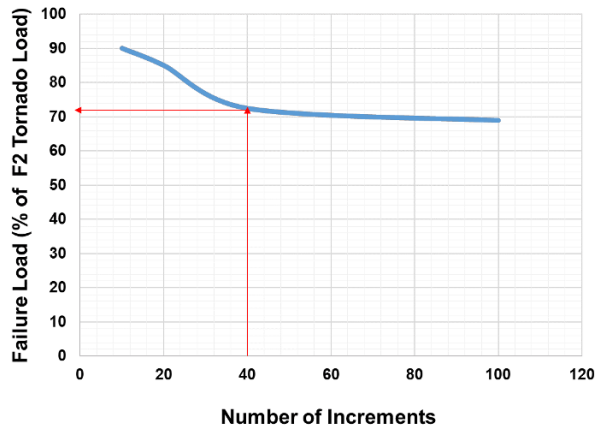


Figure 2-5: Flow chart outlining the progressive failure analysis for each critical tornado configuration.

To determine the suitable loading increment for the non-linear analysis, a sensitivity analysis has been conducted (Figure 2-6). The sensitivity analysis is conducted using the GL1 transmission line system under Hangan’s tornado [2]. The sensitivity analysis compares the failure load and the failure wind speed, as a percentage of the full F2 tornado load and wind speed, respectively, to the number of loading increments. This is critical to ensure accuracy in the results while minimizing the time required to perform the analysis. The sensitivity analysis data shown in Figure 2-6A demonstrates that a number of 40 loading increments (2.5% loading increment) is the most optimal as beyond that point there is a plateau at a failure load of approximately 72% of the full load associated with an F2 tornado. The results shown in Figure 2-6B indicate that 40 loading increments ensure accuracy in capturing the failure wind speed as beyond that point there is a plateau at the failure wind speed at approximately 84% of the full F2 tornado wind speed.

A.



B.

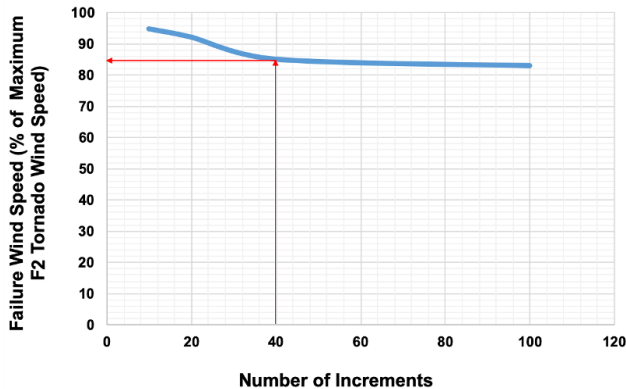


Figure 2-6: Sensitivity analysis to determine the loading increment.

2.4.1 Verification of Numerical Model

The fluid-structure numerical model, utilized in analyzing the tower systems in this study, is verified by comparing the critical tornado configurations associated with towers G1 and G2 to those obtained by Hamada and El Damatty [28, 29]. The verification is conducted using Hangan's tornado wind field [2] following the same scaling procedure and factors used by Hamada and El Damatty [28]. Table 2-3 summarizes the verification outcomes by comparing the critical configuration and the failure wind speed using the numerical model to the findings obtained by Hamada and El Damatty [29] for each of the two towers. For G1, the critical tornado configuration that is obtained in the current study is $R = 120$ m, $\theta = 165^\circ$, whereas Hamada and El Damatty [28, 29] detected $R = 125$ m, $\theta = 180^\circ$, as shown in Table 2-3. The discrepancy in the θ value between the two studies is a result of using a smaller θ increment in the parametric study outlined in the current study. Moreover, the failure load value in this study is comparable to the value reported by Hamada and El Damatty [29]. Further verification is done considering the G2 tower. Table 2-3 shows an excellent agreement in the case of G2 tower for the failure wind speeds and the two critical configurations.

Table 2-3: Summary of the verification study.

Structures	Model	Critical configuration (R, θ)	Failure wind speed (m/s)	Failure wind speed (% of F2 tornado wind speed)
G1	Current Study	120 m, 165°	63	85
	Hamada et al. [29]	125 m, 180°	65	84
G2	Current Study	100 m, 165°	42	57
	Hamada et al. [29]	100 m, 180°	43	55
G2	Current Study	120 m, 150°	45	61
	Hamada et al. [29]	125 m, 330°	42	54

2.4.2 Progressive Failure Analysis Results

2.4.2.1 The failure mode for G1 under Hangan's tornado wind field

The critical tornado configuration is $R = 120$ m and $\theta = 165^\circ$ with the maximum demand-to-capacity ratio, $\lambda = 4.3$. The failure of the tower is initiated in the diagonal member of the guy's cross-arms at 25% of the full F2 tornado load (Figure 2-7A, B). The resultant of the horizontal components of the tornado wind speed will then cause slacking of guy 3 at 32.5% of the full F2 tornado load (Figure 2-7C). The failure continues to propagate until two plastic hinges are formed at the highlighted members (Figure 2-7D) at 67.5% of the full F2 tornado load, which then results in losing the overall stability of the tower at 70% of the full F2 tornado load (Figure 2-7E). The tower fails at a tornado wind speed of 58.6 m/s which represents 84% of the maximum resultant wind speed of the full F2 tornado.

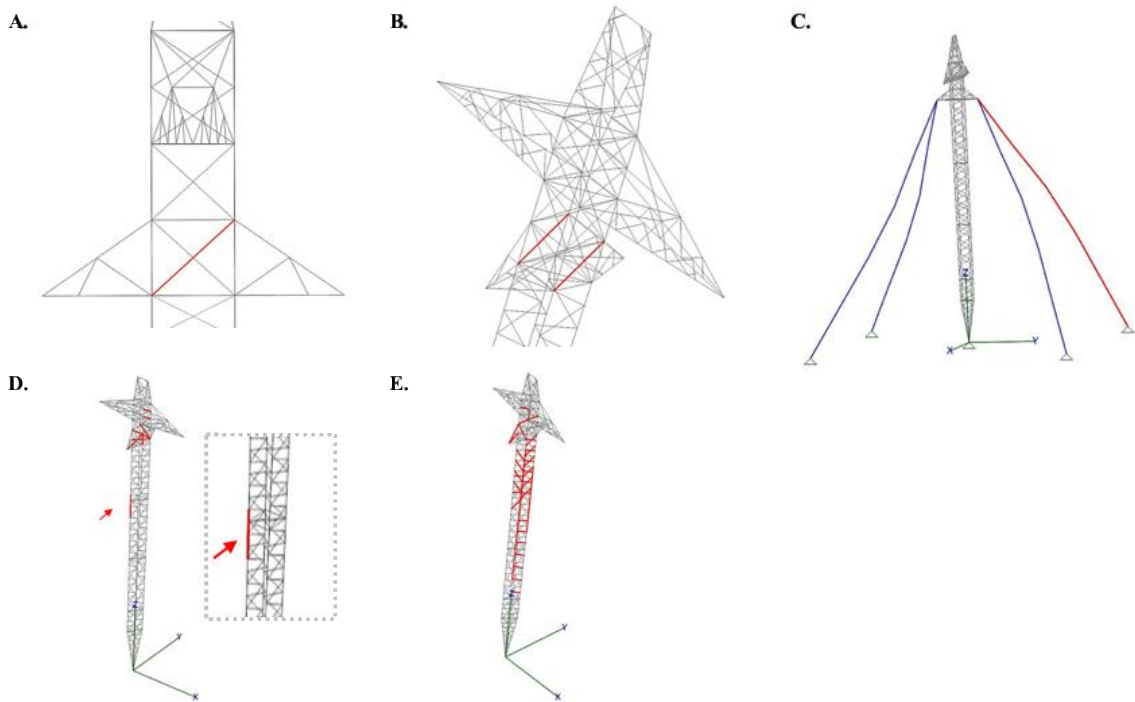
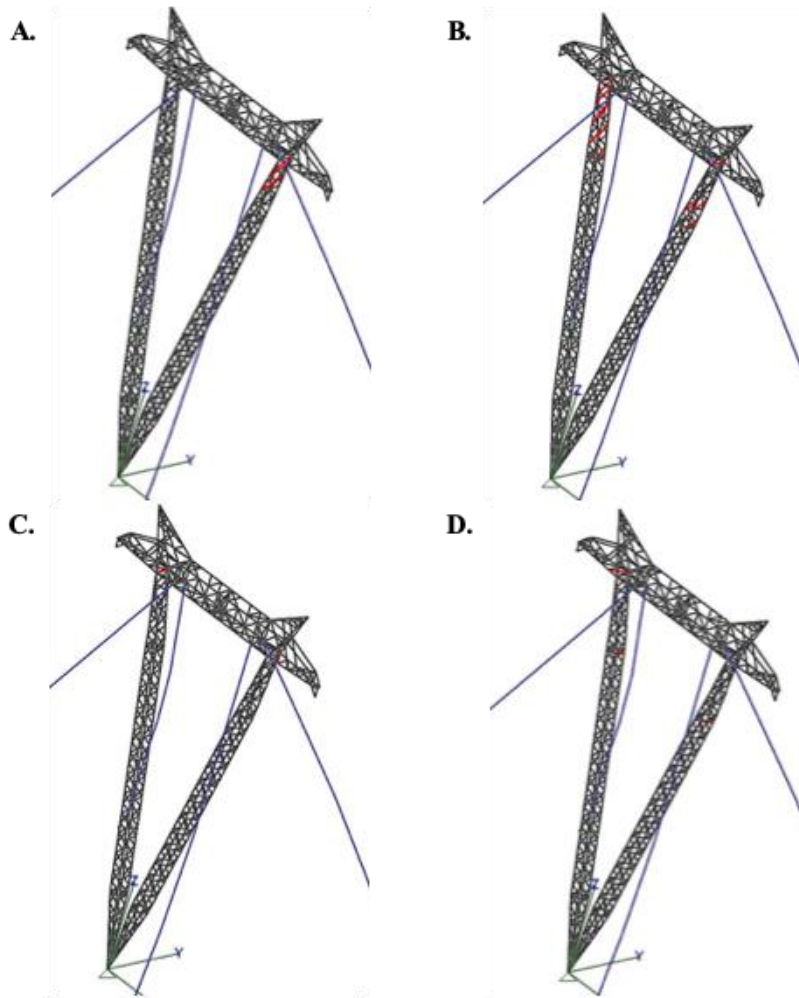


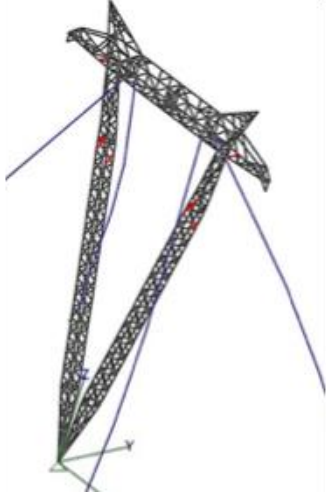
Figure 2-7: Progressive failure of G1 tower in the first scenario, $\lambda = 4$. (A,B) 25%; (C) 32.5%; (D) 67.5%; and (E) 70%.

2.4.2.2 The failure mode for G2 under Hangan's tornado wind field

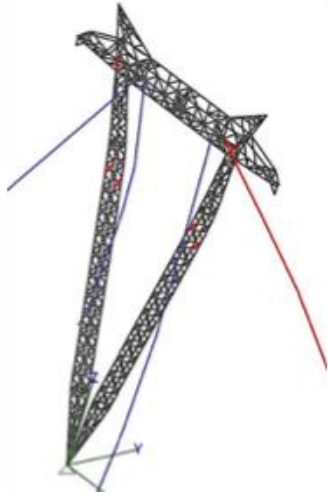
The critical tornado configuration is $R = 100$ m and $\theta = 165^\circ$ with the demand-to-capacity ratio, $\lambda = 11.4$. The failure of the tower is initiated at 10% of the full F2 tornado load in the main chord just below the cross-arm (Figure 2-8A). The progression of failure continues through the tower as shown in Figure 2-8B-I at 12.5%, 15%, 17.5%, 20%, 22.5%, 25%, 27.5%, and 30% respectively. The failure continues to propagate as shown until two plastic hinges are formed in the main chords at the highlighted members (Figure 2-8J) at 32.5% of the full F2 tornado load, which then results in losing the overall stability of the tower at 37.5% of the full F2 tornado load (Figure 2-8K-L). The tower failed at 43 m/s which represents 61% of the maximum resultant wind speed of the full F2 tornado.



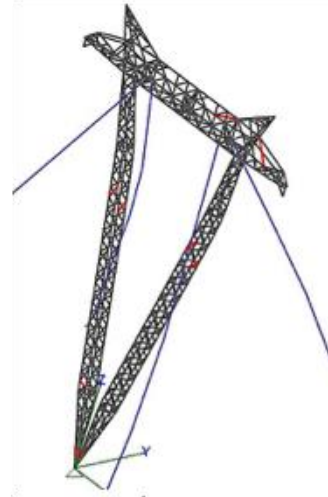
E.



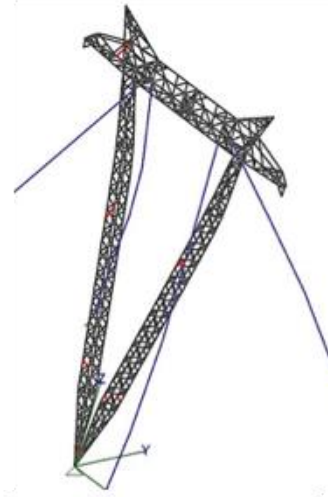
F.



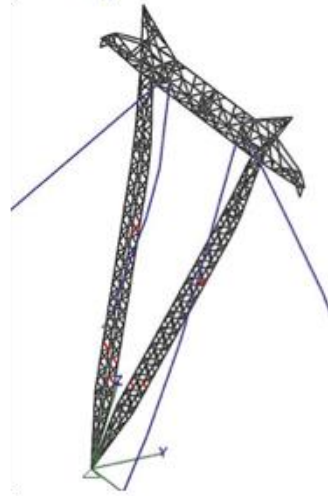
G.



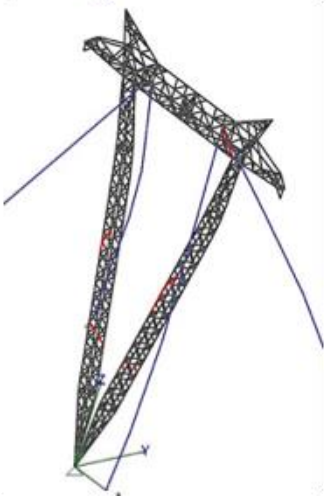
H.



I.



J.



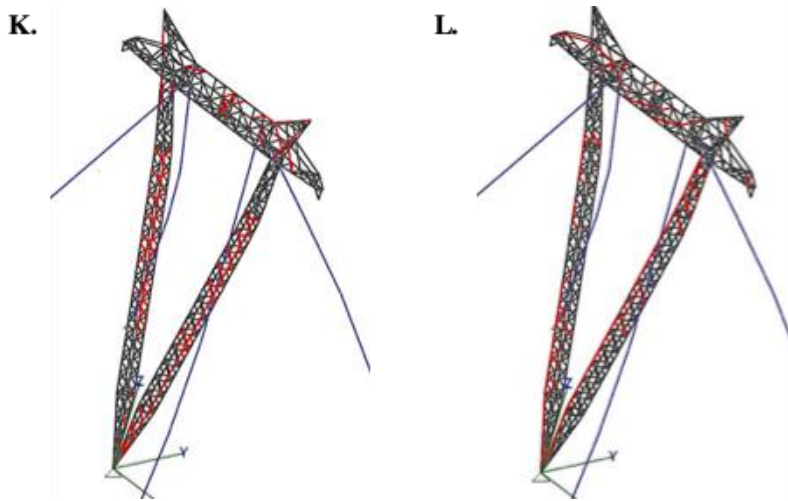


Figure 2-8: Progressive failure of G2 tower. (A) 10%; (B) 12.5%; (C) 15%; (D) 17.5%; (E) 20%; (F) 22.5%; (G) 25%; (H) 27.5%; (I) 30%; (J) 32.5%; (K) 35%; and (L) 37.5%.

2.4.2.3 The failure mode for S1 under Hangan's tornado wind field

The critical tornado configuration is $R = 160$ m and $\theta = 75^\circ$ with the demand-to-capacity ratio, $\lambda = 12.6$. The failure of the tower is initiated at 7.5% of the full F2 tornado load in the highlighted members shown in Figure 2-9A. The failure continues to propagate until a plastic hinge is formed at the outlined area shown in blue at 20% of the full F2 tornado load (Figure 2-9B). This leads to the loss of the overall stability of the tower at 22.5% of the full F2 tornado load. The tower fails at a tornado wind speed of 33.3 m/s which represents 47% of the maximum resultant wind speed of the full F2 tornado.

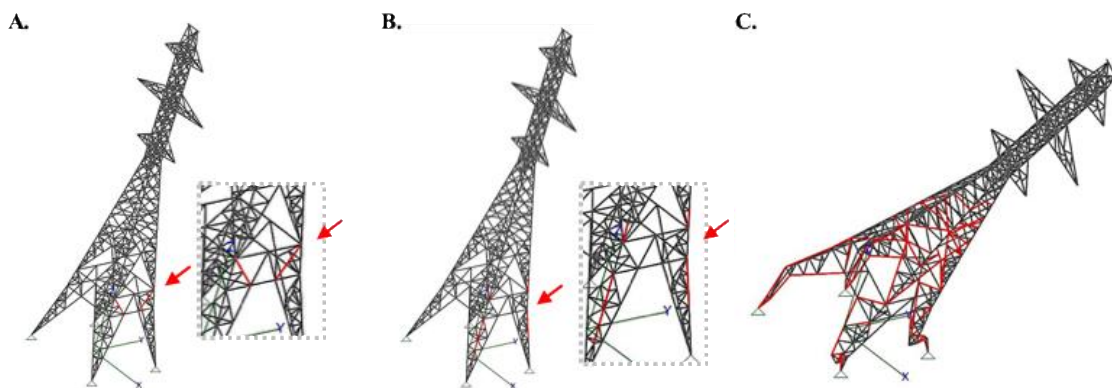


Figure 2-9: Progressive failure of S1 tower. (A) 7.5%; (B) 20%; and (C) 22.5%.

2.4.2.4 The failure mode for S2 under Hangan's tornado wind field

The critical tornado configuration is $R = 120$ m and $\theta = 225^\circ$. The failure of the tower is triggered at 10% of the full F2 tornado load in the highlighted members shown in Figure 2-10A. The progression of failure continues through the tower as shown in Figure 2-10B-D at 17.5%, 40%, 42.5% respectively. The failure continues to progress until a formation of a plastic hinge occurs at the outlined area shown in blue at 45% of the full F2 tornado load (Figure 2-10E), which corresponds to the failure of the tower.

To investigate the reason behind the failure of the tower at a relatively lower load compared to the full tornado wind load, the tower was subjected to a constant wind profile. This allowed the determination of the failure wind speed. The analysis revealed that the tower fails at a tornado wind speed of 30 m/s, which is less than the maximum F2 tornado wind speed of 70 m/s.

According to the followed methodology of analysis, the critical scenario is determined based on the highest demand-to-capacity ratio, $\lambda = 11$, in the first scenario. At this critical failure scenario, the tower collapsed at 45% of the full tornado load. However, the fourth critical scenario ($R = 120$ m and $\theta = 285^\circ$), which has a peak demand-to-capacity ratio of $\lambda = 9.4$, failed at 42.5% of the full tornado load. Hence, this is evidence that the fourth scenario is more critical compared to the first scenario. The progressive failure in the fourth scenario is shown in Figure 2-11. The failure of the tower is triggered at 10% of the full F2 tornado load in the highlighted members shown in Figure 2-11A. The progression of failure continues through the tower as shown in Figure 2-11B-D at 12.5%, 17.5%, and 32.5% respectively. The formation of the plastic hinge is triggered after the failure of the main chord member highlighted in Figure 2-11E at 40% of the full F2 tornado load. This ultimately leads to the failure of the tower at 42.5% of the full tornado load (Figure 2-11F). The tower fails at a tornado wind speed of 45.8 m/s which represents 65% of the maximum resultant wind speed of the full F2 tornado.

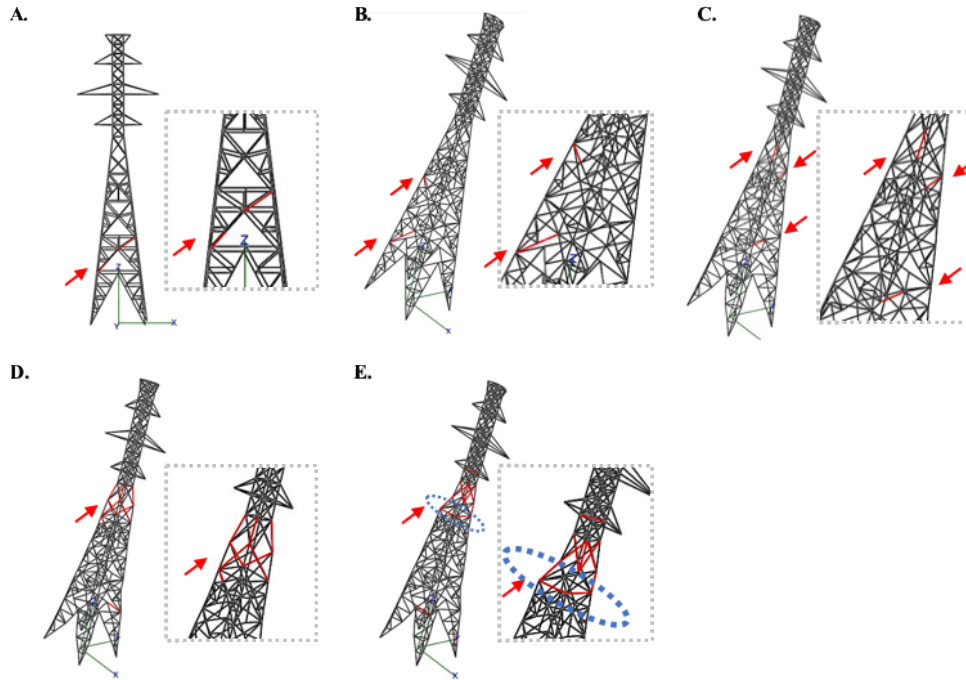


Figure 2-10: Progressive failure of S2 tower in first critical scenario, $\lambda = 11$. (A) 10%; (B) 17.5%; (C) 40%; (D) 42.5%; and (E) 45%.

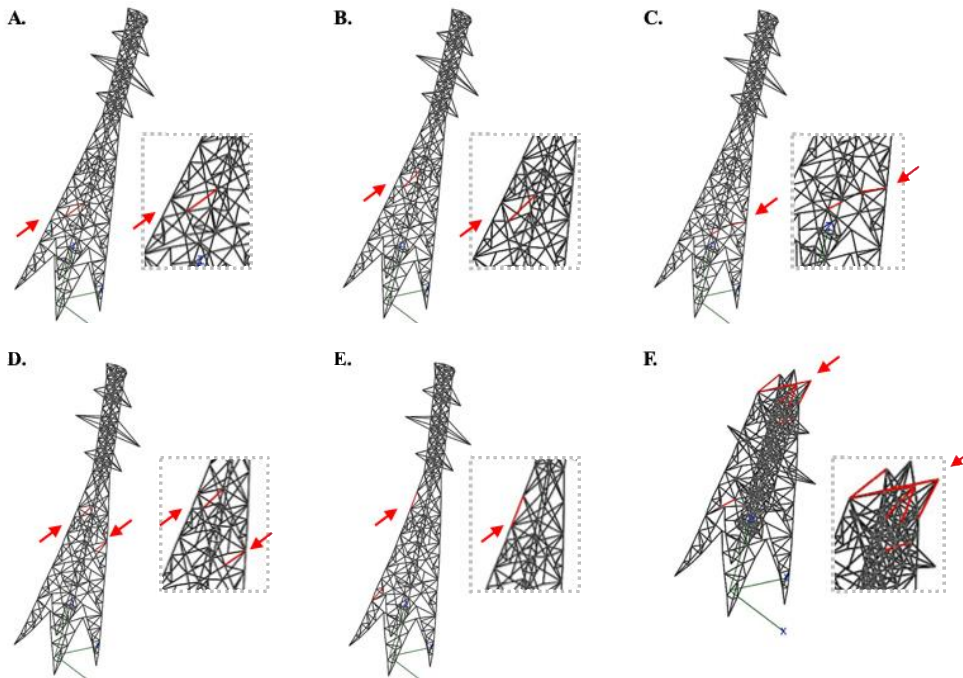
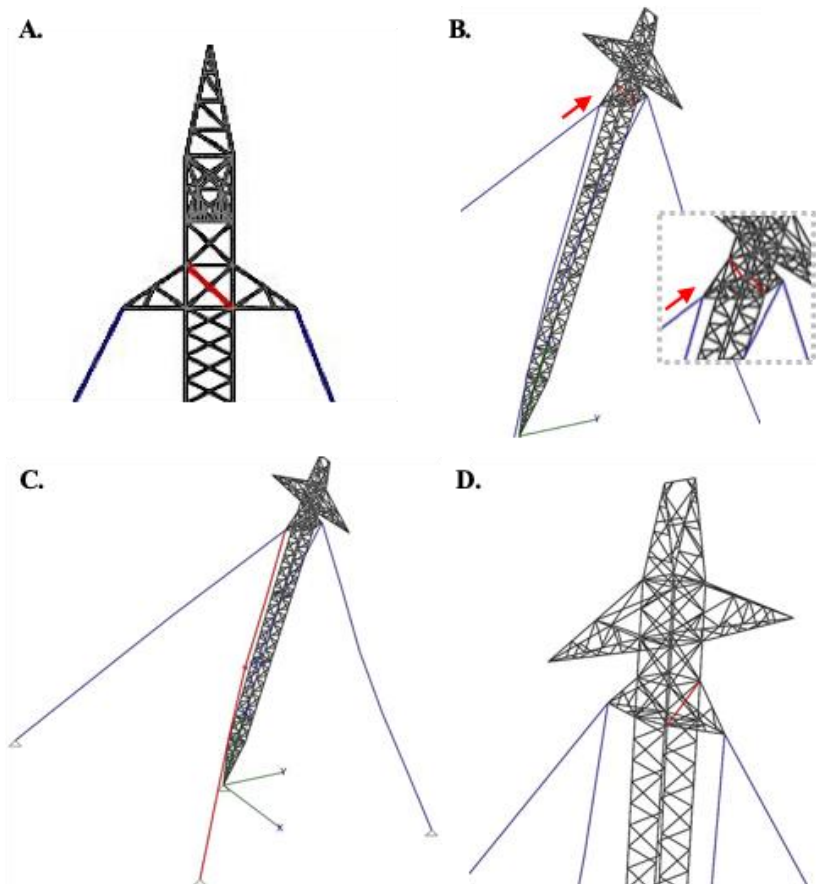


Figure 2-11: Progressive failure of S2 tower in the fourth critical scenario, $\lambda = 9.4$. (A) 10%; (B) 12.5%; (C) 17.5%; (D) 32.5%; (E) 40%; and (F) 42.5%.

2.4.2.5 The failure mode for G1 under the Stockton 2005 tornado

The critical tornado configuration is $R = 200$ m and $\theta = 0^\circ$ with a maximum demand-to-capacity ratio, $\lambda = 4.7$. At 25% of the full F2 tornado load, failure starts in the diagonal member of the guy's cross-arms (Figure 2-12A, B). Then at 30% of the full F2 tornado load, the resultant of the horizontal components of the tornado will cause slacking of guy 2 (Figure 2-12C). The progression of failure continues through the tower at 50% (Figure 2-12D), 60% (Figure 2-12E, F showed from different angles of view), and 62.5% (Figure 2-12G, H showed from different angles of view). The failure propagates until 65% of the tornado load, where a plastic hinge is formed in the main chord (Figure 2-12I) followed by the overall collapse of the tower at 67.5% (Figure 2-12J). The tower fails at a tornado wind speed of 57.5 m/s which represents 82% of the maximum resultant wind speed of the full F2 tornado.



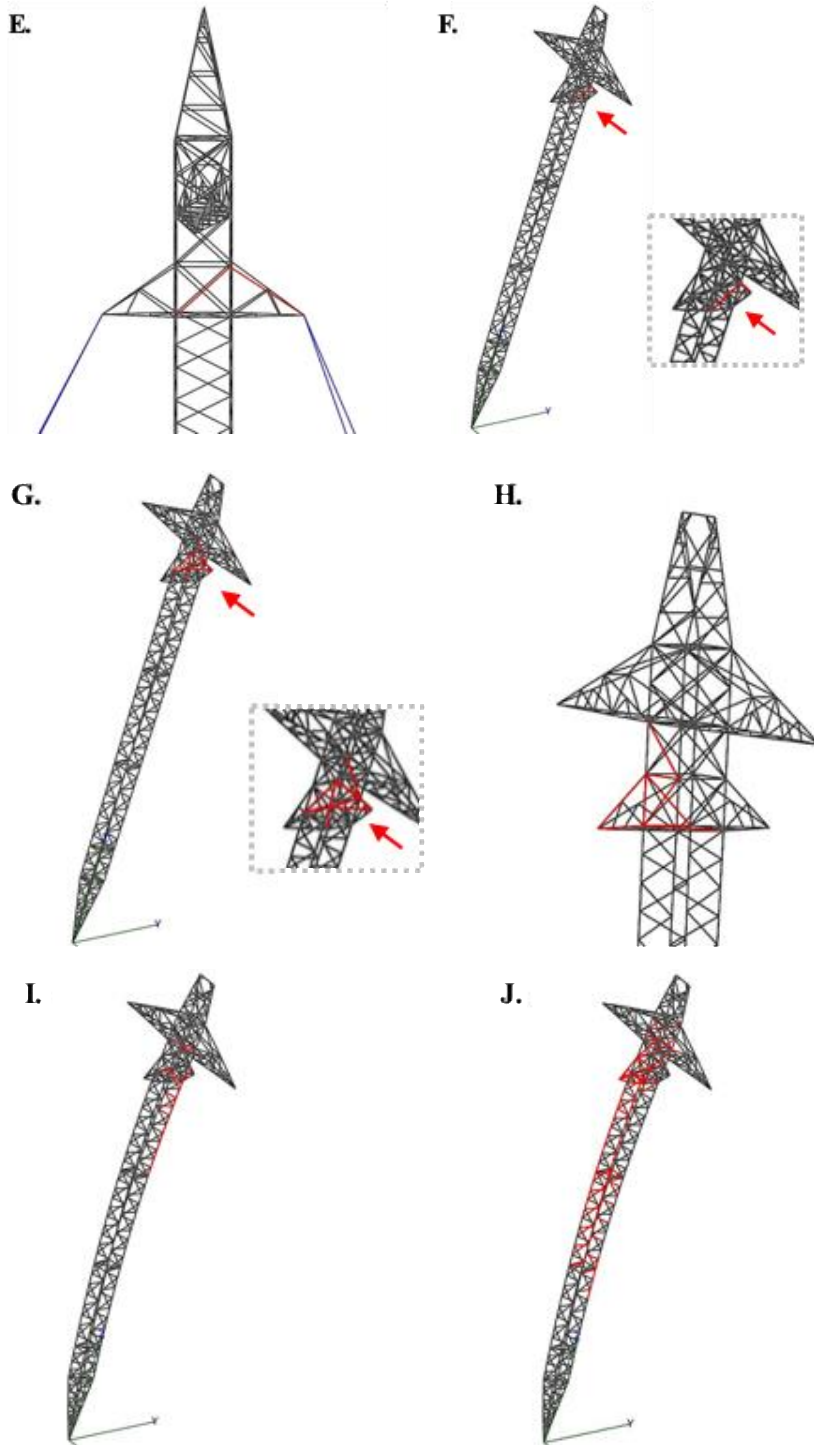
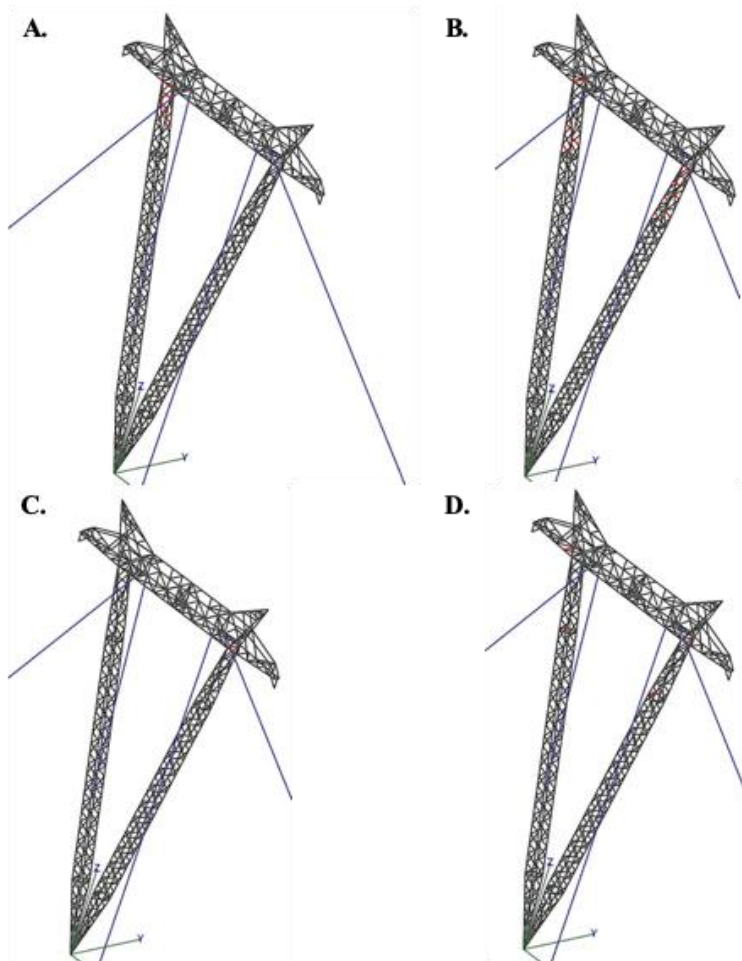
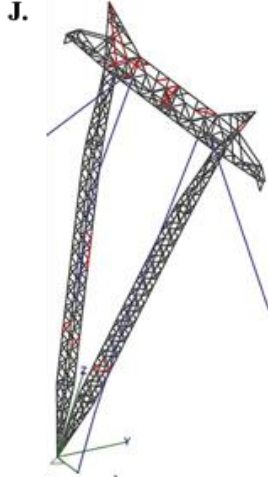
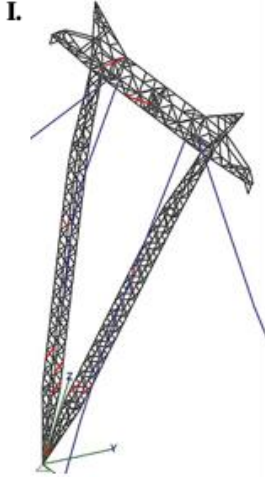
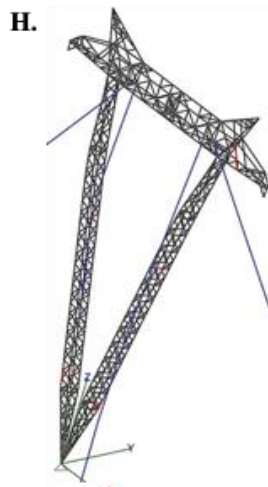
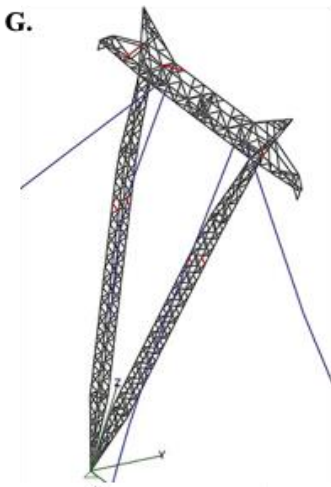
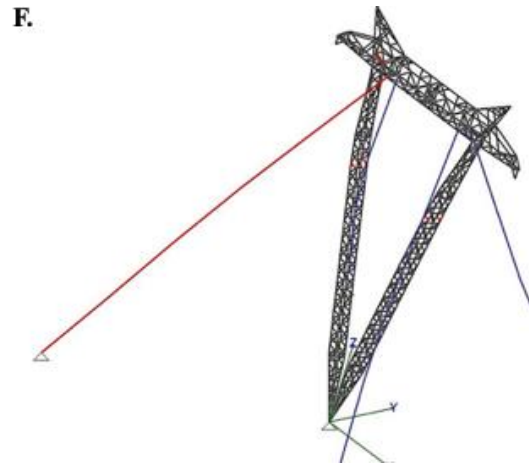
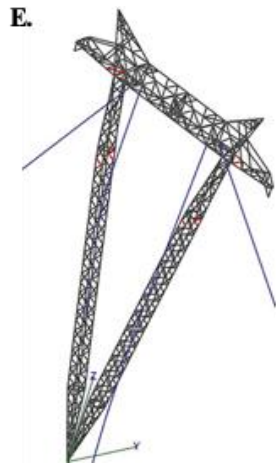


Figure 2-12: Progressive failure of G1 tower in the first scenario. (A, B) 25%; (C) 30%; (D) 50%; (E,F) 60%; (G,H) 62.5%; (I) 65%; and (J) 67.5%.

2.4.2.6 The failure mode for G2 under the Stockton 2005 tornado

The critical tornado configuration is $R = 180$ m and $\theta = 0^\circ$ with a maximum demand-to-capacity ratio, $\lambda = 11.5$. At 10% of the full F2 tornado load, failure starts in the main chord member below the guy's cross-arms (Figure 2-13A). The progression of failure continues through the tower as shown in Figure 2-13 B-J at 12.5%, 15%, 17.5%, 20%, 22.5%, 25%, 27.5%, 30%, and 32.5% respectively where a plastic hinge is formed at the highlighted location of the main chord of the left shaft. It is then followed by the formation of another plastic hinge, at 35% of the full load, in the second main chord of the right shaft at the highlighted position (Figure 2-13K) which leads to the failure of the structure at 37.5% of the full F2 tornado load (Figure 2-13L).





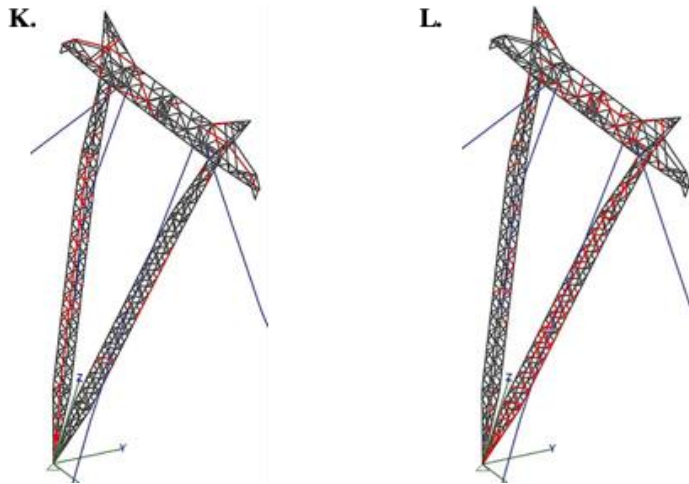
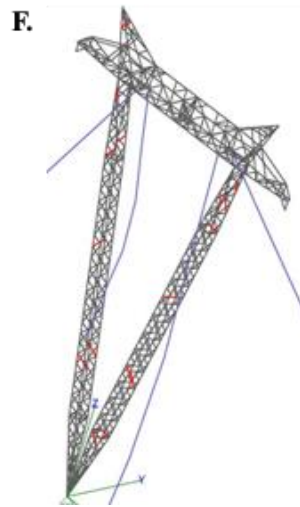
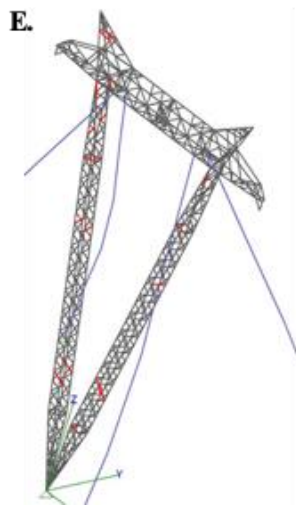
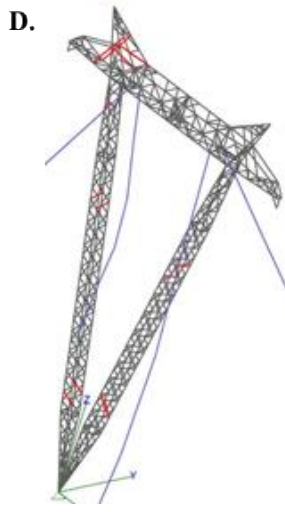
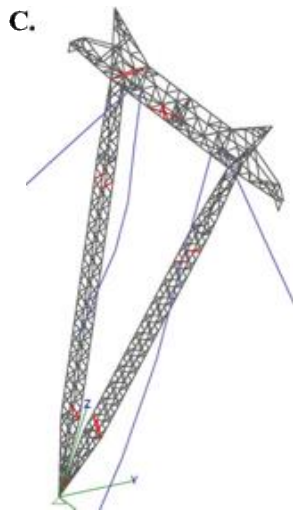
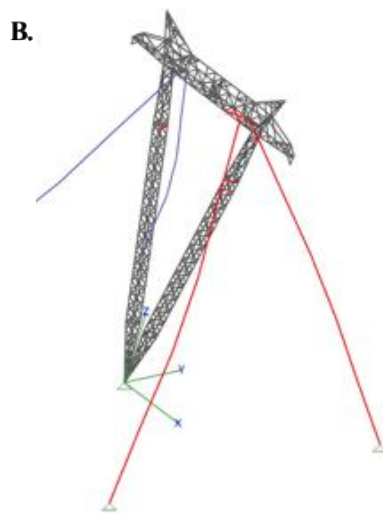
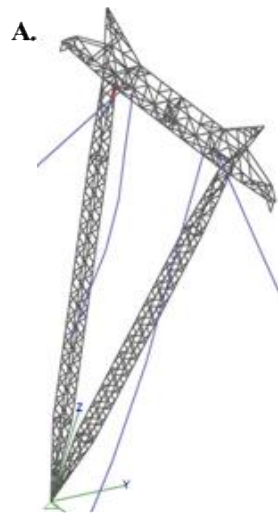


Figure 2-13: Progressive failure of G2 tower in the first scenario. (A) 10%; (B) 12.5%; (C) 15%; (D) 17.5%; (E) 20%; (F) 22.5%; (G) 25%; (H) 27.5%; (I) 30%; (J) 32.5%; (K) 35%; and (L) 37.5%.

In the first critical failure scenario, where the highest demand-to-capacity ratio, $\lambda = 11.5$, the tower collapsed at 37.5% of the full tornado load. However, the fourth critical scenario ($R = 200$ m and $\theta = 75^\circ$), which has a peak demand-to-capacity ratio of $\lambda = 7.5$, failed at 32.5% of the full tornado load. This provides evidence that the fourth critical scenario is more critical. The progressive failure in the fourth scenario is shown in Figure 2-14. The failure is initiated by the slacking of the guy at 17.5% of the full F2 tornado load (Figure 2-14B). The progression of the failure stages in the tower is shown in Figure 2-14C-G at 20%, 22.5%, 25%, 27.5%, and 30% respectively until overall collapse occurs at 32.5% (Figure 2-14H). The tower fails at a tornado wind speed of 40 m/s which represents 57% of the maximum resultant wind speed of the full F2 tornado.



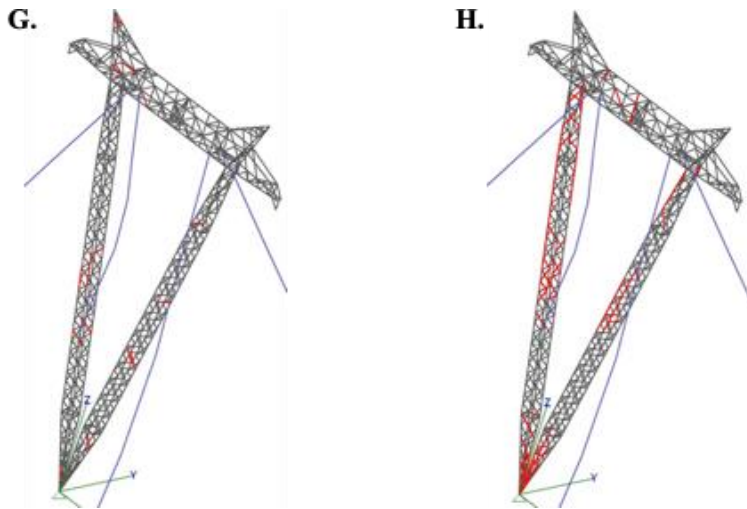
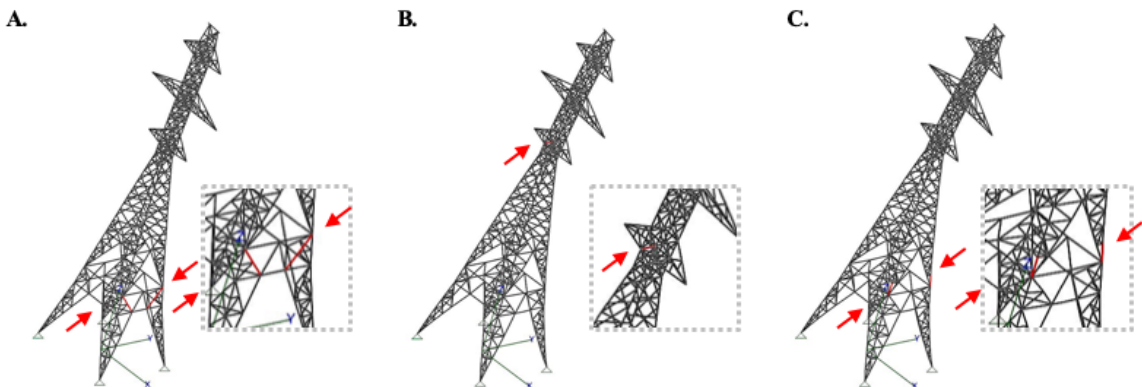


Figure 2-14: Progressive failure of G2 tower in the fourth scenario. (A) 15%; (B) 17.5%; (C) 20%; (D) 22.5%; (E) 25%; (F) 27.5%; (G) 30%; and (H) 32.5%.

2.4.2.7 The failure mode for S1 under the Stockton 2005 tornado

The critical tornado configuration is $R = 220$ m and $\theta = 75^\circ$ with a maximum demand-to-capacity ratio, $\lambda = 14.0$. The stages of failure are shown in Figure 2-15A-D at 7.5%, 15%, 17.5%, and 20%, respectively where a plastic hinge is formed as highlighted in Figure 2-15D which is then followed by the overall collapse at 22.5% of the full F2 tornado load (Figure 2-15F). The tower fails at a tornado wind speed of 33.3 m/s which represents 47% of the maximum resultant wind speed of the full F2 tornado.



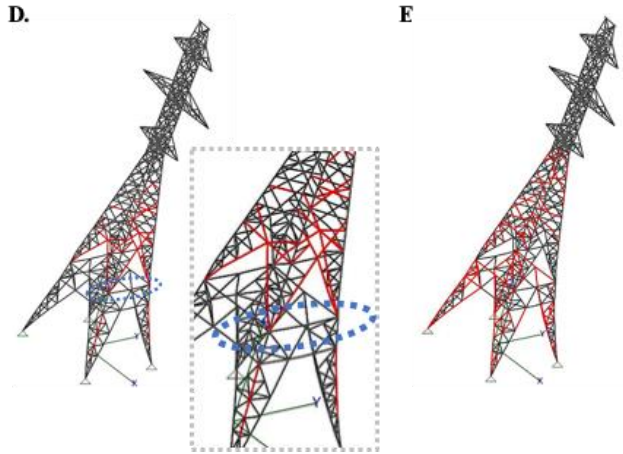


Figure 2-15: Progressive failure of S1 tower in the first scenario. (A) 7.5%; (B) 15%; (C) 17.5%; (D) 20%; and (E) 22.5%.

2.4.2.8 The failure mode for S2 under the Stockton 2005 tornado

The critical tornado configuration is $R = 200$ m and $\theta = 30^\circ$ with a maximum demand-to-capacity ratio, $\lambda = 11$. The stages of failure are shown in Figure 2-16A-G at 10%, 12.5%, 15%, 32.5%, 35%, 37.5%, and 40%, respectively. The plastic hinge is formed at 35% of the full F2 tornado load (Figure 2-16E).

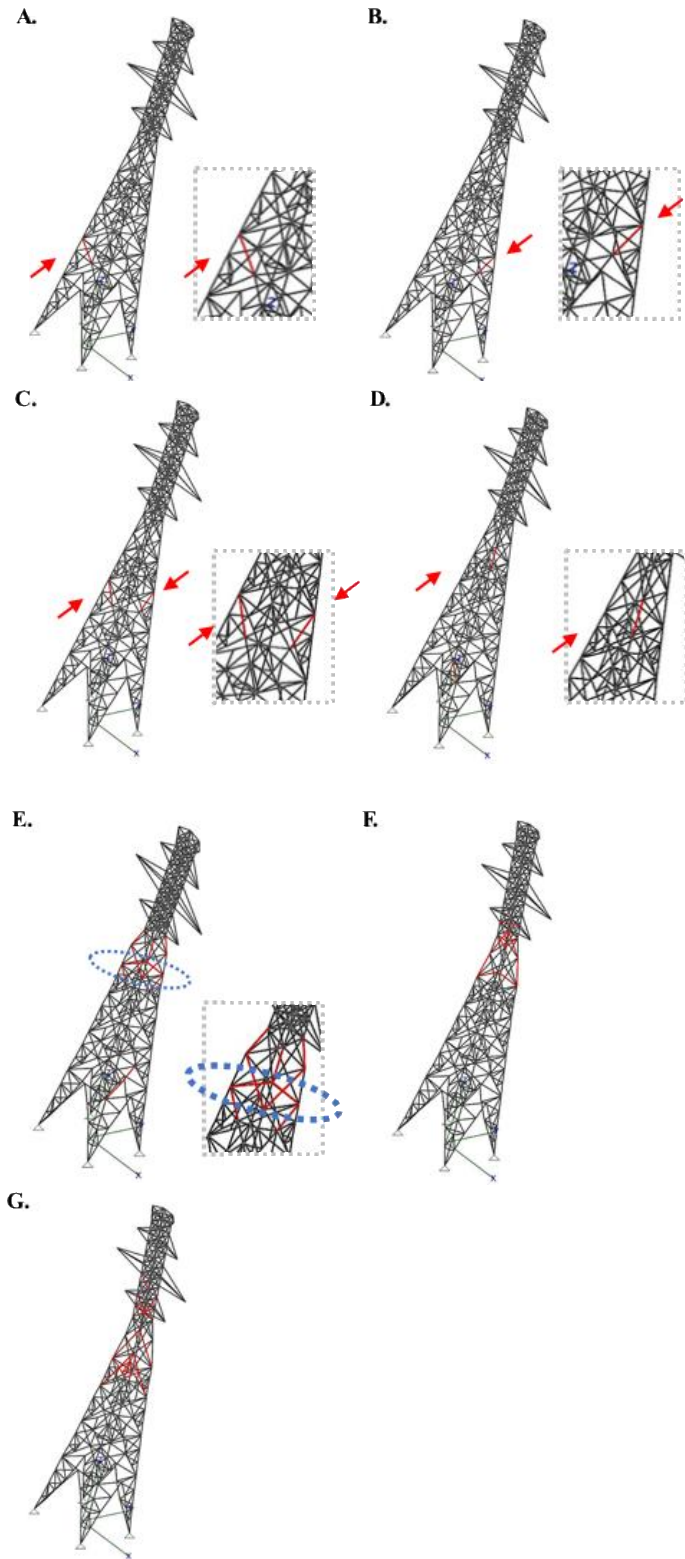


Figure 2-16: Progressive failure of S2 tower in the first scenario. (A) 10%; (B) 12.5%; (C) 15%; (D) 32.5%; (E) 35%; (F) 37.5%; and (G) 40%.

In the first critical failure scenario, where the highest demand-to-capacity ratio, $\lambda = 11$, the tower collapsed at 40% of the full tornado load. However, the second critical scenario ($R = 260$ m and $\theta = 75^\circ$), which has a peak demand-to-capacity ratio of $\lambda = 10.5$, failed at 35% of the full tornado load. This provides evidence that the second critical scenario is more critical. The progression of failure in the second scenario is shown in Figure 2-17A-H at 10% - 35%, where the plastic hinge is formed at 32.5%. The tower fails at a tornado wind speed of 41.5 m/s which represents 59% of the full F2 tornado wind speed.

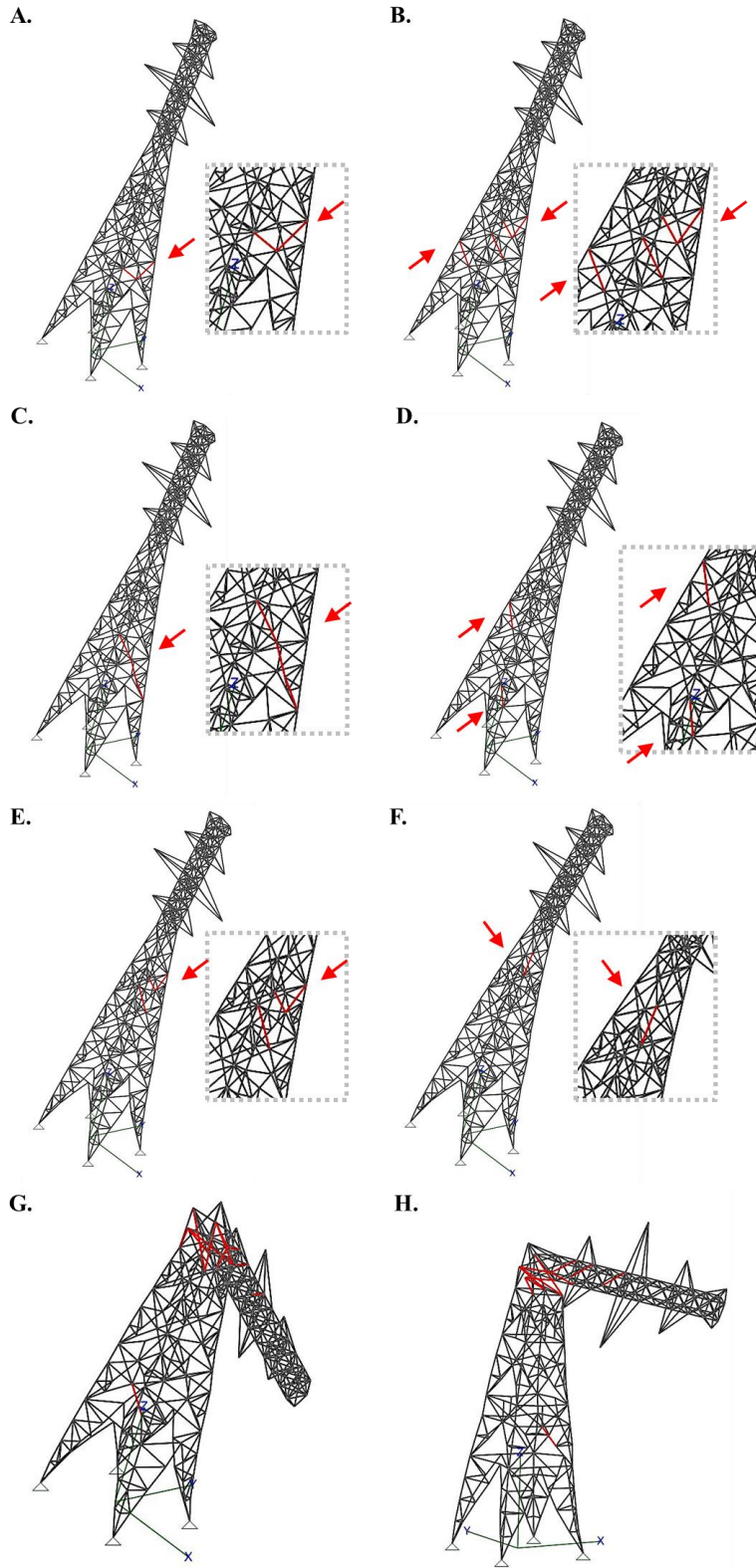


Figure 2-17: Progressive failure of S2 tower in the second scenario. (A) 10%; (B) 12.5%; (C) 15%; (D) 22.5%; (E) 25%; (F) 32.5%; and (G,H) 35%.

2.4.2.9 Summary of the Progressive Failure Analysis Results

Table 2-4 summarizes the results of the progressive failure analysis presented in Sections 2.4.2.1 - 2.4.2.8. The critical configuration, as well as the highlights of the failure progression, are presented for each of the studied towers under Hangan's [2] and Stockton [22] tornado wind fields.

Table 2-4: Summary of the progressive failure analysis results.

Tower		Hangan's tornado wind field [2]	Stockton 2005 tornado [22]
G1	Most critical configuration	R = 120 m $\theta = 165^\circ$	R = 200 m $\theta = 0^\circ$
	Demand-to-capacity ratio (λ)	4.3	4.7
	Failure Initiation (% of F2 tornado load)	25%	25%
	Load at Plastic hinge formation	67.5% of the full F2 tornado load	65% of the full F2 tornado load
	Failure Load (% of F2 tornado load)	70%	67.5%
	Failure wind speed	58.6 m/s	57.5 m/s
	Failure wind speed (% of F2 tornado wind speed)	84%	82%
G2	Most critical configuration	R = 100 m $\theta = 165^\circ$	R = 200 m $\theta = 75^\circ$ (fourth scenario)
	Demand-to-capacity ratio (λ)	11.4	7.5
	Failure Initiation (% of F2 tornado load)	10%	17.5%
	Load at Plastic hinge formation	32.5% of the full F2 tornado load	30% of the full F2 tornado load
	Failure Load (% of F2 tornado load)	37.5%	32.5%
	Failure wind speed	43m/s	40m/s

	Failure wind speed (% of F2 tornado wind speed)	61%	57%
S1	Most critical configuration	R = 160 m $\theta = 75^\circ$	R = 220 m $\theta = 75^\circ$
	Demand-to-capacity ratio (λ)	12.6	14.0
	Failure Initiation (% of F2 tornado load)	7.5%	7.5%
	Load at Plastic hinge formation	20% of the full F2 tornado load	20% of the full F2 tornado load
	Failure Load (% of F2 tornado load)	22.5%	22.5%
	Failure wind speed	33.3m/s	33.3m/s
	Failure wind speed (% of F2 tornado wind speed)	47%	47%
S2	Most critical configuration	R = 120 m $\theta = 285^\circ$ (fourth scenario)	R = 260 m $\theta = 75^\circ$ (second scenario)
	Demand-to-capacity ratio (λ)	9.4	10.5
	Failure Initiation (% of F2 tornado load)	10%	10%
	Load at Plastic hinge formation	40% of the full F2 tornado load	32.5% of the full F2 tornado load
	Failure Load (% of F2 tornado load)	42.5%	35%
	Failure wind speed	45.8 m/s	41.5 m/s
	Failure wind speed (% of F2 tornado wind speed)	65%	59%

As shown in Table 2-4, all the towers fail at smaller failure loads under Stockton tornado compared to the failure loads under Hangan's tornado. This indicates that the Stockton tornado wind field is more critical than Hangan's tornado even though both tornado wind fields are scaled so that they have the same resultant horizontal wind speeds. This can be interpreted by comparing the vertical profiles of both tornado wind fields provided in

Figure 2-1, where the peak tangential velocity for Stockton tornado is nearly uniform across the height of the tower. This causes more loads on the members of the tower under Stockton tornado compared to Hangan's tornado.

2.5 Strengthening of Towers

Failure of TLs causes detrimental economic losses and societal damages. To minimize these losses, the towers need to sustain F2 tornado loads. After investigating the progressive failure of the towers, several steps are taken to strengthen the failed towers (Figure 2-18). These steps can be summarized as follows: i) a parametric study of the towers is conducted to determine the critical configuration, ii) considering the critical configurations obtained from step i) a non-linear incremental analysis is conducted to identify the failed member of the tower. A failed member is identified when the demand-to-capacity ratio, λ , exceeds 1, iii) Members with demand/capacity ratio greater than 1.0 are then replaced with larger size members to strengthen the tower, and the analysis is repeated (steps i) to iii)) until the tower can withstand the full F2 tornado load in all the possible configurations. The resulting tower's percentage of added weight is then calculated. It is worth mentioning that symmetry is maintained during the strengthening process as TL towers are symmetrical structures. G1 and S2 towers are investigated as a sample from each system. Nine iterations of strengthening were attempted until the G1 tower could sustain the full F2 tornado load. On the other hand, 19 iterations were attempted until S2 tower could sustain the full F2 tornado wind load.

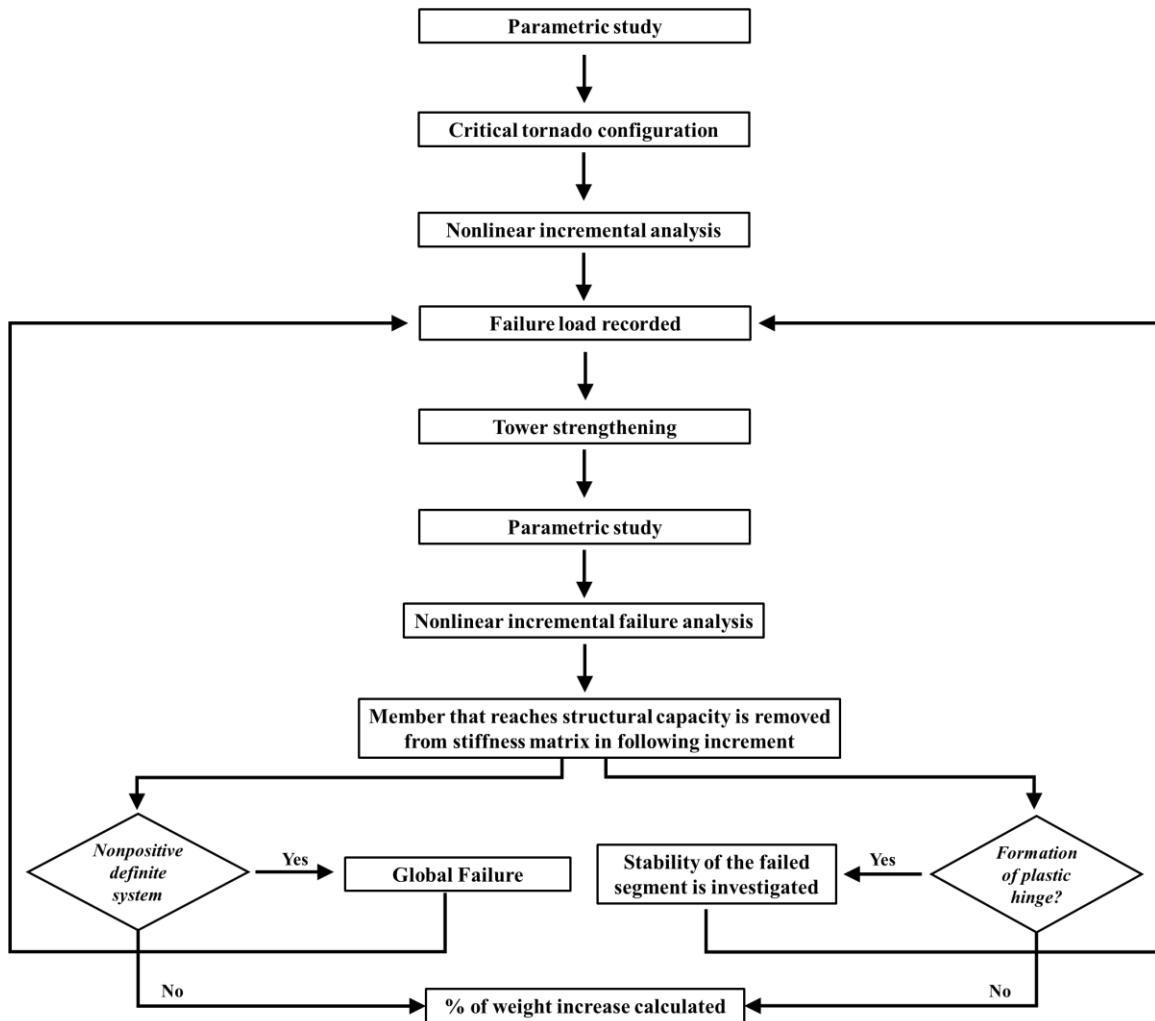


Figure 2-18: Flow chart describing the tower strengthening procedure.

It is concluded that for the towers to withstand a full load of an F2 tornado, the G1 tower needs an additional weight of 5.6%, while S2 tower requires 65%. The huge difference between the aforementioned percentages can be interpreted by the fact that the investigated self-supported towers are supporting six conductors and two ground wires, while the guyed towers are supporting two conductors and one ground wire. Hence, the effect of unbalanced load on the self-supported towers due to tornadoes is higher than that of the guyed towers.

The sequence of strengthening G1 tower is presented as a sample for the results. After four attempts of strengthening, where 125 tower members, mainly the main chord and the guys' cross-arm members, are strengthened. The increase in the members' sizes can be

represented by an additional 2.9% of the tower's original weight. Although the failure is initiated in the guys' cross arms similar to the location of the initiation of the failure before strengthening, the failure is initiated at 42.5% of the full F2 tornado wind load instead of being initiated at 25% before strengthening. Figure 2-19A shows the formation of the plastic hinge, at 72.5% of the full F2 tornado load, located at the lower zone of the tower. The failure propagates until failure of the tower at 80% of the full F2 tornado load. The tower fails at a tornado wind speed of 62.8 m/s which represents 89.4% of the full F2 tornado wind speed. The failure loads recorded throughout the nine attempts are summarized in Table 2-5.

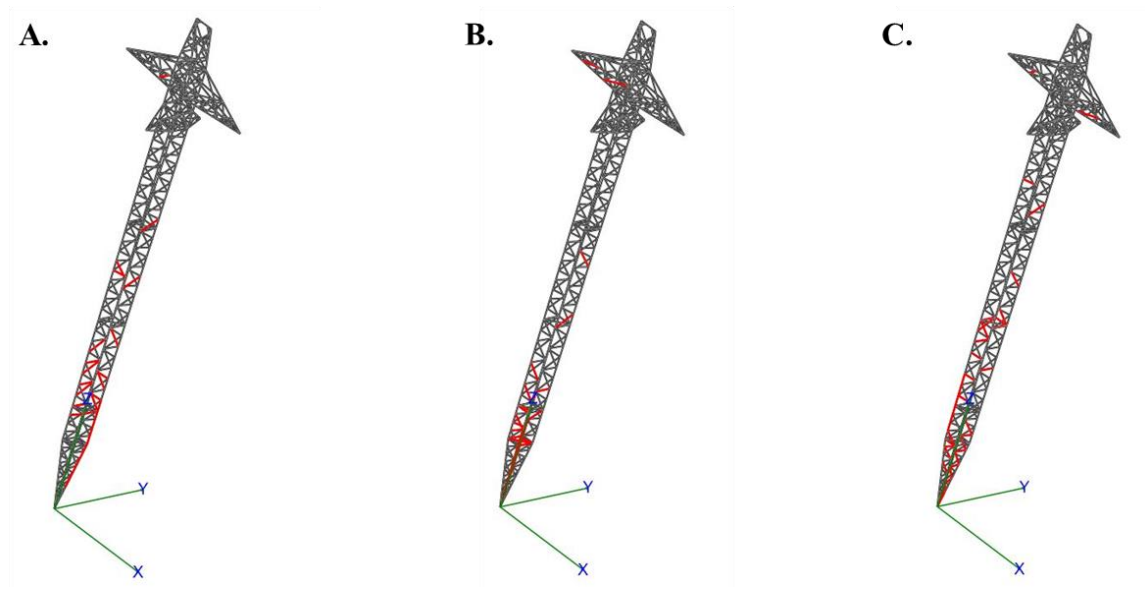


Figure 2-19: Progressive failure of G1 tower after attempting four iterations of strengthening. (A) 72.5%; (B) 75%; (C) 77.5%.

Table 2-5: Summary of the strengthening attempts for G1 tower.

	Before strengthening	Fourth attempt	Ninth attempt
Number of strengthened members	0	125	145
Most critical configuration	R = 120 m $\theta = 165^\circ$	R = 120 m $\theta = 255^\circ$	R = 120 m $\theta = 255^\circ$
Demand-to-capacity ratio (λ)	4.3	2.0	1.9
Failure Initiation (% of F2 tornado load)	25%	42.5%	55%
Load at Plastic hinge formation	67.5% of the full F2 tornado load	75% of the full F2 tornado load	N/A
Failure Load (% of F2 tornado load)	70%	80%	N/A
Failure wind speed	58.6 m/s	62.8 m/s	N/A
Failure wind speed (% of F2 tornado wind speed)	84%	89.4%	N/A

For S1 tower, the 19 strengthening attempts can be represented by the following gradual increase in the tower weight: 1.8%, 4.57%, 9.38%, 10 %, 16.5%, 19%, 22.9%, 27.2%, 28.8%, 31.1%, 31.6%, 33.4%, 35.1%, 38.3%, 39.5%, 41%, 50.1%, 55%, and 65.3%, respectively. The attempts lead to a reduction in the peak demand-to-capacity ratio (λ) from 11 to 1.3.

Additionally, the differences in the highest demand-to-capacity ratio, λ , recorded in the parametric study for each tower before and after the strengthening of the towers are shown in Table 2-6.

Table 2-6: Comparison between the highest capacity ratio, λ , before and after strengthening of the transmission line towers.

Tower	% of weight added	Highest demand-to-capacity ratio, λ, before strengthening	Highest demand-to-capacity ratio, λ, after strengthening
G1	5.6	4.3	1.9
S2	65	11	1.3

2.6 Conclusion

In the current study, a non-linear finite element analysis integrated with CFD models has been utilized to investigate the progressive failure of two guyed and two self-supported TL towers under two different tornado wind fields.

An extensive parametric study is conducted to identify the critical tornado configurations by varying the location of the tornado relative to the studied tower. Considering the identified critical configurations, progressive failure analysis is conducted for four different towers designed and constructed following current code provisions to resist synoptic normal wind loading.

The results of the parametric study, as well as the progressive failure analysis, are reported for each tower. The results include the critical configuration of the tornado with respect to the structure, associated failure load, and a description of the failure mode. The study is then repeated to investigate the difference in the progression of failure in the TL towers under a different tornado wind field. The study demonstrates that none of the investigated towers can sustain the full load produced by the various F2 tornado wind fields. The results also indicate that Hangan's tornado wind field is less critical than the Stockton tornado wind field although both tornado wind fields are scaled so that they have equal horizontal resultant wind speeds.

Moreover, the strengthening of the guyed and self-supported TL towers is also investigated to assess cost implications associated with designing TLs that can sustain F2 tornadoes. The progressive failure analysis results are used as an input for the strengthening study. The iterative procedure of strengthening outlined in the study shows that the guyed tower requires an additional 5.6% of its own weight in order to sustain a full load of an F2 tornado, while the self-supported tower needs 65% additional weight increase. This concludes that the investigated guyed towers that are designed as per current code provisions are found to be more resilient to F2 tornadoes and require less strengthening to sustain the full F2 tornado.

2.7 References

- [1] H. B. Ishac, M.F.; White, “Effect of tornado loads on transmission lines,” in *IEEE Transactions on Power Delivery*, 1995, p. Volume: 10; Issue: 1; pages: 445-451.
- [2] H. Hangan and J. D. Kim, “Swirl ratio effects on tornado vortices in relation to the Fujita scale,” *Wind Struct.*, vol. 11, pp. 291–302, Aug. 2008, doi: 10.12989/was.2008.11.4.291.
- [3] E. O. of the President, “White House 2013 - Grid Resiliency and Economic Benefit,” 2013.
- [4] T. T. Fujita, “Tornadoes and Downbursts in the Context of Generalized Planetary Scales,” *Journal of the Atmospheric Sciences*, vol. 38, no. 8. pp. 1511–1534, 1981, doi: 10.1175/1520-0469(1981)038<1511:TADITC>2.0.CO;2.
- [5] M. J. Newark, “Canadian tornadoes, 1950–1979,” *Atmos. - Ocean*, vol. 22, no. 3, pp. 343–353, 1984, doi: 10.1080/07055900.1984.9649203.
- [6] J. Sarkar, P., Haan, F., Gallus, Jr., W., Le, K. and Wurman, “Velocity measurements in a laboratory tornado simulator and their comparison with numerical and full-scale data,” in *37th Joint Meeting Panel on Wind and Seismic Effects*.
- [7] W. C. Lee and J. Wurman, “Diagnosed three-dimensional axisymmetric structure of the Mulhall tornado on 3 May 1999,” *J. Atmos. Sci.*, vol. 62, no. 7 II, pp. 2373–2393, 2005, doi: 10.1175/JAS3489.1.
- [8] C. A. Wan and C. C. Chang, “Measurement of the Velocity Field in a Simulated Tornado-Like Vortex Using a Three-Dimensional Velocity Probe,” *Journal of the Atmospheric Sciences*, vol. 29, no. 1. pp. 116–127, 1972, doi: 10.1175/1520-0469(1972)029<0116:motvfi>2.0.co;2.
- [9] N. B. Ward, “The exploration of certain features of tornado dynamics using a laboratory model,” *J. Atmos. Sci.*, vol. 29, pp. 1194–1204, 1972.
- [10] R. P. Davies-Jones, “The Dependence of Core Radius on Swirl Ratio in a Tornado Simulator,” *Journal of the Atmospheric Sciences*, vol. 30, no. 7. pp. 1427–1430,

- 1973, doi: 10.1175/1520-0469(1973)030<1427:tdocro>2.0.co;2.
- [11] C. R. Church, J. T. Snow, and E. M. Agee, “Tornado Vortex Simulation at Purdue University,” *Bull. Am. Meteorol. Soc.*, vol. 58, no. 9, pp. 900–908, 1977, doi: 10.1175/1520-0477(1977)058<0900:tvsapu>2.0.co;2.
- [12] E. M. Church, C. R., Snow, J. T., Baker, G. L. and Agee, “Characteristics of tornado-like vortices as a function of swirl ratio: A laboratory investigation,” *J. Atmos Sci.*, vol. 36, pp. 1755–1776, 1979.
- [13] G. L. Baker and C. R. Church, “Measurements of the core radii and peak velocities in modeled atmospheric vortices,” *J. Atmos. Sci.*, vol. 36, no. 12, Dec. 1979. pp. 2413–2424, 1979.
- [14] R. Rotunno, “A study in tornado like vortex dynamics,” *J. Atmos. Sci.*, vol. 36, no. 1, Jan.1979. pp. 140–155, 1979.
- [15] W. S. Lewellen, “A solution for three-dimensional vortex flows with strong circulation,” *J. Fluid Mech.*, vol. 14, no. 3, pp. 420–432, 1962, doi: 10.1017/S0022112062001330.
- [16] W. S. Lewellen, D. C. Lewellen, and R. I. Sykes, “Large-Eddy simulation of a tornado’s interaction with the surface,” *J. Atmos. Sci.*, vol. 54, no. 5, pp. 581–605, 1997, doi: 10.1175/1520-0469(1997)054<0581:LESOAT>2.0.CO;2.
- [17] D. C. Lewellen, W. S. Lewellen, and J. Xia, “The influence of a local swirl ratio on tornado intensification near the surface,” *J. Atmos. Sci.*, vol. 57, no. 4, pp. 527–544, 2000, doi: 10.1175/1520-0469(2000)057<0527:TIOALS>2.0.CO;2.
- [18] D. C. Lewellen and W. S. Lewellen, “Near-surface intensification of tornado vortices,” *J. Atmos. Sci.*, vol. 64, no. 7, pp. 2176–2194, 2007, doi: 10.1175/JAS3965.1.
- [19] J. Xia, W. S. Lewellen, and D. C. Lewellen, “Influence of Mach number on Tornado corner flow dynamics,” *J. Atmos. Sci.*, vol. 60, no. 22, pp. 2820–2825, 2003, doi: 10.1175/1520-0469(2003)060<2820:IOMNOT>2.0.CO;2.
- [20] R. P. Selvam and P. C. Millett, “Computer modeling of tornado forces on

- buildings,” *Wind Struct. An Int. J.*, vol. 6, no. 3, pp. 209–220, 2003, doi: 10.12989/was.2003.6.3.209.
- [21] A. Gairola and G. Bitsuamlak, “Numerical tornado modeling for common interpretation of experimental simulators,” *J. Wind Eng. Ind. Aerodyn.*, vol. 186, no. November 2017, pp. 32–48, 2019, doi: 10.1016/j.jweia.2018.12.013.
- [22] A. El Damatty, N. Ezami, and A. Hamada, “Case Study for Behaviour of Transmission Line Structures under Full-Scale Flow Field of Stockton, Kansas, 2005 Tornado,” in *Electrical Transmission and Substation Structures 2018*, 2018, pp. 257–268.
- [23] E. Savory, G. A. R. Parke, M. Zeinoddini, N. Toy, and P. Disney, “Modeling of tornado and microburst induced wind loading and failure of a lattice transmission tower,” vol. 23, pp. 365–375, 2001.
- [24] A. Y. Shehata, A. A. El Damatty, and E. Savory, “Finite element modeling of transmission line under downburst wind loading,” *Finite Elem. Anal. Des.*, vol. 42, no. 1, pp. 71–89, 2005, doi: 10.1016/j.finel.2005.05.005.
- [25] A. Y. Shehata and A. El Damatty, “Behaviour of guyed transmission line structures under downburst wind loading,” *Wind Struct.*, vol. 10, pp. 249–268, Jun. 2007, doi: 10.12989/was.2007.10.3.249.
- [26] A. Y. Shehata and A. El Damatty, “Failure analysis of a transmission tower during a microburst,” *Wind Struct.*, vol. 11, Jun. 2008, doi: 10.12989/was.2008.11.3.193.
- [27] A. Hamada, A. A. E. Damatty, H. Hangan, and A. Y. Shehata, “Finite element modelling of transmission line structures under tornado wind loading,” *Wind Struct. An Int. J.*, vol. 13, no. 5, pp. 451–469, 2010, doi: 10.12989/was.2010.13.5.451.
- [28] A. Hamada and A. A. El Damatty, “Behaviour of guyed transmission line structures under tornado wind loading,” *Comput. Struct.*, vol. 89, no. 11–12, pp. 986–1003, 2011, doi: 10.1016/j.compstruc.2011.01.015.
- [29] A. Hamada and A. El Damatty, “Failure analysis of guyed transmission lines

during F2 tornado event,” *Eng. Struct.*, vol. 85, Feb. 2015, doi: 10.1016/j.engstruct.2014.11.045.

- [30] F. Inc., “FLUENT 6.2 User’s Guide.” Lebanon, NH, 2005.
- [31] A. A. El Damatty and A. Hamada, “F2 tornado velocity profiles critical for transmission line structures,” *Eng. Struct.*, vol. 106, pp. 436–449, 2016, doi: 10.1016/j.engstruct.2015.10.020.
- [32] A. 74, *ASCE - 74*, Third ed., no. 74. Reston, Virginia: American Society of Civil Engineers, 2009.
- [33] H. Aboshosha and A. El Damatty, “Effective technique to analyze transmission line conductors under high intensity winds,” *Wind Struct. An Int. J.*, vol. 18, no. 3, pp. 235–252, 2014, doi: 10.12989/was.2014.18.3.235.
- [34] *Design of Latticed Steel Transmission Structures (10-15)*. American Society of Civil Engineers, 2015.

Chapter 3

3 Progressive Failure of Self-supported Transmission Line Towers under Different Tornado Wind Fields

3.1 Introduction

Transmission lines (TLs) are the main element in an electrical power network. Within a TL, there are two main elements: i) the conductors that transfer electricity; ii) the towers that support the conductors. Failure of TL towers results in power outages, which ultimately lead to social and economic consequences. Globally, the failure of TLs generally results from high-intensity wind (HIW) events, including downbursts and tornadoes [1, 2]. Annual economic loss can be up to \$33 billion for the 600+ power outages due to severe weather, as reported by the White House in Washington in 2013 [3]. Many previous studies available in the body of the literature, studied the behaviour of TLs under downbursts. However, the literature review in this paper will focus on tornadoes, which is the main scope of the current study.

Fujita defined tornadoes as “highly convergent swirling wind affecting a relative narrow path” [4]. In 1971, Fujita categorized tornadoes into seven categories according to the tornado wind speed and the related structural damage based on the damage surveys [5]. The Fujita-Pearson scale was introduced in 1973 [6] to categorize tornadoes into seven categories based on tornado wind speed, path length and width as shown in Table 3-1.

Southwestern Ontario in Canada experiences an F3 tornado every five years on average, and 92% of the tornadoes that cause TL failures are F2 or less on the Fujita scale [7].

Table 3-1: Ranges of wind speed, path length, and pathwidth from the Fujita-Pearson scales [6].

Scale	Fujita scale wind speed (mph)	Pearson path length (mile)	Pearson path width (yards)
0	40-72	0.3-0.9	6-17
1	73-112	1.0-3.1	18-55
2	113-157	3.2-9.9	56-175
3	158-506	10-31	176-556
4	207-260	32-99	0.-0.9 miles
5	261-318	100-315	1.0-3.1 miles
6	319-380	316-999	3.3-9.9 miles

Furthermore, tornadoes cause the most weather-related TL failure in Ontario Hydro due to the significant likelihood of a tornado touching down near a TL [1]. Although these statistics are alarming, only conventional boundary layer wind profiles are considered in practice manuals and design guidelines. The lack of consideration of HIW events, especially tornadoes, is problematic due to the various differences in the nature of these wind events. The differences include the locality of tornadoes, narrow path width, and wind profiles, which include a vertical velocity component. Therefore, to ensure that failure preventative measures are in place, tornado wind fields need to be investigated to understand the mechanisms of weather-related TL failures. Particularly, previous studies attempted to record field measurement data [8, 9] without being able to get measurements for the zone near the ground surface; this is of interest to structural engineers as it covers all structures. Research laboratory simulations that characterize tornado wind fields have been performed by numerous groups, including Sarkar et al. [8]; Wan and Chang [10]; Ward [11]; Davies-Jones [12]; Church et al. [13]; Church et al. [14]; Baker and Church [15]; and Rotunno [16], as well as numerical simulations conducted by Hangan and Kim [2]; Lewellen [17]; Lewellen et al. [18]; Lewellen et al. [19]; Lewellen and Lewellen [20]; Xia et al. [21]; Selvam and Millett [22]; Gairola and Bitsuamlak [23]; and El Damatty et al. [24].

In 1996, a microburst event led to the collapse of transmission towers in Winnipeg, Canada, that consequently led to starting an extensive research program examining the behaviour of TLs under HIW events at Western University. Failure of self-supported towers under tornadoes and downbursts was investigated by Savory et al. [25] with the limitation of not including the modelling of the conductors and the vertical velocity component of the tornado wind field. The efforts at Western University led to the development of an in-house software [26] that can predict and assess the TL behaviour [27] and failure analysis of transmission towers under downbursts [28]. The software uses six TL spans to properly estimate the stiffness of the system and the conductors' reactions when conducting parametric studies or failure analysis of TLs under HIW events as recommended by Shehata et al. [26]. This software was then expanded by Hamada et al. [29] to incorporate Computational Fluid Dynamics (CFD) simulations conducted by Hangan and Kim [2], to include a tornado wind field in the software. The developed software then played a crucial role in assessing the failure of TLs under tornadoes [29]. Subsequently, the model evolved further to include geometric nonlinearity of the tower members [30] to analyze two guyed transmission systems and its failure modes [31] under two critical tornado configurations previously identified from parametric studies [29, 30].

A previous study by Hamada and El Damatty [31] shows the progression of failure within single guyed TL towers under one tornado wind field, which does not address the knowledge gap of how failure propagates within TL systems. Observations from damage surveying, such as the one shown in Figure 3-1, show that towers may fail within the TL without causing the collapse of the entire TL in a domino effect. This triggered researchers to investigate the progressive failure of the TL as a unit composed of multiple TL towers and conductors. Shehata and El Damatty [32] extended the software to capture the incremental deformation and the post-failure geometry of the tower to be used in predicting the forces transmitted through the conductors to the adjacent towers within the line. This novel technique allows calculating the conductors' reactions using the extensible catenary approach developed by Shehata and El Damatty [33]. This is imperative for predicting how the failure of a TL tower within the unit will impact the adjacent towers.

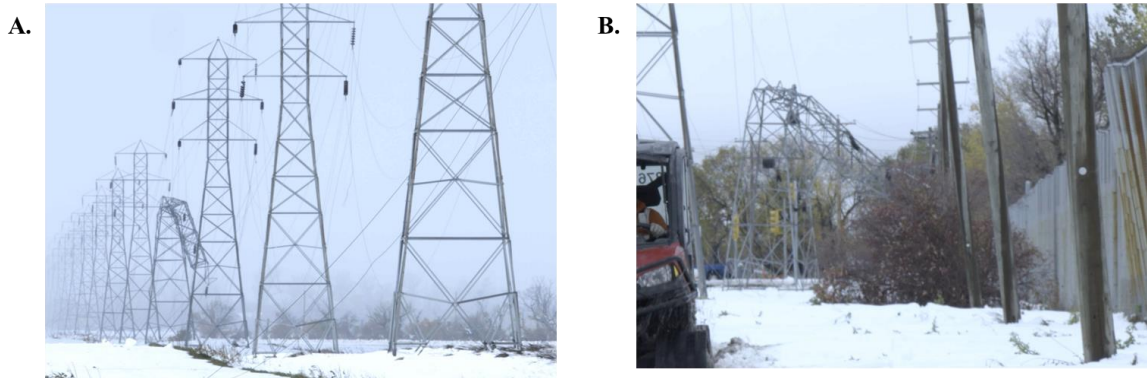


Figure 3-1: (A) Failure of one transmission line tower within the line. (B) Close-up image of a failed transmission line tower within a TL. “Manitoba Hydro, 2019”.

The current study builds on the findings of previous studies conducted by Hamada et al. [29] and Hamada and El Damatty [30, 31] as well as the findings of Shehata and El Damatty [32, 33]. Two tornado wind fields, obtained from CFD simulations conducted by Hangan and Kim [2] and El Damatty et al. [24], are incorporated in the fluid-structure program [32]. The program is then used to conduct a parametric study to identify the critical tornado configurations for the self-supported tower under each of the two tornado wind fields [2, 24] incorporated in this study.

To verify this extended version of the numerical model the critical tornado configurations for two guyed TLs are compared to those identified by Hamada and El Damatty [29, 30]. Accordingly, these critical tornado configurations are considered in a non-linear finite element analysis to identify failure modes of the investigated guyed towers and then compare them to those reported by Hamada and El Damatty [31].

After validating the numerical model, the program is used to examine the progression of failure of TL systems under F2 tornadoes. This study is considered the first of its kind to: i) conduct a progressive failure analysis for a self-supported TL unit, consisting of seven towers and eight spans, under different F2 tornado wind fields; ii) assess the performance of as-built towers, designed following current code provisions under the effect of normal wind, when exposed to different F2 tornado wind fields; iii) investigate the effect of components within the TL (insulator length) on the progressive failure of the TL; iv) conduct a parametric study to investigate the effect of changing the span length on the progressive failure of the TL.

3.2 Description of the Numerical Model

The current study presents the results of numerical simulations that incorporate different tornado wind fields into finite element models that simulate TL systems. The tornado wind fields are obtained from CFD simulations conducted by Hangan and Kim [2] and El Damatty et al. [24]. The description of each component of the numerical model is outlined in the following subsections.

3.2.1 Description of Tornado Wind Fields

Three velocity components: the tangential (V_{mt}), radial (V_{mr}), and axial (V_{ma}) represent the tornado wind fields. The velocity components are each presented as a function of the cylindrical coordinates, r , θ , z , measured from the center of the tornado.

To investigate the difference in the progressive failure of self-supported TL systems under different tornado wind fields, two different tornado wind fields are incorporated into the fluid-structure software.

The first tornado wind field is obtained from the findings of Hangan and Kim [2]. Hangan and Kim [2] conducted CFD simulations using the commercial software FLUENT [34] to simulate tornado wind fields. The maximum scaled-up velocities of the three velocity components for this wind field [35] are: the maximum tangential velocity is 78 m/s at radius, $r = 96$ m and height, $z = 19$ m; the maximum radial velocity is 49 m/s at the radius, $r = 146$ m and height, $z = 6$ m; the maximum axial velocity is 37 m/s at the radius, $r = 171$ m and height, $z = 127$ m.

The second tornado wind field is obtained from the findings of El Damatty et al. [24]. El Damatty et al. [24] conducted CFD simulation for the Stockton, Kansas, 2005 tornado [24] using the commercial software Star CCM+. The maximum velocity of the three velocity components are: the maximum tangential velocity is 53 m/s at radius, $r = 205$ m and height, $z = 60$ m; the maximum radial velocity is 14 m/s at radius, $r = 241$ m and height, $z = 158$ m; the maximum axial velocity is 32.9 m/s at radius, $r = 287$ m and height, $z = 269$ m.

The vertical profiles of the tangential velocity component for both tornado wind fields are shown in Figure 3-2.

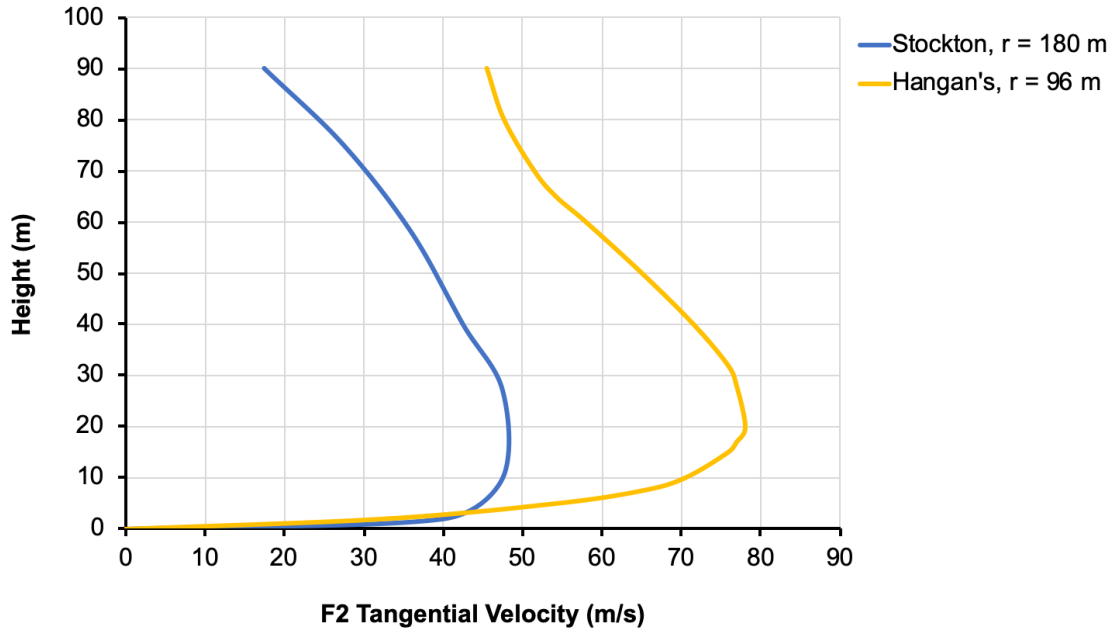


Figure 3-2: Vertical profiles of tangential velocity component of Stockton [24] and Hangan's [3, 30] tornado wind fields for radial distances, r , from tornado center.

The velocity components of the simulated wind fields are scaled. Specifically, the procedure scales the maximum resultant of the radial and tangential components to match the maximum wind speed for F2 tornadoes on the Fujita scale which is 70 m/s [36]. This allows predicting the members' demand-to-capacity ratios and comparing the progressive failure of the towers under different tornado wind fields.

3.2.2 Description of the Considered Towers

Self-supported TLs are the most common type of built TL systems. The self-supported tower's structural system can be simplified as a cantilever beam fixed at the base. A self-supported TL is considered in the current study as a sample to investigate the progressive failure of self-supported TLs under different F2 tornado wind fields. The examined self-supported TL system is shown in Figure 3-3 and labelled as SL.

The self-supported towers within SL are labelled S2. The towers support six conductors, which are connected to the towers through 2.438 m insulators, and two ground-wires. The

conductors and ground-wires have initial sag of 19.5 m and 14 m, respectively. The height of the S2 tower is 51.81 m. The physical parameters for conductors and ground-wires in SL are outlined in Table 3-2. The numbering of the towers within the TL is outlined in Figure 3-3, where the intermediate tower is referred to as Tower 1 or the Subject tower. The investigated towers are designed to resist synoptic wind with design wind speeds shown in Table 3-2. Figure 3-4 shows a detailed schematic of an S2 tower.

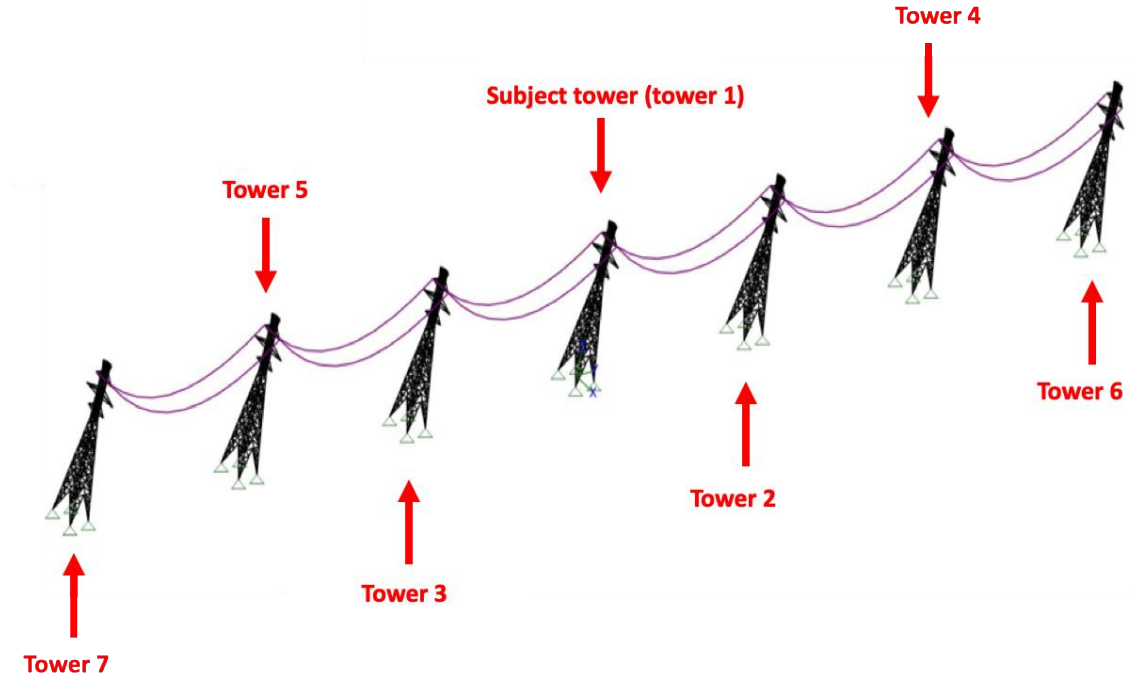


Figure 3-3: Schematic of the SL transmission line.

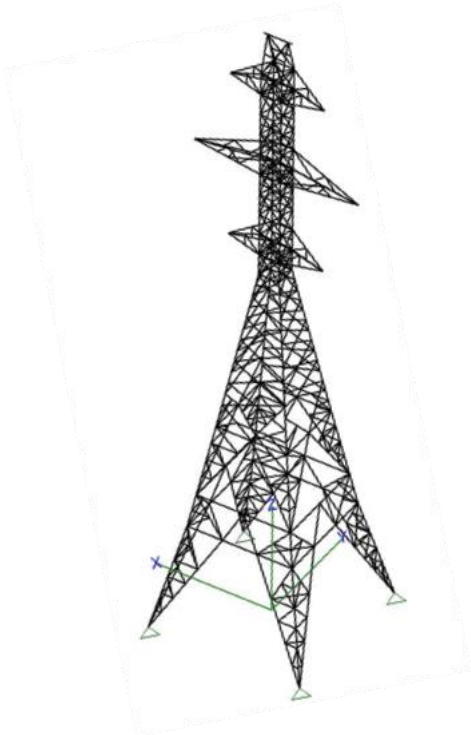


Figure 3-4: Schematic illustrating studied S2 TL towers.

Table 3-2: Properties of TL.

Tower	S2
Type	Self-supported
Tower Weight (kN)	78.1
Span (m)	450
Guy Diameter (m)	N/A
Tower Height (m)	51.81
Number of Conductors	6
Number of Ground Wires	2
Conductor Weight (N/m)	20.14
Ground Wire Weight (N/m)	3.823
Conductor Sag (m)	19.5
Ground Wire Sag (m)	14
Insulator Length (m)	2.438
Design Wind Speed (m/s)	34

3.2.3 Description of the Finite Element Model

The TL system consists of two main components: the tower, and the conductors. Two noded three-dimensional frame elements are used to model the tower members. Rigid connections are assumed between the primary chord members to simulate the multi-bolted connections, while hinged connections are used to simulate the single-bolt connections between the diagonal and the primary chord members.

For the parametric study, the conductors' reactions are calculated based on modelling the line system by considering six spans. The numerical model consists of two hinged support at the ends and five towers, which include the tower of interest and two adjacent towers on each side. The number of towers is chosen based on the recommendations concluded by Shehata and et al. [26] to ensure an accurate reflection of the appropriate stiffness of the system and the forces transferred from the conductors and ground wires to the tower of interest. The technique developed by Aboshosha and El Damatty [37] is used to calculate the reactions of the conductors of a multi-spanned TL system under tornado loads using a semi-closed form solution. The semi-closed form technique requires significantly less computational time compared to non-linear finite element methods, which is a crucial factor when conducting extensive parametric studies.

After identifying the critical tornado configurations using the results of the parametric study, progressive failure analysis is conducted for the five most critical scenarios. In the progressive failure analysis of a multiple-tower TL system where the propagation of failure from one tower to the adjacent tower, each line system is modelled by considering eight spans as recommended by Shehata and El Damatty [32]. This is due to Shehata and El Damatty's recommendation to consider six spans to accurately the conductors' reactions transmitted to the tower of interest [26]. The numerical model comprises seven towers (the tower of interest and the three adjacent towers from each side) and two hinged supports at both ends restraining the translational motion in three directions. The reactions of the conductors are calculated using the technique developed by Shehata and El Damatty [32]. The technique allows calculating the conductors' reactions of a multi-spanned TL system under tornado loads based on the deformed shape and the post-failure geometry using the extensible catenary approach developed by Shehata and El Damatty [33].

3.3 Parametric Study

The extensive parametric study considers different cases in which the location of the tornado changes relative to the subject tower (Figure 3-5). To identify the most critical tornado configurations, a non-linear analysis of the TL systems under the full F2 tornado loads is conducted for each case. The parametric study is necessary when investigating structures under local events, such as tornadoes. This can be investigated by surveying a domain of polar coordinates (R, θ) , relative to the centre of the tower of interest, as shown in Figure 3-5. The radius, R , ranges from 0 m to 500 m with an increment of 20 m (26 cases). The angle, θ , ranges from 0° to 345° with an increment of $\theta = 15^\circ$ (24 cases). A total of 624 cases are investigated for the tower of interest in this parametric study.

The most critical tornado configurations that cause the loss of the overall stability (collapse) of the tower are identified from the parametric study. The critical tornado configurations are sorted based on the peak demand-to-capacity ratio (λ) recorded after non-linear analysis of the TL system under tornado wind loading. The demand-to-capacity ratio is the ratio of the internal forces of structural members to the capacities of the members. The capacity of the structural members is calculated based on ASCE 10-15 [38].

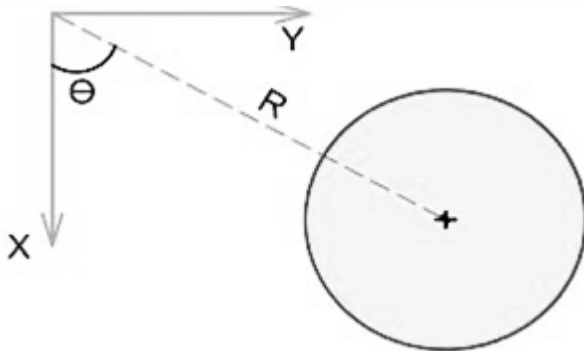


Figure 3-5: Critical tornado configurations parameters (R and θ) relative to the tower of interest.

3.3.1 Parametric Study Results

The results of the parametric study that considers the TL tower system under two different tornado wind fields are summarized in Table 3-3. The finite element model incorporates the CFD simulations developed by Hangan and Kim [2], and El Damatty et al. [24] to investigate the critical tornado configurations for the tower system. The five most critical scenarios are ranked in a descending order based on the maximum demand-to-capacity ratio (λ) experienced within all the tower members. The most critical tornado configuration for the tower under each tornado wind field is bolded in Table 3-3.

Table 3-3: Results of the parametric study.

Tower	Tornado Wind Field	Scenario	Critical configuration (R, θ)	λ
S2	Hangan and Kim [2]	1	(120,225)	11.0
		2	(120,45)	10.8
		3	(120,240)	9.8
		4	(120,285)	9.4
		5	(160,75)	9.3
	Stockton [24]	1	(200,30)	11.0
		2	(260,75)	10.5
		3	(200,210)	10.3
		4	(240,75)	9.9
		5	(180,75)	9.3

3.4 Progressive Failure Analysis

Based on the critical configurations identified in the parametric study, progressive failure analysis of the towers is investigated for the five most critical configurations. For each of the identified critical tornado configuration, a non-linear analysis that involves geometric non-linearity is conducted. A non-linear analysis is conducted, where the subject tower is being solved at each increment of loading to identify the members that have reached the structural capacity. The identified members are then eliminated from the structural stiffness matrix in subsequent increments, where incrementally, deformed shape and the plastic hinge formation are detected.

Once the structure cumulatively loses its overall stability, failure load and the associated failure mode for the tower are recorded. The numerical tool allows predicting the location of the plastic hinge and the post-failure geometry for the collapsed segment of the failing tower above the plastic hinge. The geometry of the collapsed segment can be predicted by investigating its stability under the combination of its own weight, the forces in the conductors due to the tornado loads, and the forces on the nodes of the collapsed segment of the tower as well. This can be achieved through numerical iterations that eventually identifies the geometry that causes a zero-value overturning moment at the location of the plastic hinge. The analysis is based on the assumption that the conductors remain attached to the failed segment and the adjacent towers. This assumption is based on the observations from the damage surveying reported by the industry.

The location of the collapsed segment can be defined using three parameters: height of the plastic hinge (Z_{ph}) and two angles (θ_F , θ_D) as shown in Figure 3-6. θ_F is an angle in the vertical plane perpendicular to the TL. θ_F is measured between the projection of the collapsed segment of the tower on the plane and the centerline of the tower. On the other hand, θ_D is an angle in the horizontal plane that is measured between the projection of the collapsed segment of the tower on the plane and the centerline of the tower. The post-failure geometry is then used to calculate the conductors' forces that are transmitted to the adjacent towers. The conductors' forces are calculated based on the extensible catenary approach developed by Shehata and El Damatty [33]. Shehata and El Damatty [33] modified the basic extensible catenary mathematical equations to solve 3D space catenary

equations. This allows solving for the TL conductors' forces of multi-spanned TL systems with a difference in the horizontal and the vertical levels of the conductors' supports. It is worth mentioning that the mathematical approach accounts for the non-linearity of the system, and the insulators' flexibility. For more details on modifying the mathematical equations, the reader is referred to Shehata and El Damatty [33]. Hence, the progressive failure analysis of the adjacent towers can be investigated, where the adjacent towers are analyzed under the combination of the tornado loads from the critical tornado configuration and the conductors' forces transmitted to the tower after the increment of failure of the main tower. Figure 3-7 the procedure followed to conduct the progressive failure analysis.

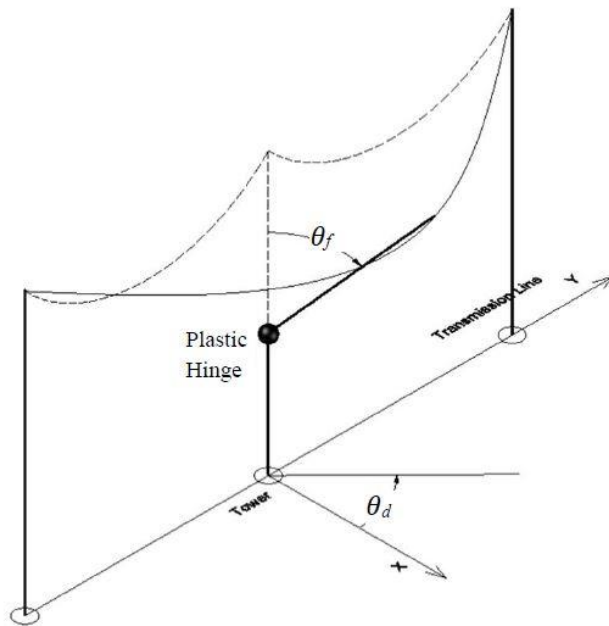


Figure 3-6: Post failure geometry [32].

To determine the suitable loading increment for the non-linear analysis, a sensitivity analysis has been performed (Figure 3-8). The sensitivity analysis is done considering the GL1 transmission line system (described in Section 3.4.1.1) under Hangan's tornado [2]. The sensitivity analysis compares the failure load and the failure wind speed, as a percentage of the full F2 tornado load and wind speed, respectively, to the number of loading increments. This is critical to ensure accuracy in the results while minimizing the

time required to perform the analysis. The sensitivity analysis data shown in Figure 3-8A demonstrates that a number of 40 loading increments (2.5% loading increment) is the most optimal as beyond that point there is a plateau at the failure load at approximately 72% of the full load associated with an F2 tornado. The results shown in Figure 3-8B also show that 40 loading increments ensure accuracy in capturing the failure wind speed as beyond that point there is a plateau at the failure wind speed at approximately 84% of the full F2 tornado wind speed.

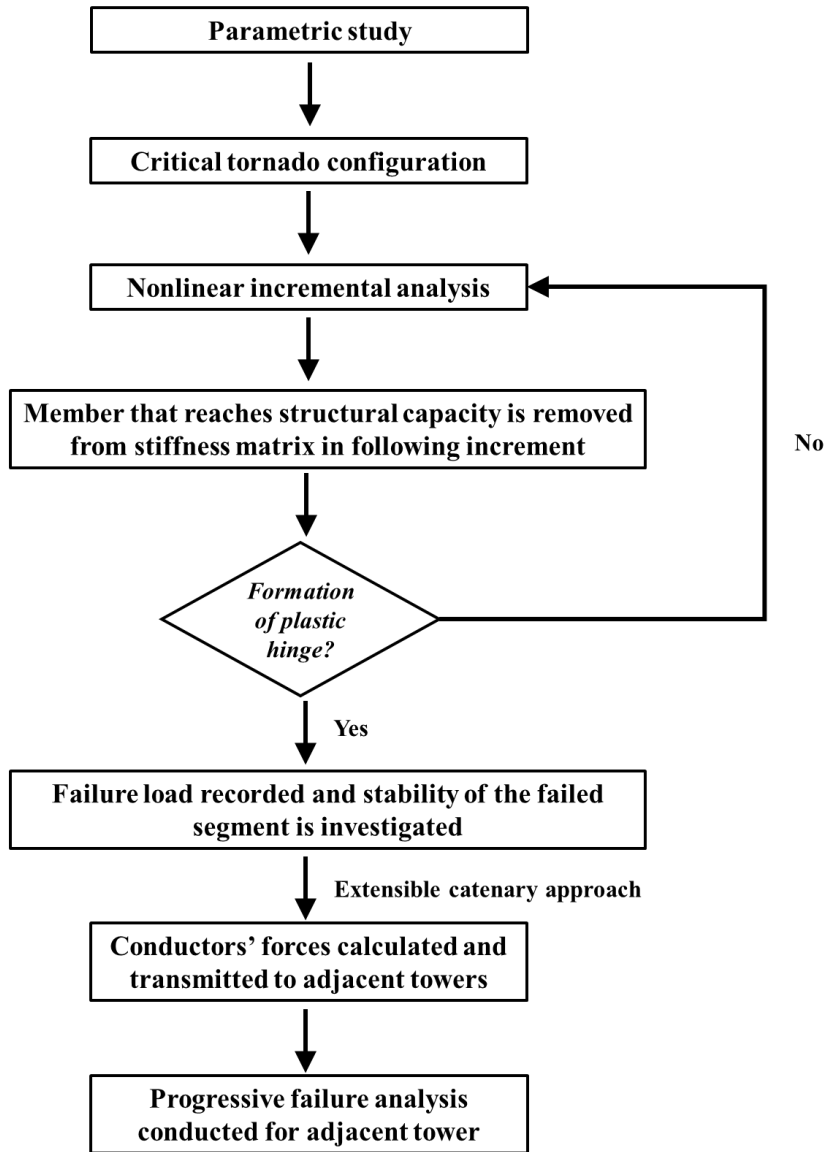


Figure 3-7: Flow chart outlining the progressive failure analysis for each critical tornado configuration.

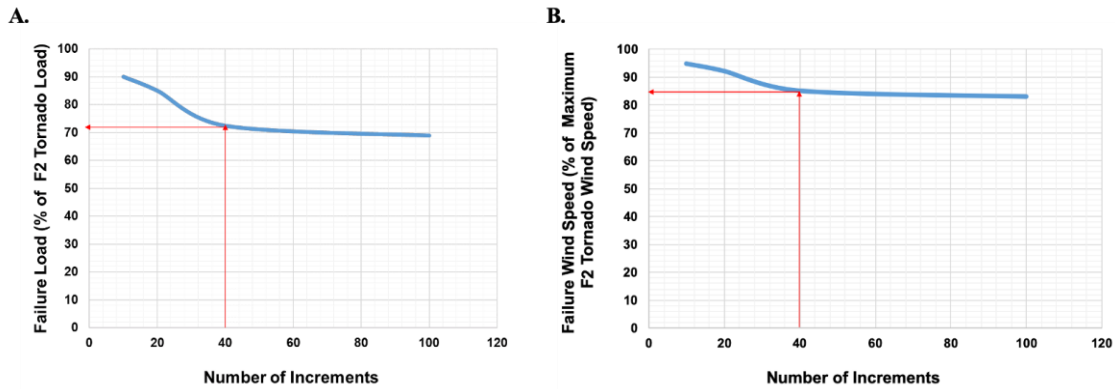


Figure 3-8: Sensitivity analysis to determine the loading increment.

3.4.1 Verification of Numerical Model

The fluid-structure numerical model, utilized in analyzing the tower systems in this study, is verified by comparing the critical tornado configuration to those obtained by Hamada and El Damatty [30, 31]. Even though the current study is focusing on the progressive failure of self-supported TL systems, the verification is conducted by considering two single guyed towers because only guyed towers have been previously studied by Hamada and El Damatty [31].

3.4.1.1 Description of the guyed towers considered in the verification

The first guyed TL system, GL1, has a line span of 480 m. The guyed towers, G1, support two conductors connected to the towers through 3.9 m insulators and one ground-wire at the top of the tower at a height of 44.39 m. The conductors and ground-wire initial sags are 20 m and 13 m, respectively. The height of the guyed tower G1 is 44.39 m and is supported by four down guys attached to G1's cross-arms at a height of 38.23 m point (Figure 3-9A).

The second guyed TL system, GL2, has a line span of 460 m. The guyed towers, G2, support two conductors, which are connected to the towers through 4.27 m insulators, and two ground-wires at the highest points of the tower at a height of 46.57 m. The conductors and ground-wire initial sags are 14 m and 16 m, respectively. The height of the guyed tower G2 is 46.57 m and is supported by four guys attached to G2's cross-arms (Figure 3-9B).

The physical parameters for conductors and ground-wires in GL1, GL2 are outlined in Table 3-4. The investigated towers are designed to resist synoptic wind with design wind speeds shown in Table 3-4. A sample of the detailed drawings for the towers is provided for G1 in Figure 3-10.

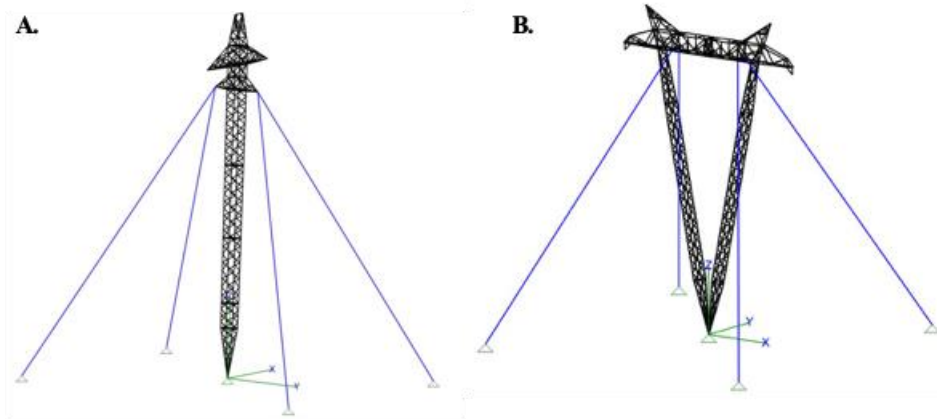


Figure 3-9: Schematic illustrating studied TL towers used in the verification. (A) G1; (B) G2 transmission line.

Table 3-4: Properties of TLs used in the verification.

Tower	G1	G2
Type	Guyed	Guyed
Tower Weight (kN)	34	78.2
Span (m)	480	460
Guy Diameter (m)	0.0165	0.0195
Tower Height (m)	44.39	46.57
Number of Conductors	2	3
Number of Ground Wires	1	2
Conductor Weight (N/m)	28.97	8.67
Ground Wire Weight (N/m)	3.9	5.45
Conductor Sag (m)	20	14
Ground Wire Sag (m)	13.54	16
Insulator Length (m)	3.9	4.27
Design Wind Speed (m/s)	32	36

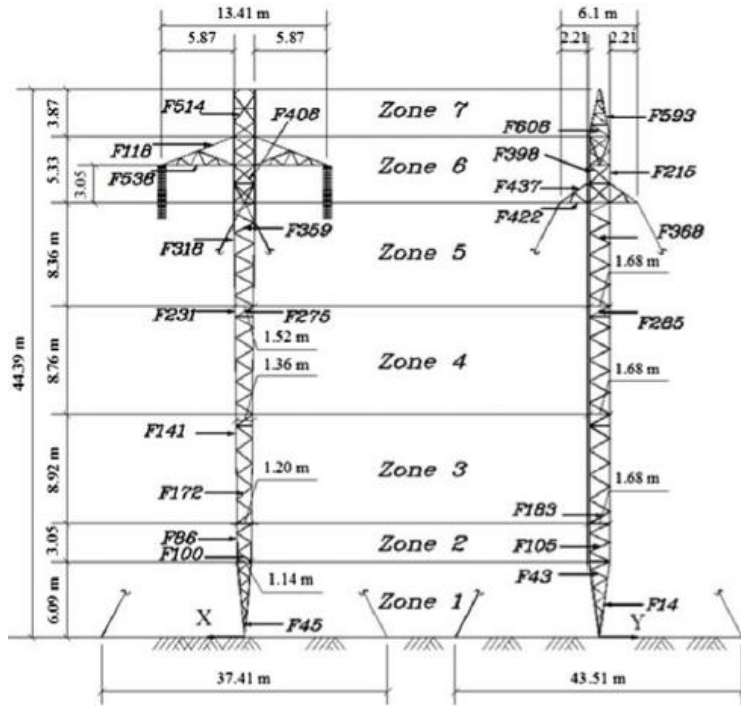


Figure 3-10: Detailed Drawing for G1 [35].

The numerical model is verified using Hangan's tornado wind field [2] following the same scaling procedure and factors used by Hamada and El Damatty [30]. Table 3-5 summarizes the results from the verification by comparing the critical configuration and the failure wind speed using the numerical model to the findings obtained by Hamada and El Damatty [31] for each of the two towers. For G1, the critical tornado configuration that is obtained in the current study is $R = 120$ m, $\theta = 165^\circ$, whereas Hamada and El Damatty [31] reported $R = 125$ m, $\theta = 180^\circ$, as shown in Table 3-5. The discrepancy in the θ value between the two studies can be interpreted by the fact of using a smaller θ increment in the parametric study outlined in the current study. Moreover, the failure load value in this study is comparable to the value reported by Hamada and El Damatty [31], where the maximum percentage of difference in the failure wind speed concluded from this comparison is 1%. Further verification is done considering the G2 tower. Table 3-5 shows an excellent agreement in the case of G2 tower for the failure wind speeds and the critical

configurations, where the maximum percentage of difference in the failure wind speed concluded from this comparison is 2%.

Table 3-5: Summary of the verification study.

Structures	Model	Critical configuration (R, θ)	Failure wind speed (m/s)	Failure wind speed (% of F2 tornado wind speed)
G1	Current Study	120 m, 165°	63	85
	Hamada et al. [31]	125 m, 180°	65	84
G2	Current Study	100 m, 165°	42	57
	Hamada et al. [31]	100 m, 180°	43	55

3.4.2 Progressive Failure Analysis Results

After validating the fluid-structure numerical model, the progressive failure analysis of the self-supported TLs is conducted. The progressive failure analysis results for S2 TL under Stockton 2005 and Hangan’s F2 tornadoes are reported below. It is worth mentioning that all the figures in Section 3.4.2 are shown in a distorted scale of 0.2:1 for horizontal: vertical distances. The numbering of the towers within the TL is outlined in Figure 3-3, where the intermediate tower is referred to as Tower 1 or the Subject tower.

3.4.2.1 The failure mode for S2 under Stockton 2005 tornado wind field

The progressive failure analysis is conducted for the S2 TL under each of the five most critical configurations of the Stockton 2005 tornado outlined in Table 3-3. The results of the progressive failure analysis are presented in Sections 3.4.2.1.1 - 3.4.2.1.5.

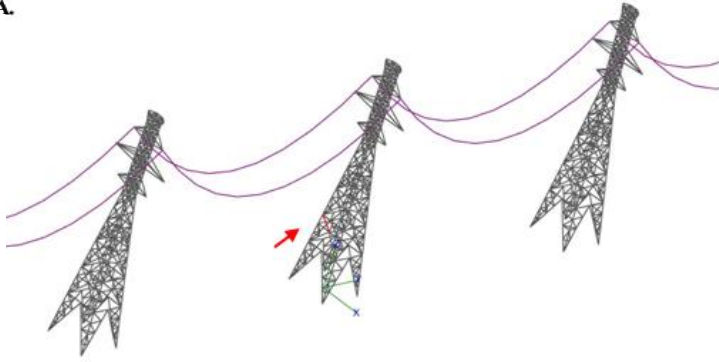
3.4.2.1.1 The first failure scenario for S2 under Stockton 2005 tornado wind field

As shown earlier in Table 3-3, the first critical tornado configuration is at $R = 200$ m and $\theta = 30^\circ$ with an associated demand-to-capacity ratio, $\lambda = 11$. Figure 3-11 shows the propagation of failure within the structural members of the TL towers in the transmission line. The first member to collapse within tower 1 is a diagonal member that fails at 10% of the full F2 tornado load (Figure 3-11A). The progression of failure continues through tower 1 until the formation of a plastic hinge at a height of 30.1 m at 32.5% of the full F2 tornado load. Tower 1 fails at 40% of the full F2 tornado load at a wind speed of 44.4 m/s, which represents 63% of the maximum resultant wind speed of the full F2 tornado.

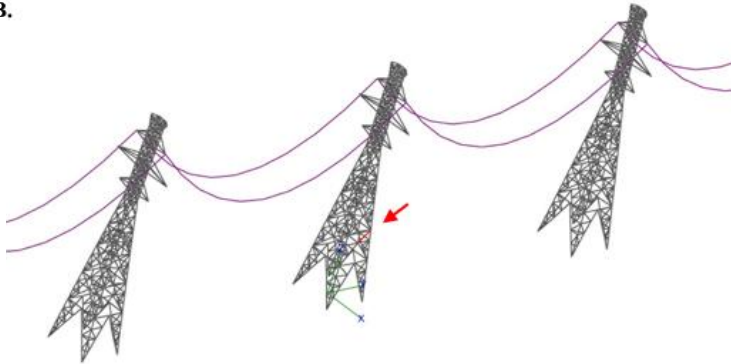
The combination of the tornado loads and the conductors' forces on tower 2 cause the formation of a plastic hinge in tower 2 at 67.5% of the full F2 tornado load. Tower 2 ultimately fails at 72.5% of the full F2 tornado load at a wind speed of 59.8 m/s, which represents 85% of the maximum resultant wind speed of the full F2 tornado.

The global tower failures within the line occur only within the towers near the tornado location (towers 1 and 2) despite that some local failures are experienced in the adjacent towers 3, 4, and 5 as shown in Figure 3-11.

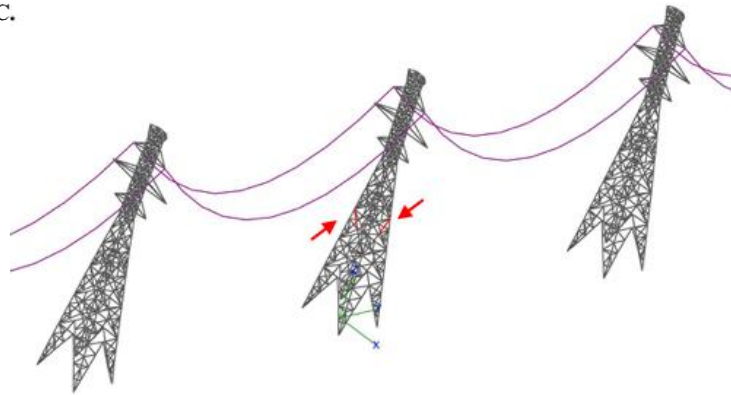
A.



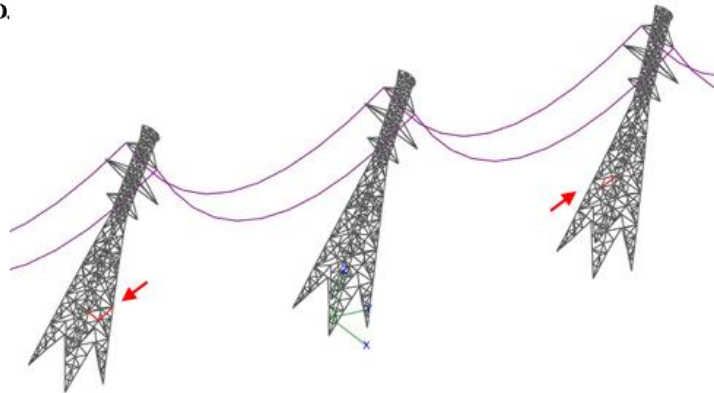
B.



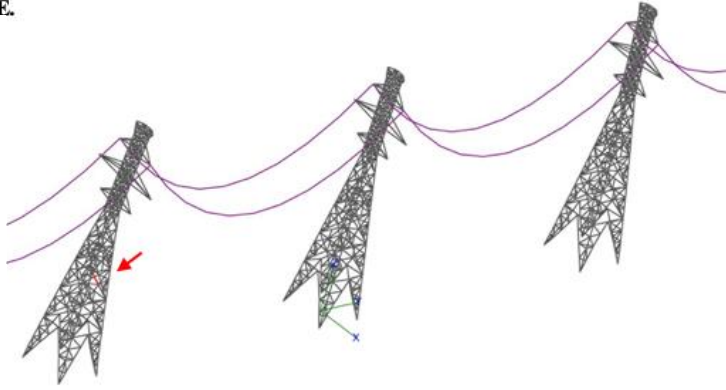
C.



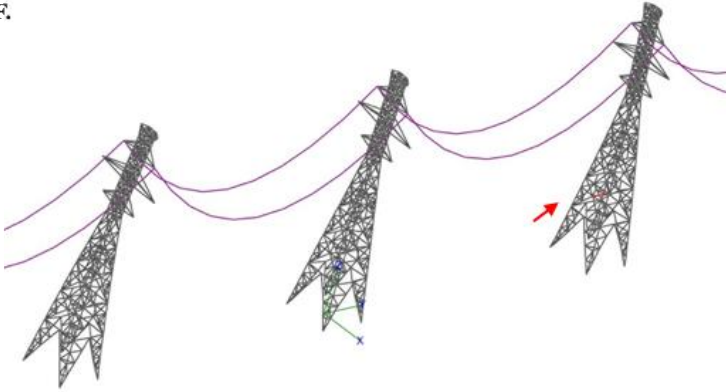
D.



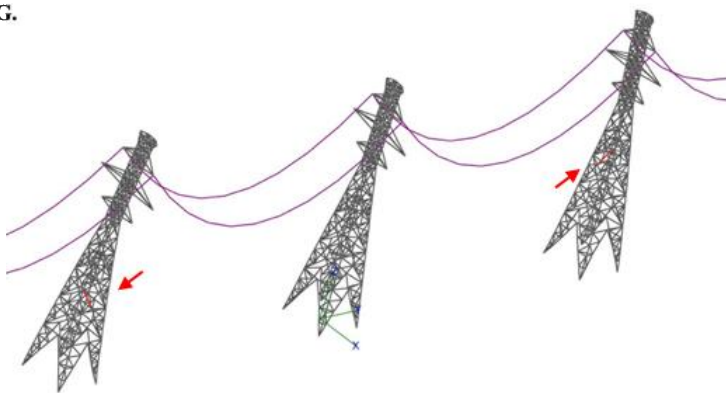
E.



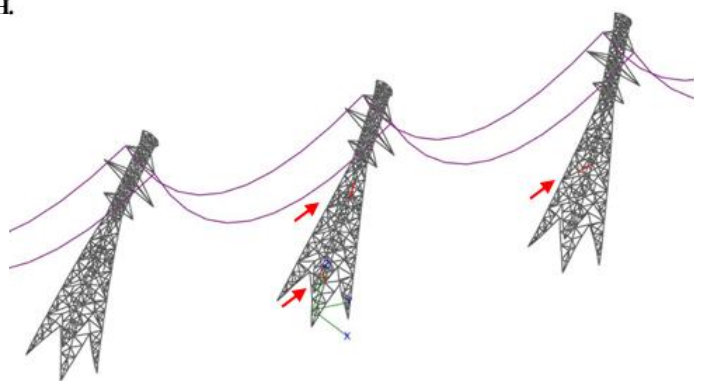
F.



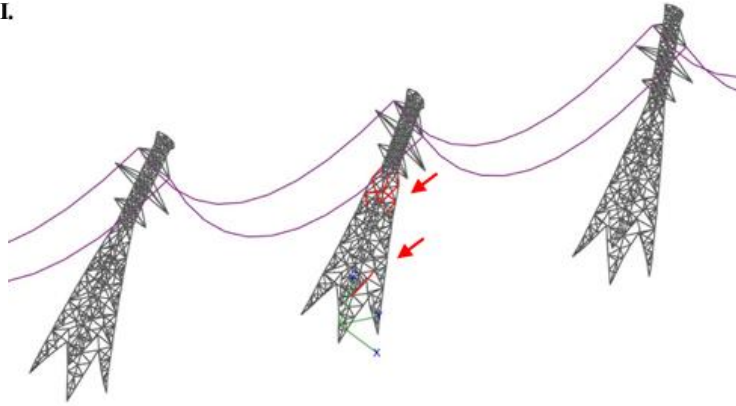
G.



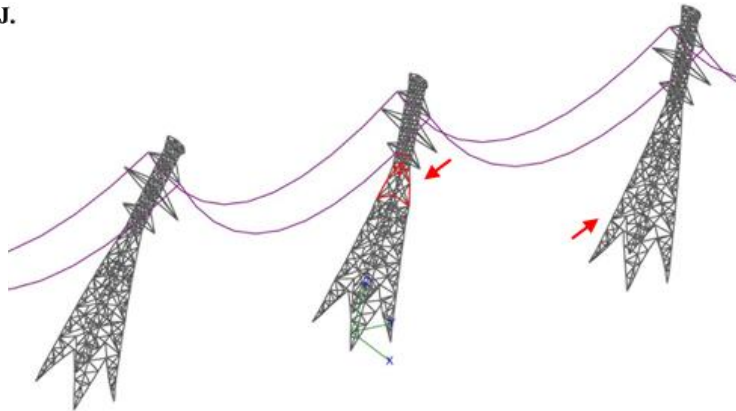
H.



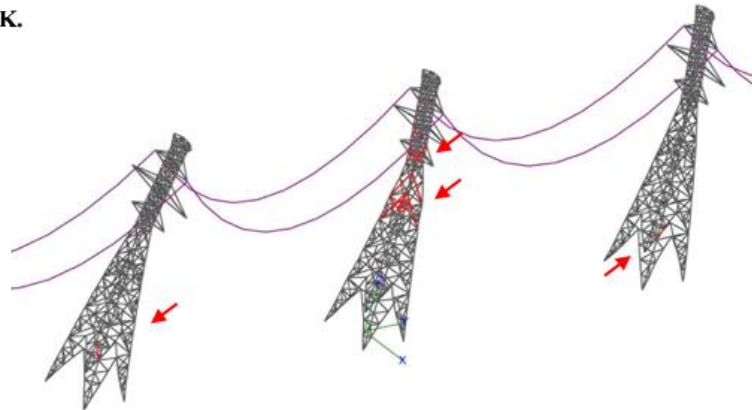
I.



J.



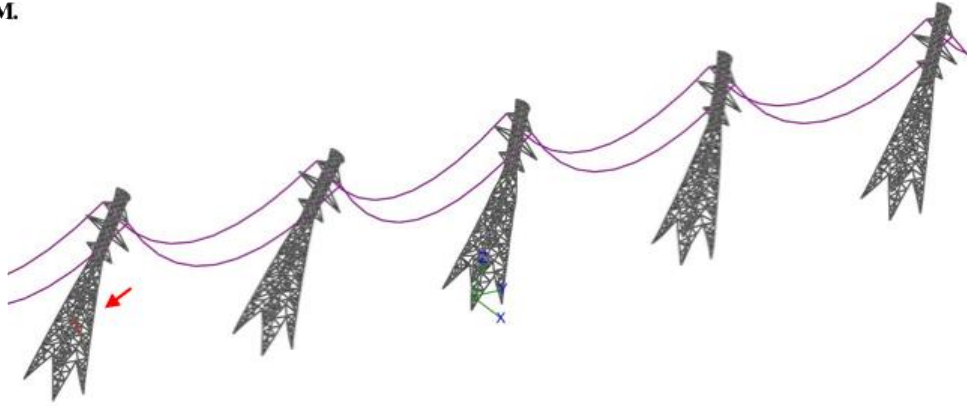
K.



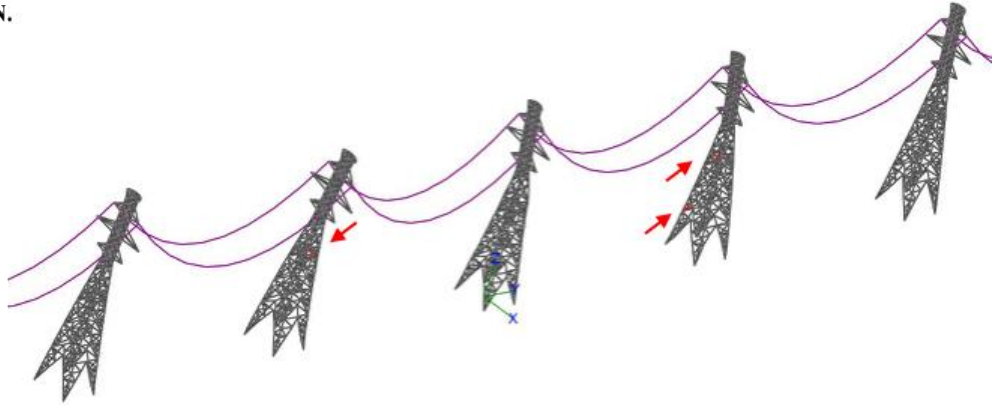
L.



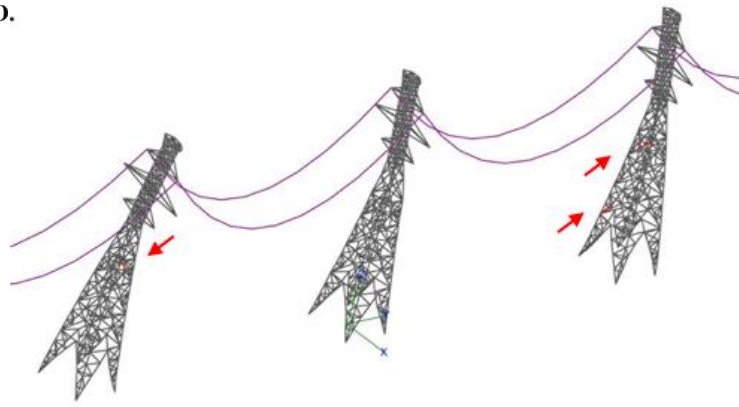
M.



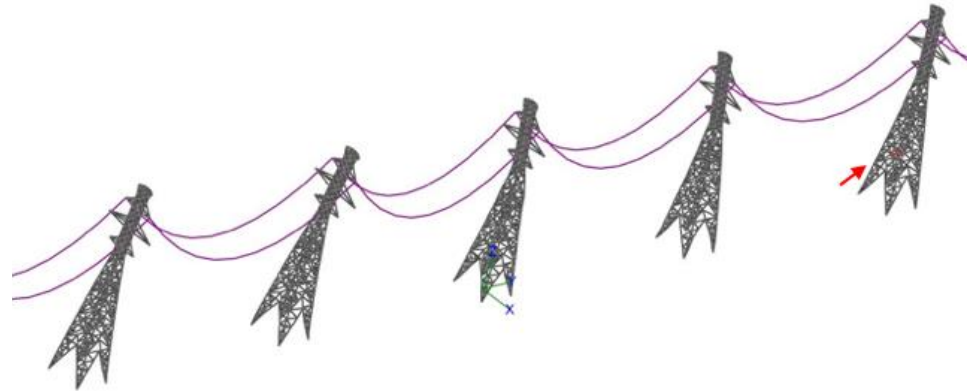
N.



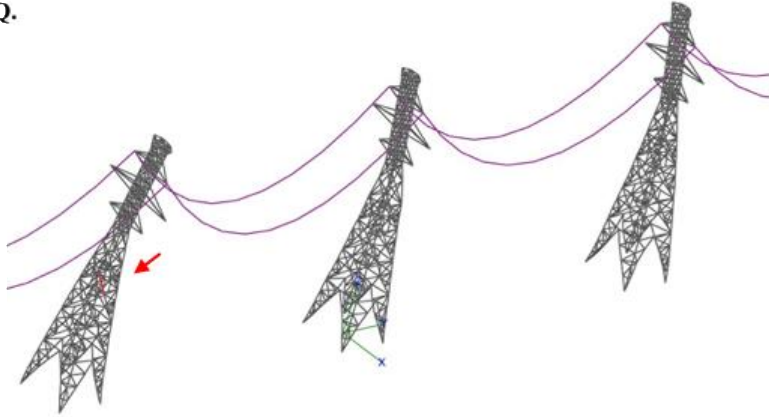
O.



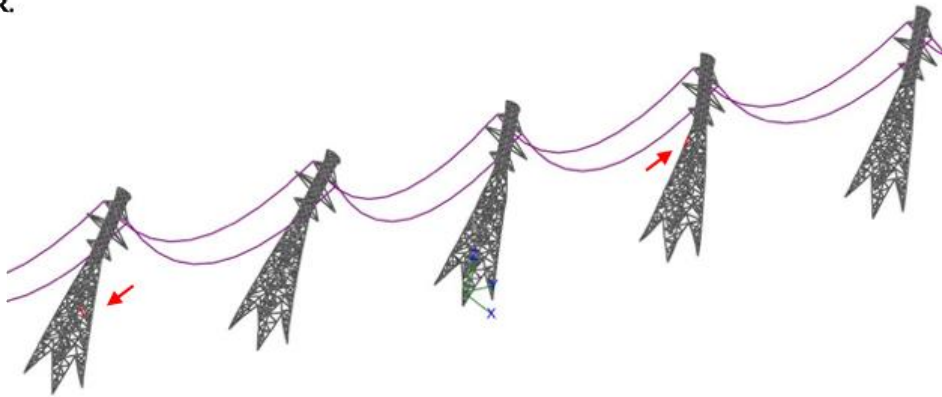
P.



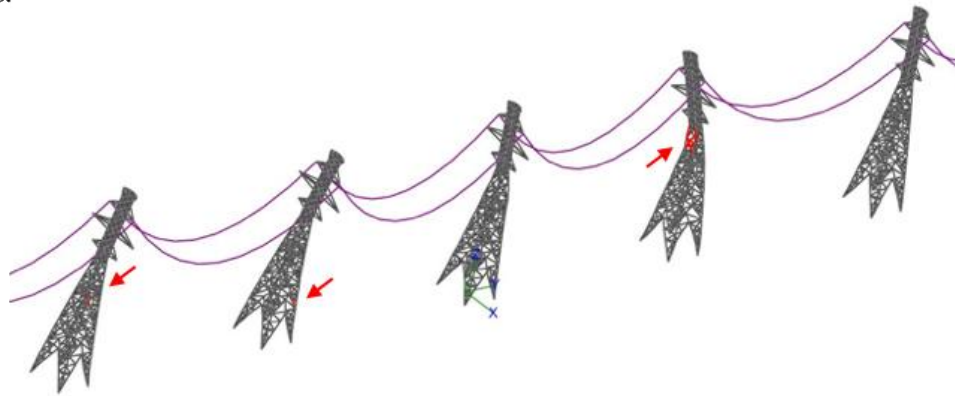
Q.



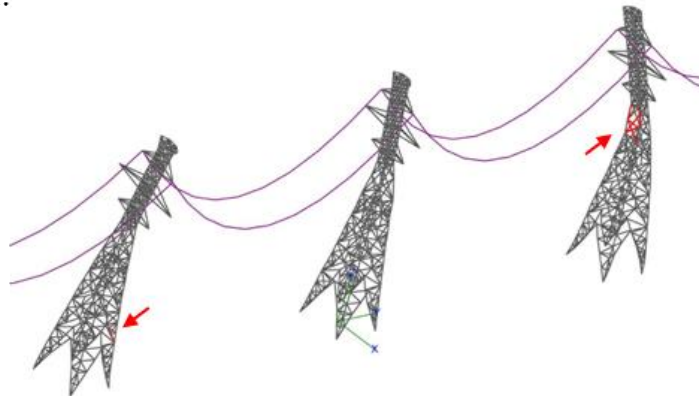
R.



S.



T.



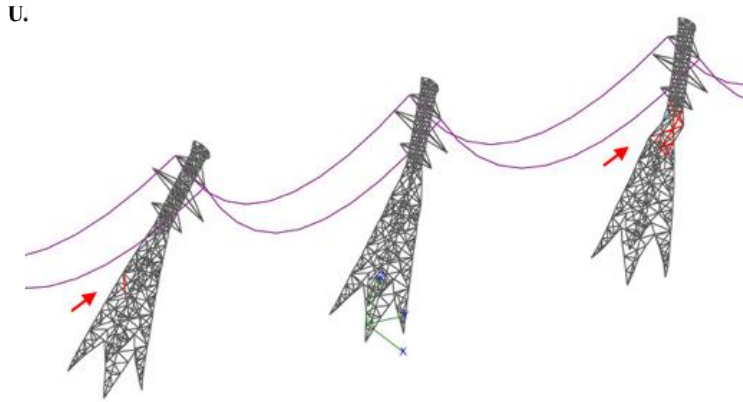


Figure 3-11: Progressive failure of S2 tower in first critical scenario, $\lambda = 11$. (A) 10%; (B) 12.5%; (C) 15%; (D) 17.5%; (E) 20%; (F) 25%; (G) 27.5%; (H) 32.5%; (I) 35%; (J) 37.5%; (K) 40%; (L) 50%; (M) 52.5%; (N,O) 55%; (P) 57.5%; (Q) 60%; (R) 67.5%; (S,T) 70; and (U) 72.5%.

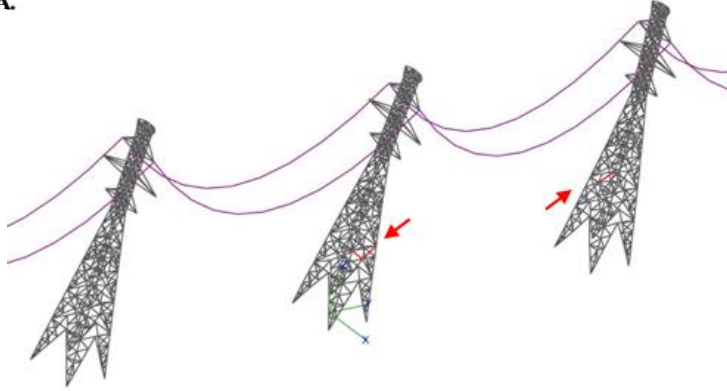
3.4.2.1.2 The second failure scenario for S2 under Stockton 2005 tornado wind field

The second critical tornado configuration is at $R = 260$ m and $\theta = 75^\circ$ with an associated demand-to-capacity ratio, $\lambda = 10.5$. Figure 3-12 shows the propagation of failure within the structural members of the TL towers in the transmission line. The first two members to collapse within tower 1 are diagonal bracing members that fail at 10% of the full F2 tornado load (Figure 3-12A). The progression of failure continues through tower 1 until the formation of a plastic hinge at a height of 30.1 m at 32.5% of the full F2 tornado load. Tower 1 fails at 37.5% of the full F2 tornado load at a wind speed of 43 m/s, which represents 61% of the maximum resultant wind speed of the full F2 tornado.

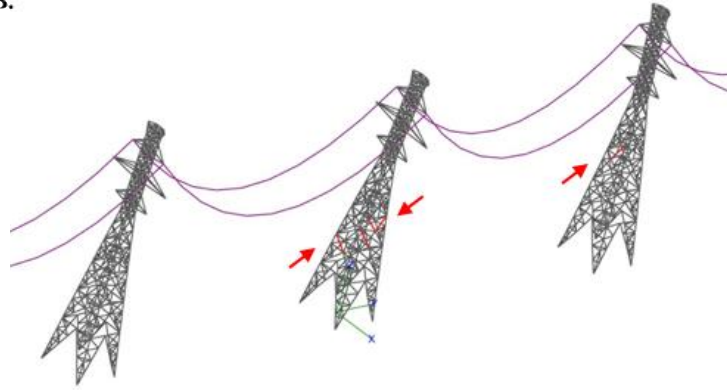
The combination of the tornado loads and the conductors' forces on tower 2 cause the formation of a plastic hinge in tower 2 at 37.5% of the full F2 tornado load. Tower 2 ultimately fails at 40% of the full F2 tornado load at a wind speed of 44.4 m/s, which represents 63% of the maximum resultant wind speed of the full F2 tornado.

The global tower failures within the line occur only within the towers near the tornado location (towers 1 and 2), despite that some local failures are experienced in the adjacent towers 3, 4, and 5 as shown in Figure 3-12.

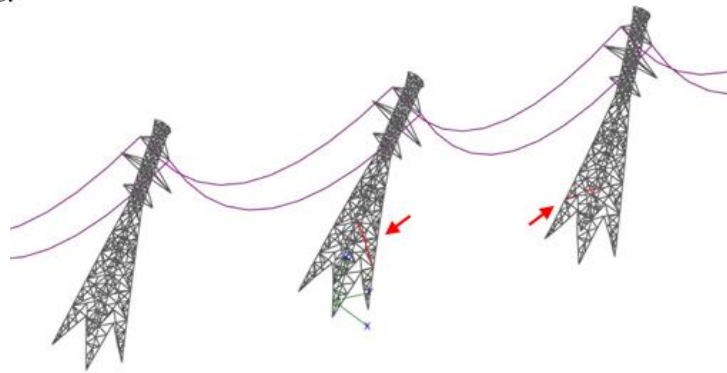
A.



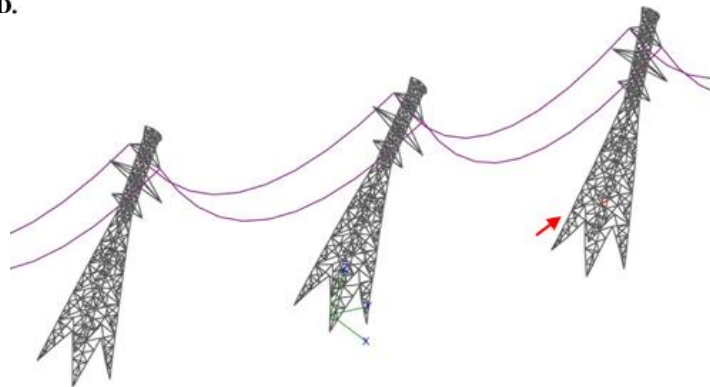
B.



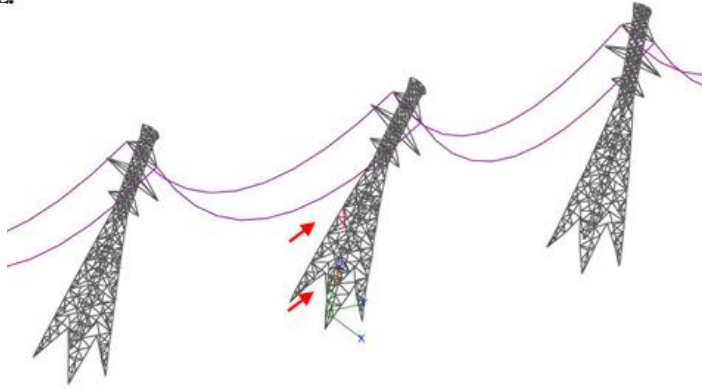
C.



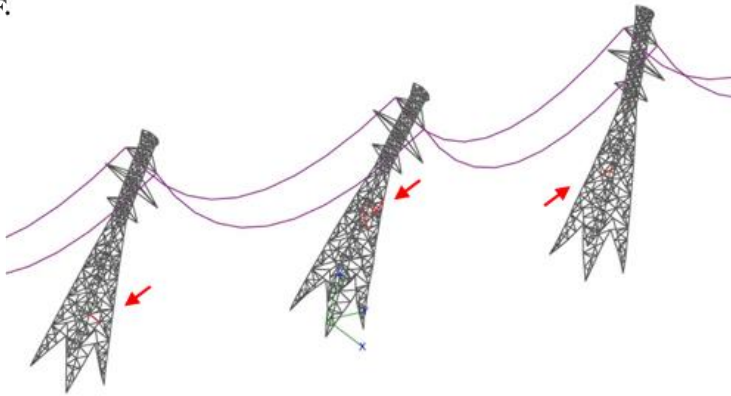
D.



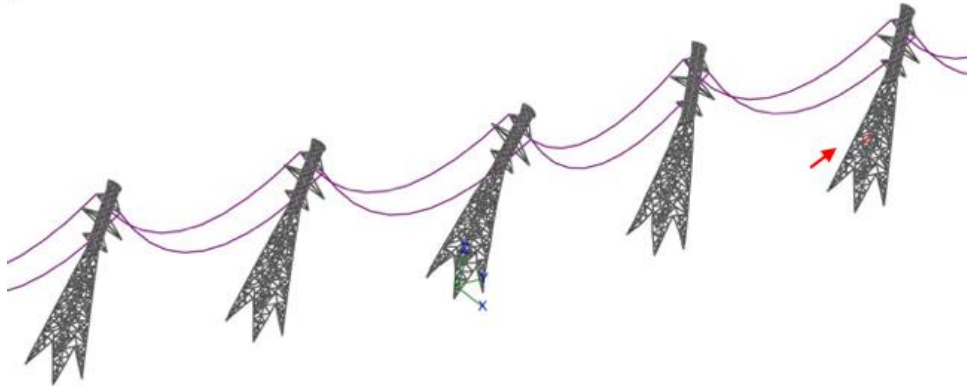
E.



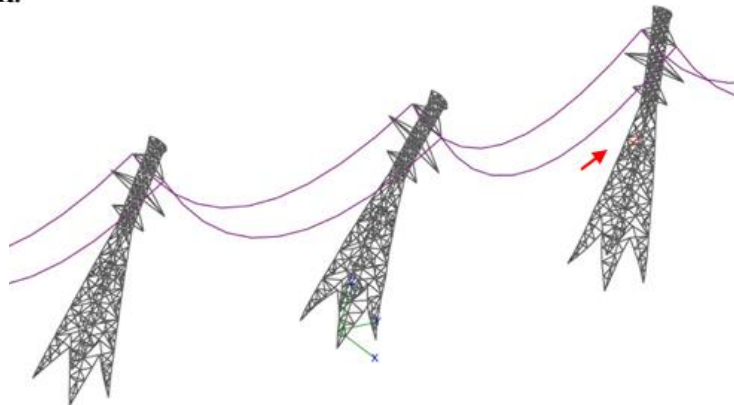
F.



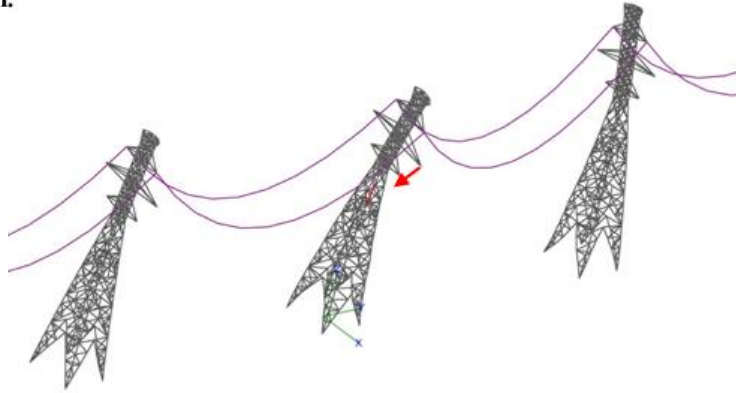
G.



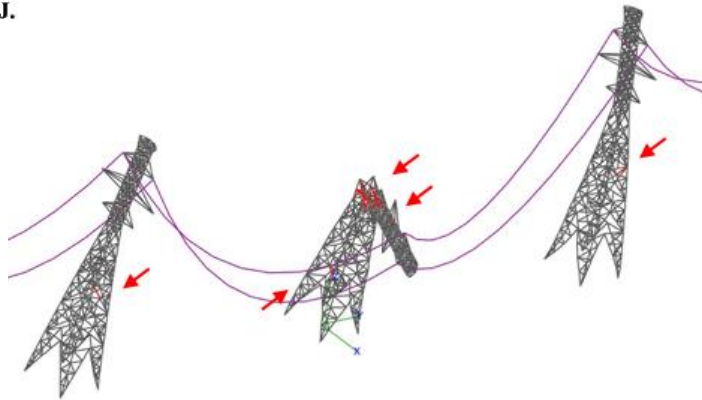
H.



I.



J.



K.

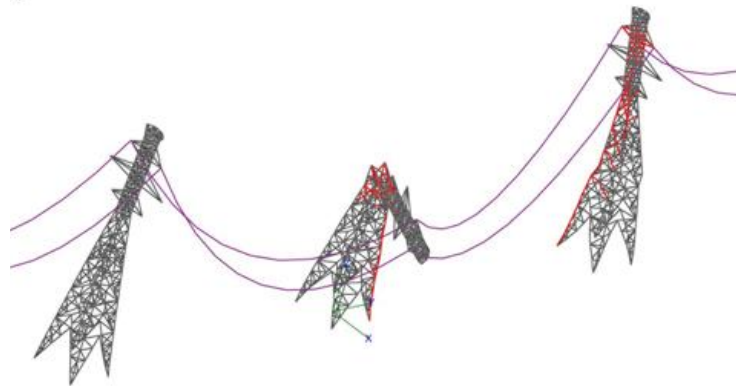




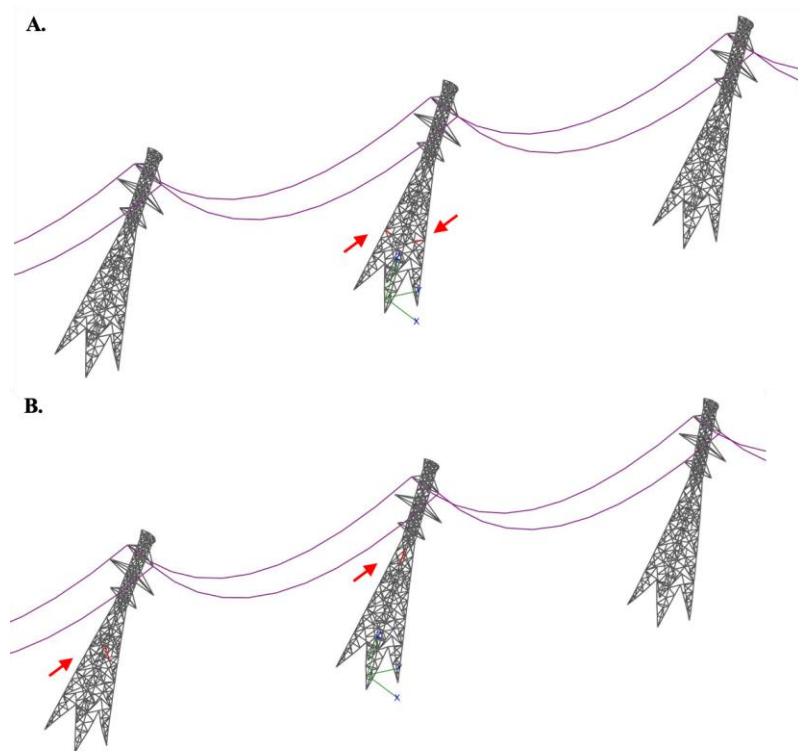
Figure 3-12: Progressive failure of S2 tower in second critical scenario, $\lambda = 9.4$. (A) 10%; (B) 12.5%; (C) 15%; (D) 17.5%; (E) 22.5%; (F) 25%; (G) 27.5%; (H) 30%; (I) 32.5%; (J) 35%; (K) 37.5%; and (L,M) 40%.

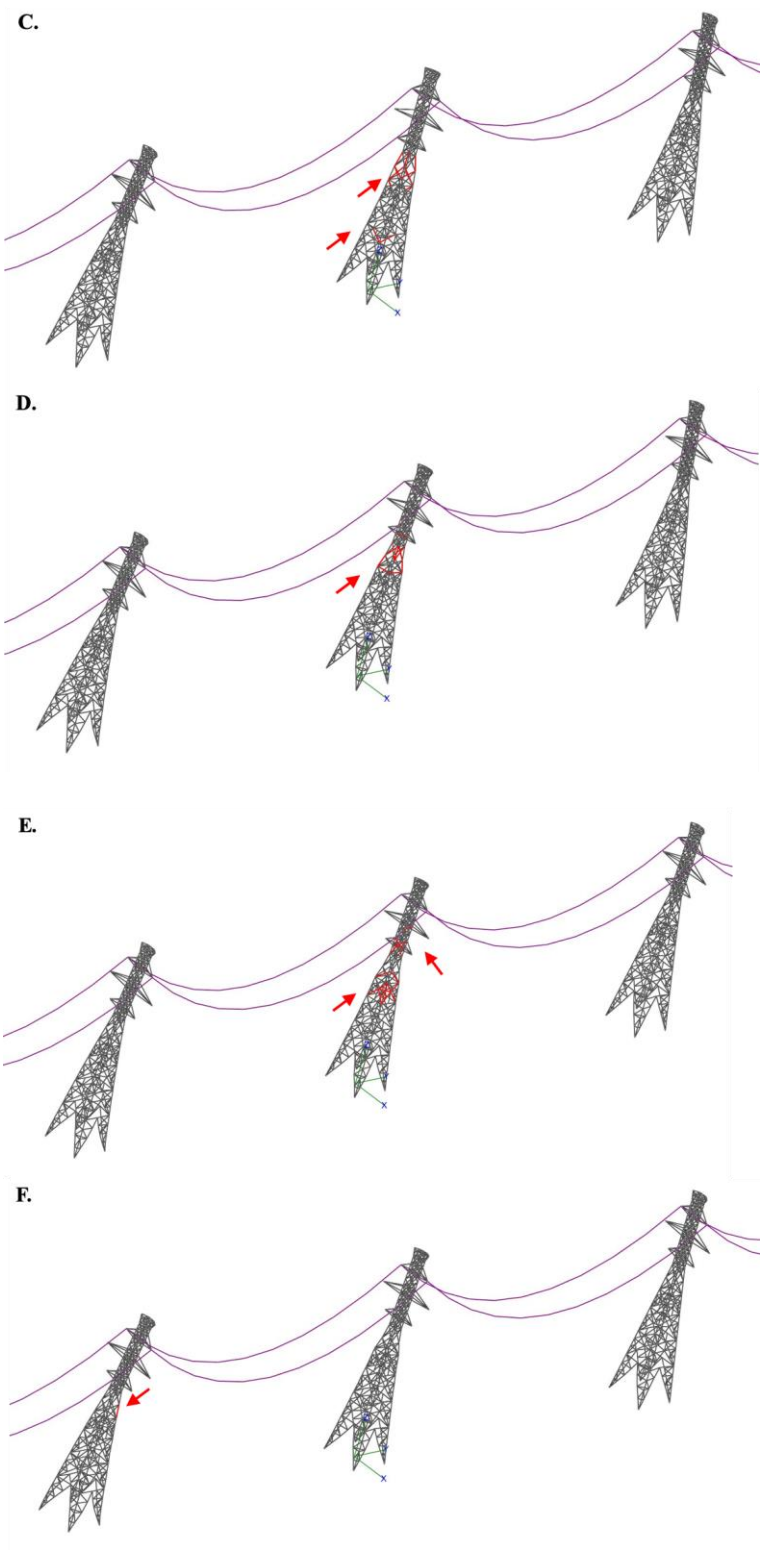
3.4.2.1.3 The third failure scenario for S2 under Stockton 2005 tornado wind field

The third critical tornado configuration is at $R = 200$ m and $\theta = 210^\circ$ with an associated demand-to-capacity ratio, $\lambda = 10.3$. Figure 3-13 shows the propagation of failure within the structural members of the TL towers in the transmission line. The first two members to collapse within tower 1 are horizontal bracing members that fail at 12.5% of the full F2 tornado load (Figure 3-13A). The progression of failure continues through tower 1 until the formation of a plastic hinge at a height of 30.1 m at 32.5% of the full F2 tornado load. Tower 1 fails at 40% of the full F2 tornado load at a wind speed of 44.4 m/s, which represents 63% of the maximum resultant wind speed of the full F2 tornado.

The combination of the tornado loads and the conductors' forces on tower 3 cause the formation of a plastic hinge in tower 3 at 62.5% of the full F2 tornado load. Tower 3 ultimately fails at 70% of the full F2 tornado load at a wind speed of 58.7 m/s, which represents 84% of the maximum resultant wind speed of the full F2 tornado.

The global tower failures within the line occur only within the towers near the tornado location (towers 1 and 3), despite that some local failures are experienced in the adjacent towers 2, 4, and 5.





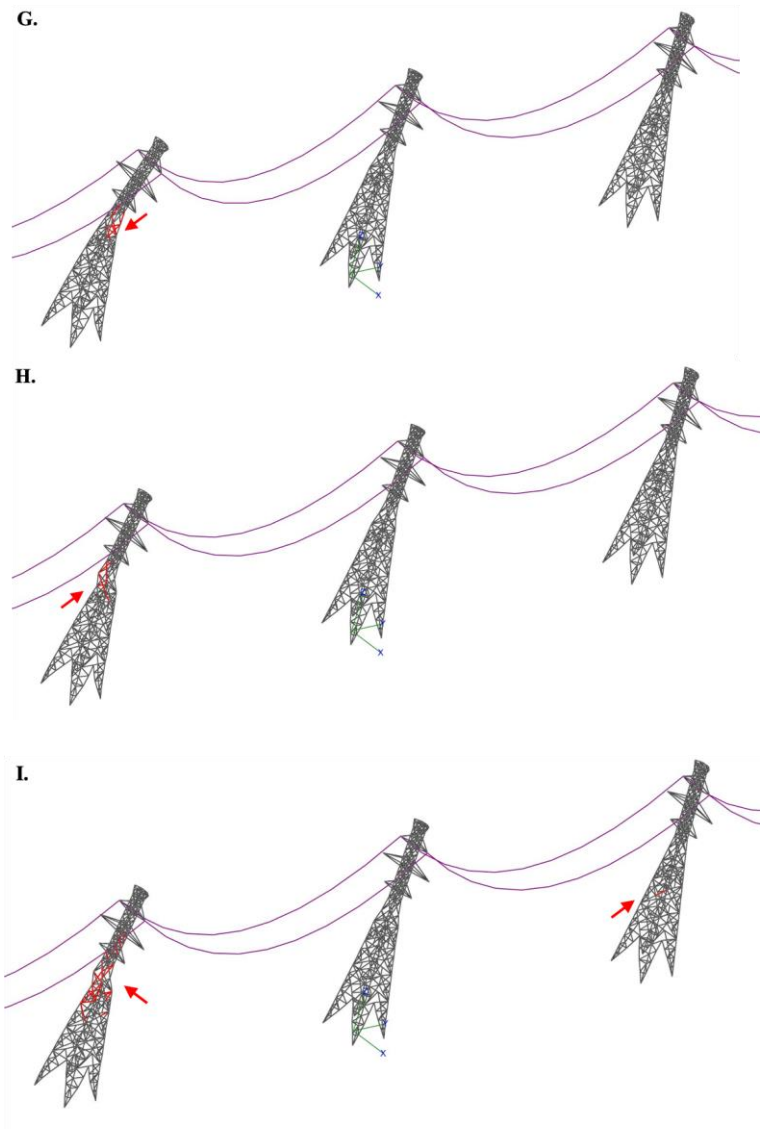


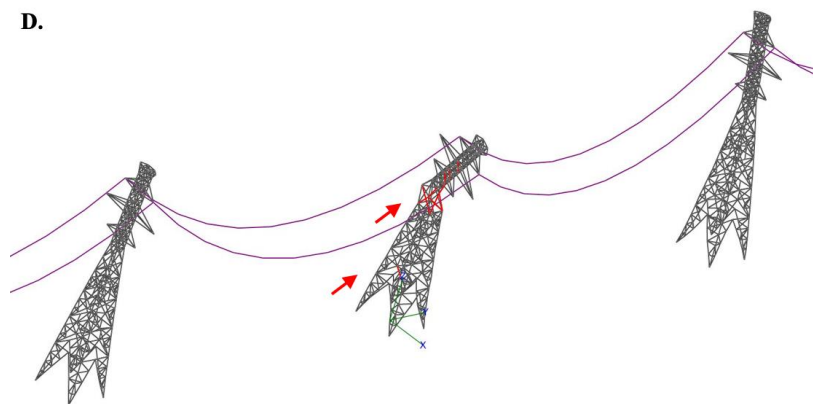
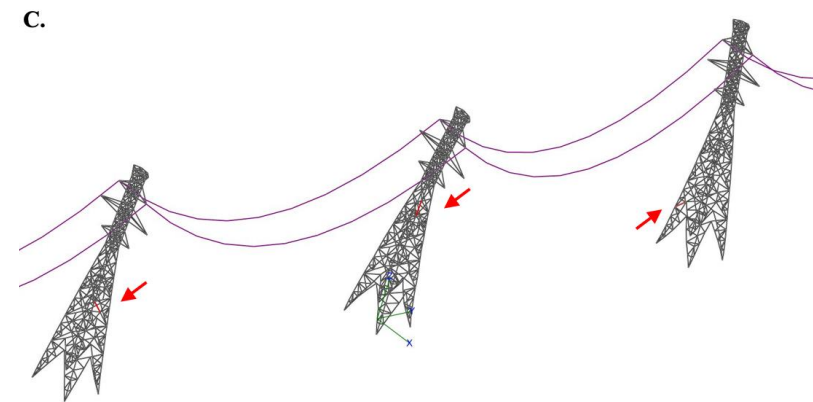
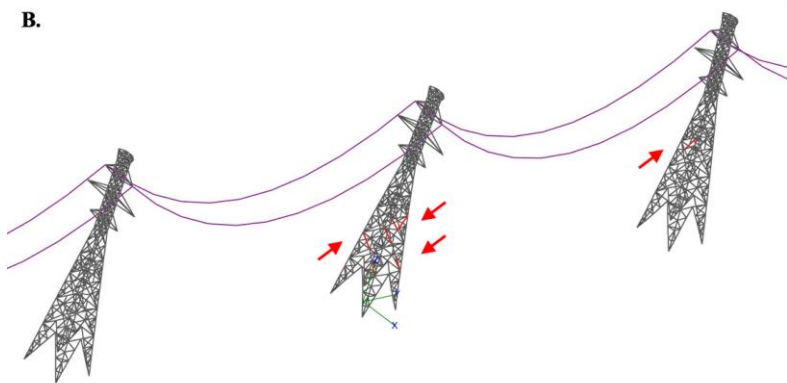
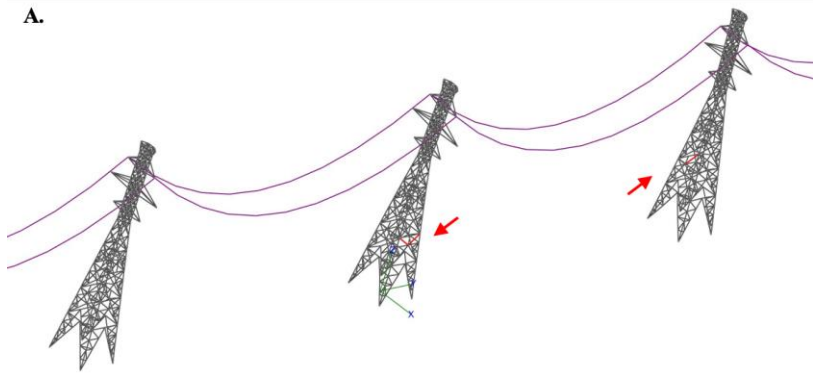
Figure 3-13: S2NL third mode. (A) 12.5%; (B) 32.5%; (C) 35%; (D) 37.5%; (E) 40%; (F) 62.5%; (G) 65%; (H) 67.5%; and (I) 70%.

3.4.2.1.4 The fourth failure scenario for S2 under Stockton 2005 tornado wind field

The fourth critical tornado configuration is at $R = 240$ m and $\theta = 75^\circ$ with an associated demand-to-capacity ratio, $\lambda = 9.9$. Figure 3-14 shows the propagation of failure within the structural members of the TL towers in the transmission line. The first two members to collapse within tower 1 are diagonal bracing members that fail at 10% of the full F2 tornado load (Figure 3-14A). The progression of failure continues through tower 1 until the formation of a plastic hinge at a height of 30.1 m at 32.5% of the full F2 tornado load. Tower 1 fails at 37.5% of the full F2 tornado load at a wind speed of 43 m/s, which represents 61% of the maximum resultant wind speed of the full F2 tornado.

The combination of the tornado loads and the conductors' forces on tower 2 cause the formation of a plastic hinge in tower 2 at 37.5% of the full F2 tornado load. Tower 2 ultimately fails at 42.5% of the full F2 tornado load at a wind speed of 45.7 m/s, which represents 65% of the maximum resultant wind speed of the full F2 tornado.

The global tower failures within the line occur only within the towers near the tornado location (towers 1 and 2), despite that some local failures are experienced in the adjacent towers 3,4, and 5.



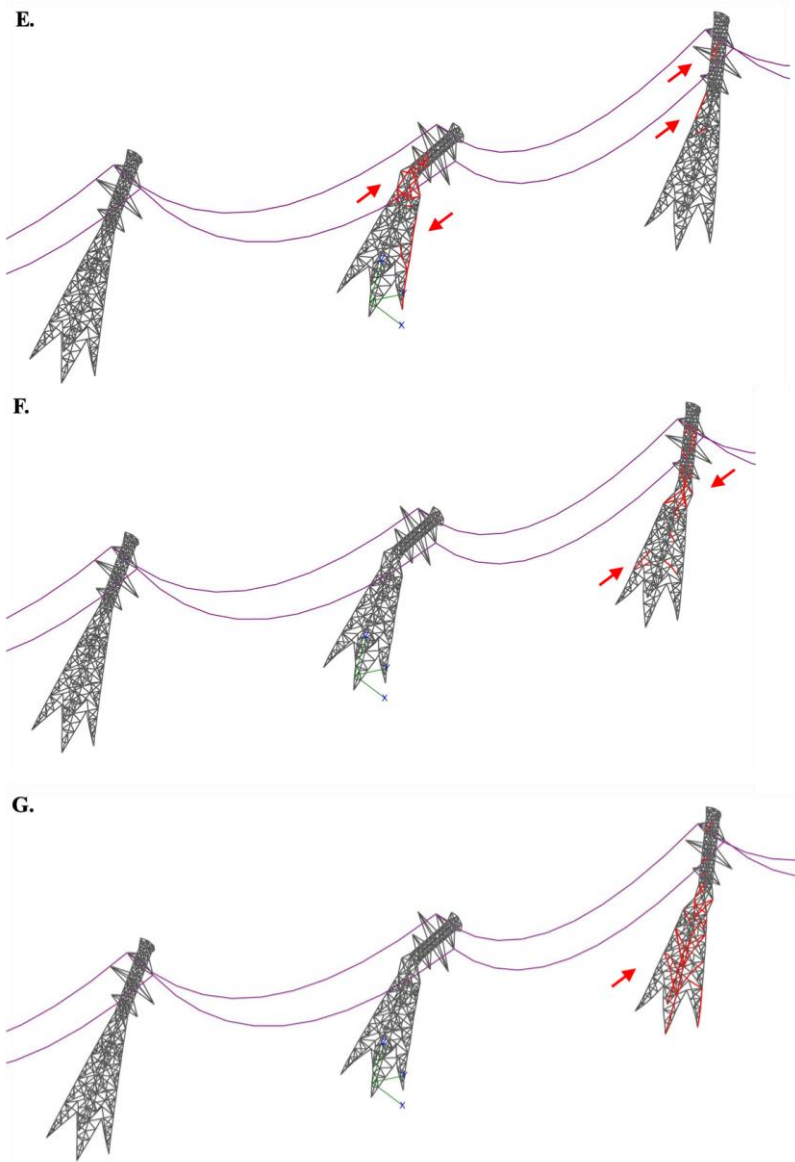


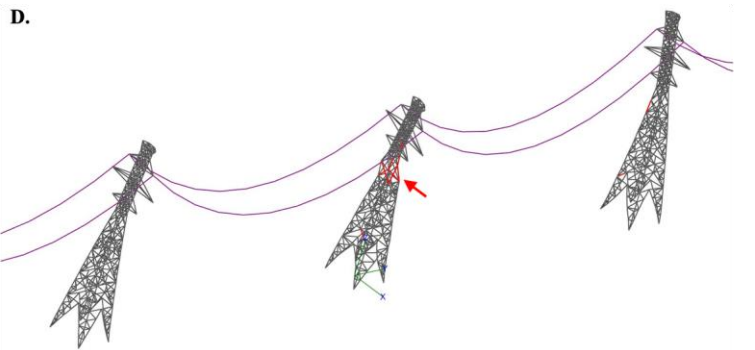
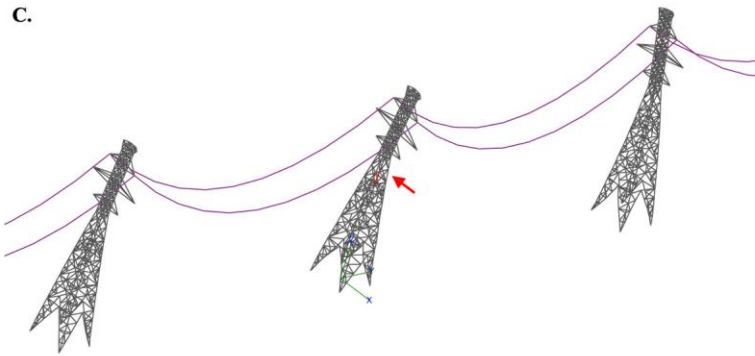
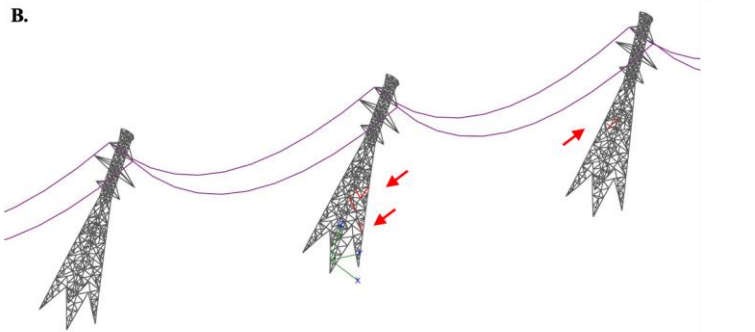
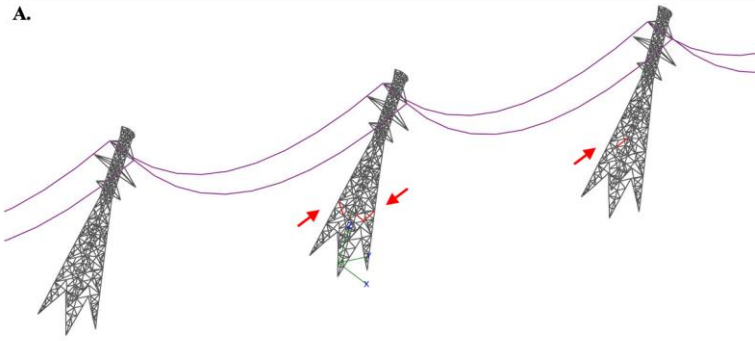
Figure 3-14: S2NL fourth mode. (A) 10%; (B) 12.5%; (C) 32.5%; (D) 35%; (E) 37.5%; (F) 40%; and (G) 42.5%.

3.4.2.1.5 The fifth failure scenario for S2 under Stockton 2005 tornado wind field

The fifth critical tornado configuration is at $R = 180$ m and $\theta = 75^\circ$ with an associated demand-to-capacity ratio, $\lambda = 9.3$. This critical configuration has the same angle as the fourth critical configuration with a closer distance to the tornado. However, it is less critical than the fourth tornado configuration. This can be interpreted by the fact that the radius of the maximum tangential velocity of the Stockton tornado is 220 m. This means that the tower is closer to the maximum tangential wind speed in the fourth critical tornado configuration compared to the fifth tornado configuration. Figure 3-15 shows the propagation of failure within the structural members of the TL towers in the transmission line. The first three members to collapse within tower 1 are diagonal bracing members that fail at 10% of the full F2 tornado load (Figure 3-15A). The progression of failure continues through tower 1 until the formation of a plastic hinge at a height of 30.1 m at 34% of the full F2 tornado load. Tower 1 fails at 40% of the full F2 tornado load at a wind speed of 44.4 m/s, which represents 63% of the maximum resultant wind speed of the full F2 tornado.

The combination of the tornado loads and the conductors' forces on tower 2 cause the formation of a plastic hinge in tower 2 at 37.5% of the full F2 tornado load. Tower 2 ultimately fails at 45% of the full F2 tornado load at a wind speed of 47 m/s, which represents 67% of the maximum resultant wind speed of the full F2 tornado.

The global tower failures within the line occur only within the towers near the tornado location (towers 1 and 2), despite that some local failures are experienced in the adjacent towers 3, 4, and 5.



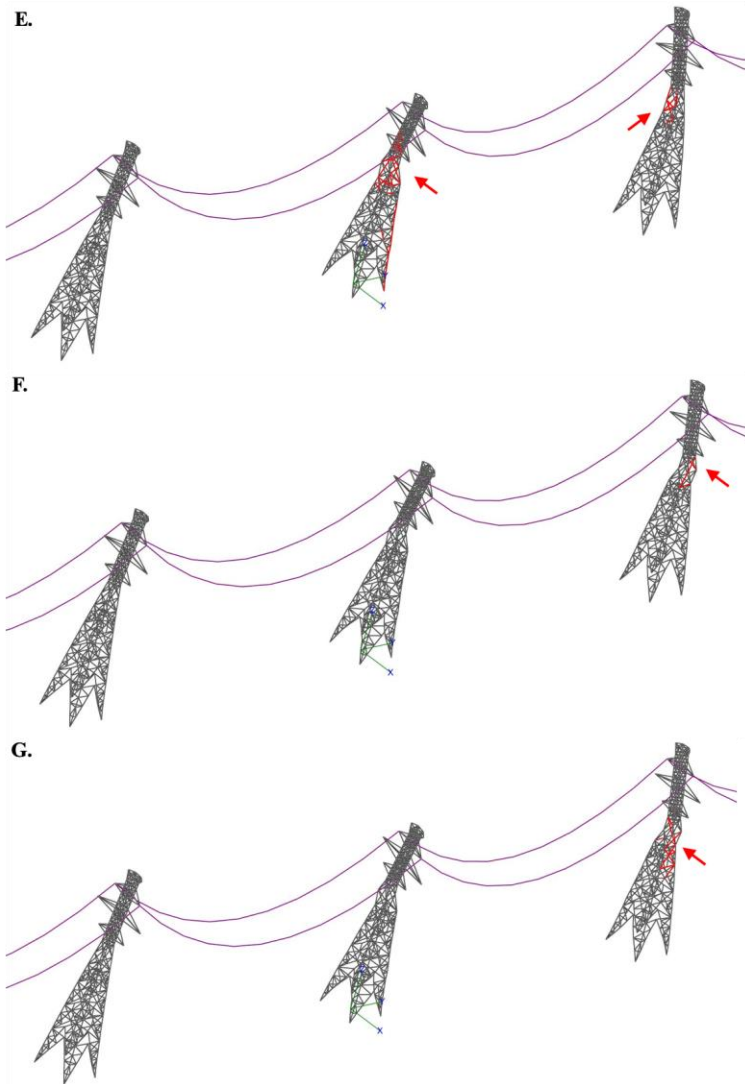


Figure 3-15: S2NL fifth mode. (A) 10%; (B) 12.5%; (C) 35%; (D) 37.5%; (E) 40%; (F) 42.5%; and (G) 45%.

3.4.2.2 The failure mode for S2 under Hangan's tornado wind field

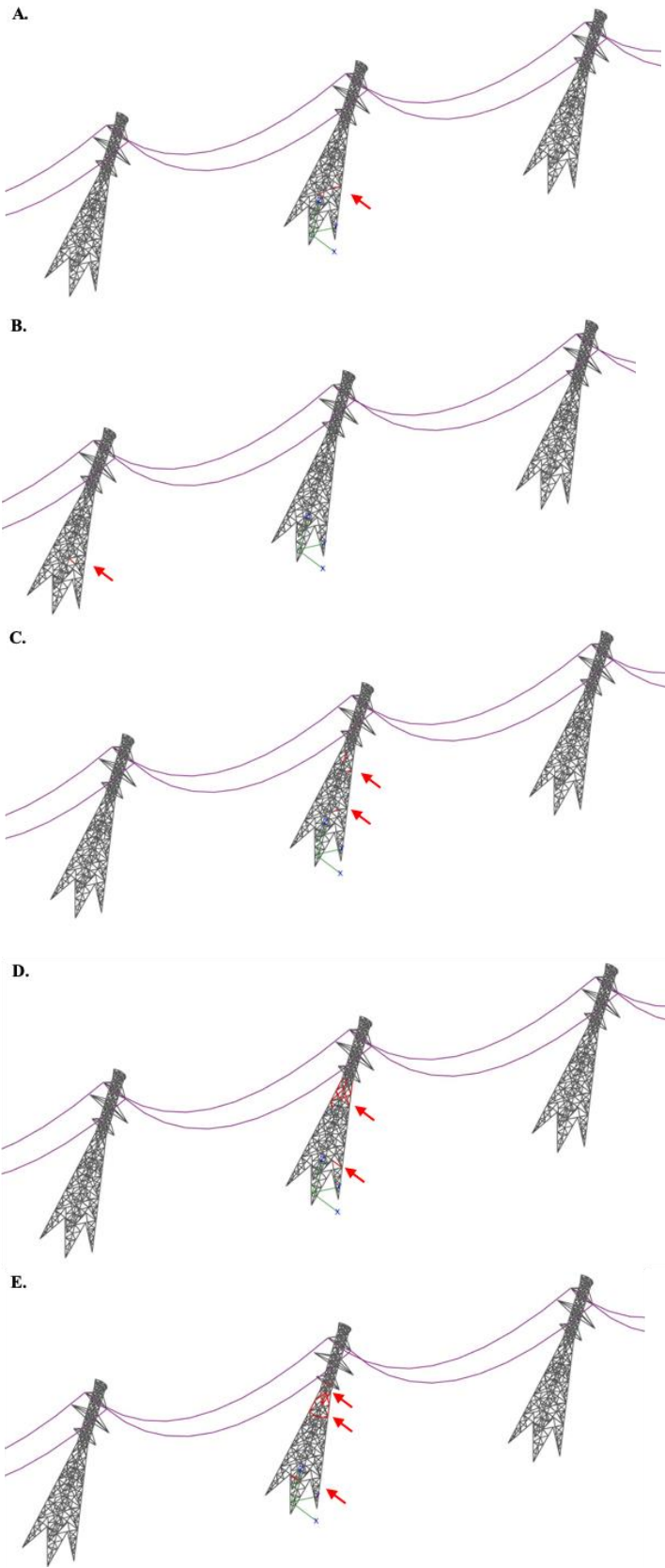
The progressive failure analysis is conducted for the S2 TL under each of the five most critical configurations of the Hangan's tornado outlined in Table 3-3. The results of the progressive failure analysis are presented in Sections 3.4.2.2.1 - 3.4.2.2.5.

3.4.2.2.1 The first failure scenario for S2 under Hangan's tornado wind field

The first critical tornado configuration is at $R = 120$ m and $\theta = 225^\circ$ with an associated demand-to-capacity ratio, $\lambda = 11$. Figure 3-16 shows the propagation of failure within the structural members of the TL towers in the transmission line. The first two members to collapse within tower 1 are diagonal bracing members that fail at 10% of the full F2 tornado load (Figure 3-16A). The progression of failure continues through tower 1 until the formation of a plastic hinge at a height of 30.1 m at 40% of the full F2 tornado load. Tower 1 fails at 45% of the full F2 tornado load at a wind speed of 47.1 m/s, which represents 67% of the maximum resultant wind speed of the full F2 tornado.

The combination of the tornado loads and the conductors' forces on tower 3 cause the formation of a plastic hinge in tower 3 at 92.5% of the full F2 tornado load. Tower 3 ultimately fails at 97.5% of the full F2 tornado load at a wind speed of 69.3 m/s, which represents 98.7% of the maximum resultant wind speed of the full F2 tornado.

The global tower failures within the line occur only within the towers near the tornado location (towers 1 and 3), despite that some local failures are experienced in the adjacent towers 2,4, and 5.



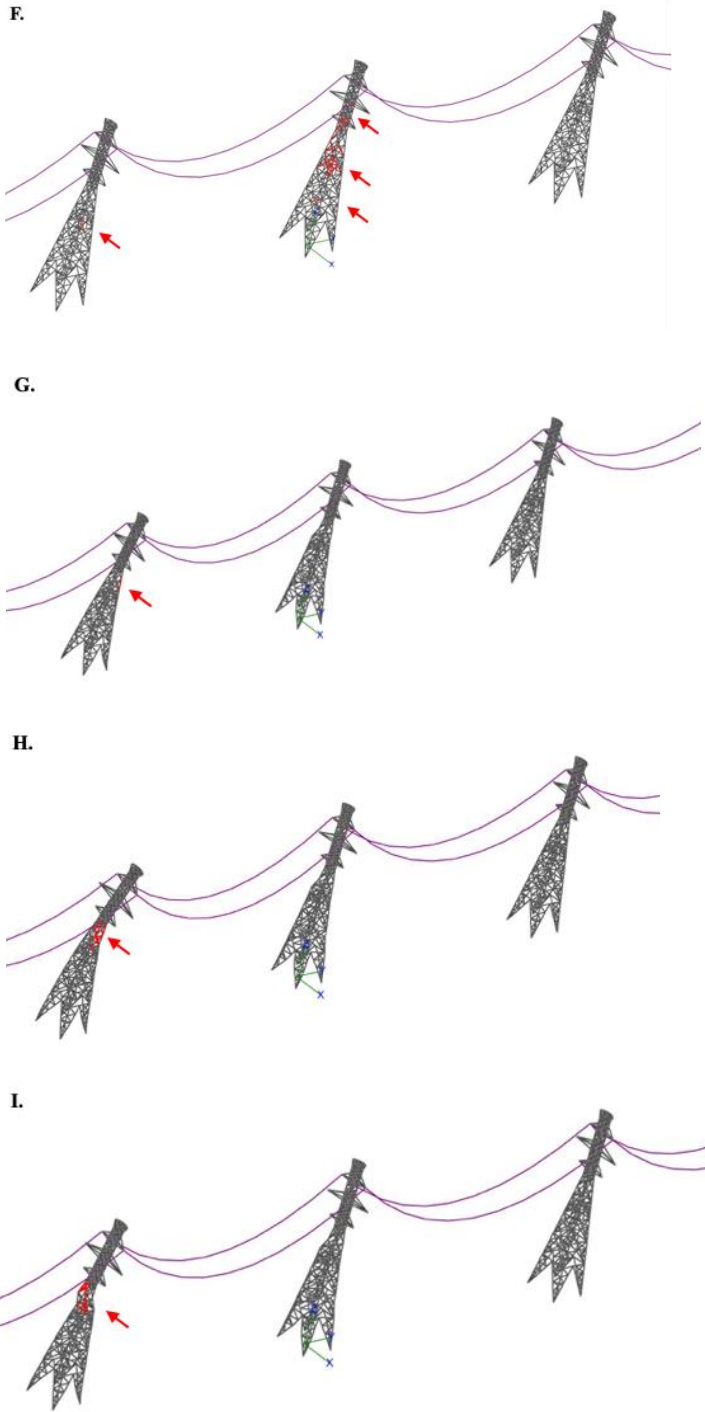
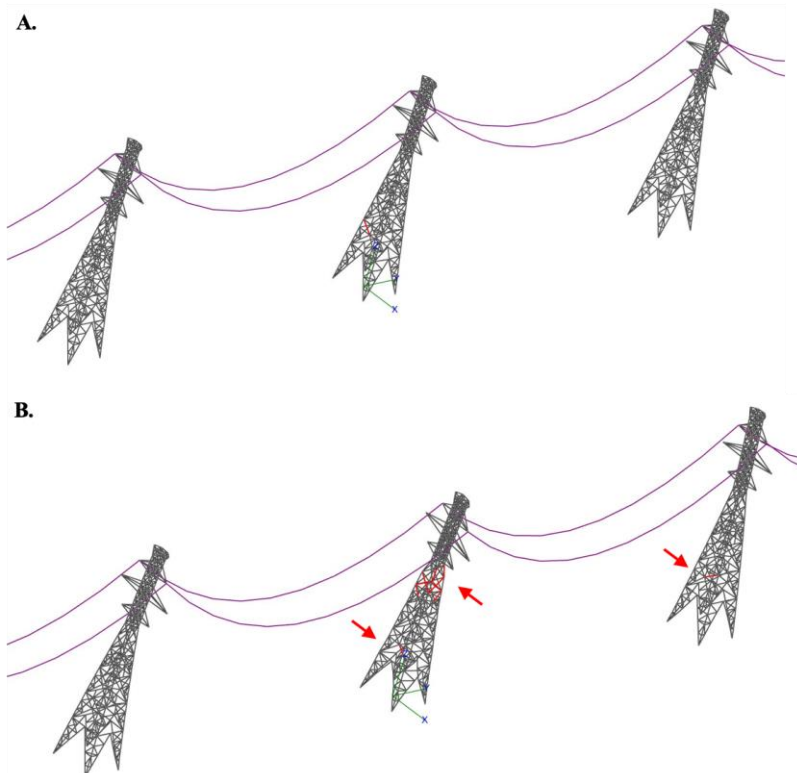


Figure 3-16: S2L first failure mode. (A) 10%; (B) 20%; (C) 40%; (D) 42.5%; (E) 45%; (F) 47.5%; (G) 92.5%; (H) 95%; and (I) 97.5%.

3.4.2.2.2 The second failure scenario for S2 under Hangan's tornado wind field

The second critical tornado configuration is at $R = 120$ m and $\theta = 45^\circ$ with an associated demand-to-capacity ratio, $\lambda = 10.8$. Figure 3-17 shows the propagation of failure within the structural members of the TL towers in the transmission line. The first member to collapse within tower 1 is a diagonal member that fails at 10% of the full F2 tornado load (Figure 3-17A). The progression of failure continues through tower 1 until the formation of a plastic hinge at a height of 30.1 m at 40% of the full F2 tornado load. Tower 1 fails at 45% of the full F2 tornado load at a wind speed of 47.1 m/s, which represents 67% of the maximum resultant wind speed of the full F2 tornado.

The global tower failures within the line occur only within tower 1, despite that some local failures are experienced in the adjacent towers 2 and 3.



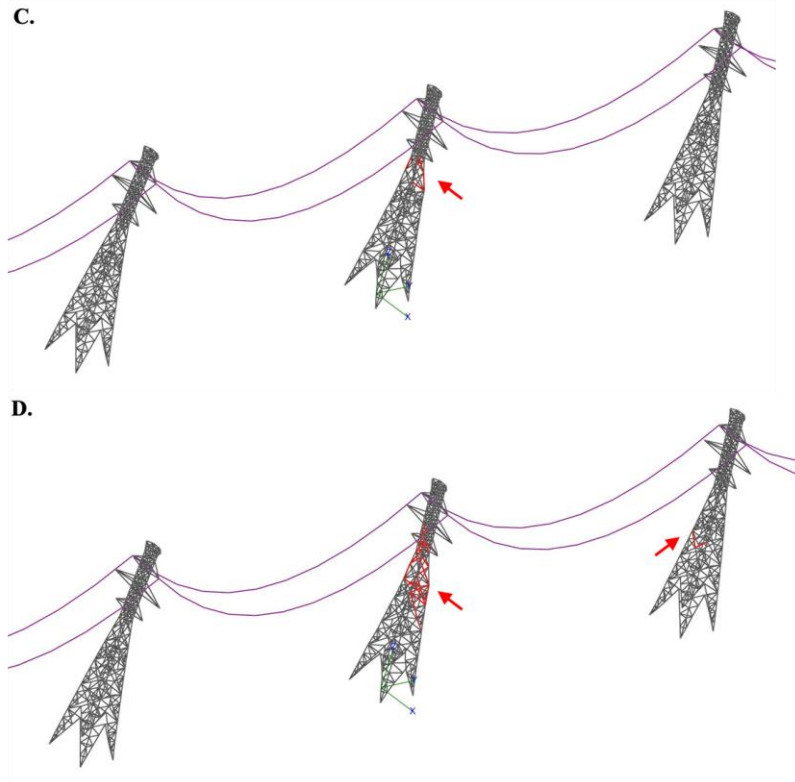


Figure 3-17: S2L second failure mode. (A) 10%; (B) 40%; (C) 42.5%; and (D) 45%.

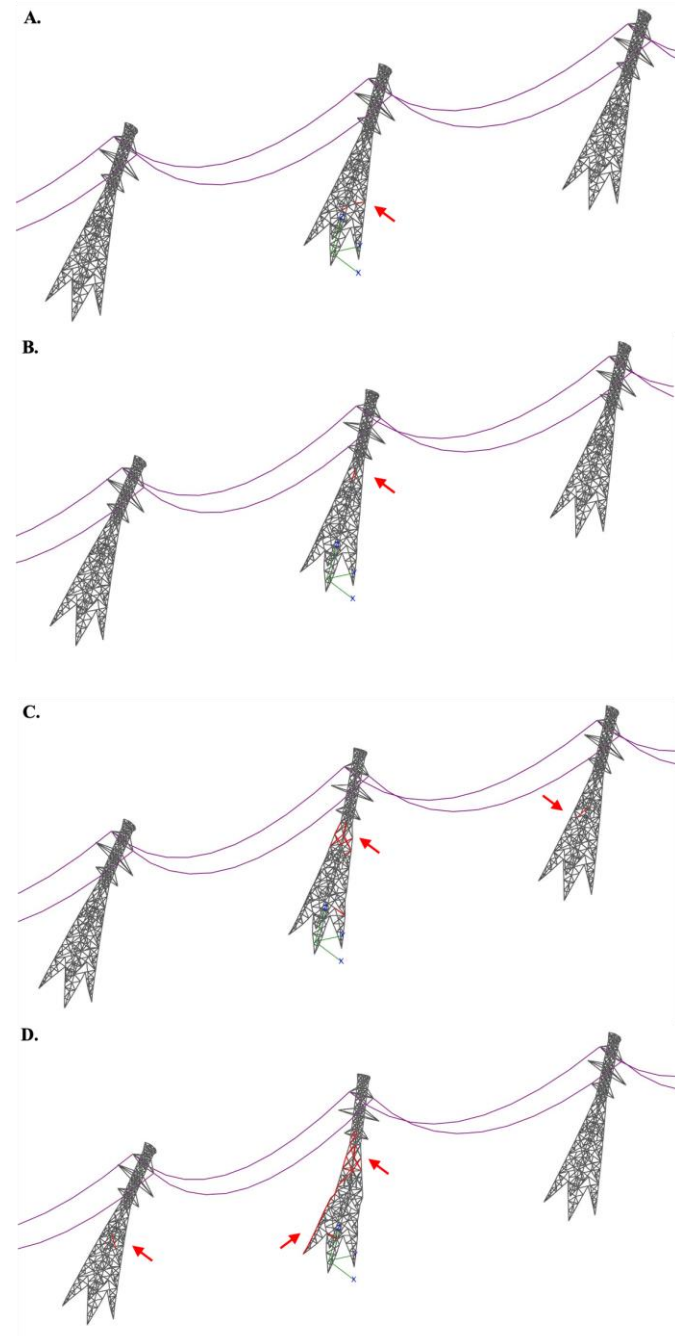
3.4.2.2.3 The third failure scenario for S2 under Hangan's tornado wind field

The third critical tornado configuration is at $R = 120$ m and $\theta = 240^\circ$ with an associated demand-to-capacity ratio, $\lambda = 9.8$. Figure 3-18 shows the propagation of failure within the structural members of the TL towers in the transmission line. The first two members to collapse within tower 1 are diagonal bracing members that fail at 10% of the full F2 tornado load (Figure 3-18A). The progression of failure continues through tower 1 until the formation of a plastic hinge at a height of 19.8 m at 40% of the full F2 tornado load. Tower 1 fails at 47.5% of the full F2 tornado load at a wind speed of 48.4 m/s, which represents 69% of the maximum resultant wind speed of the full F2 tornado.

The combination of the tornado loads and the conductors' forces on tower 3 cause the formation of a plastic hinge in tower 3 at 47.5% of the full F2 tornado load. Tower 3

ultimately fails at 55% of the full F2 tornado load at a wind speed of 52 m/s, which represents 74% of the maximum resultant wind speed of the full F2 tornado.

The global tower failures within the line occur only within the towers near the tornado location (towers 1 and 3), despite that some local failures are experienced in the adjacent towers 2, 4, and 5.



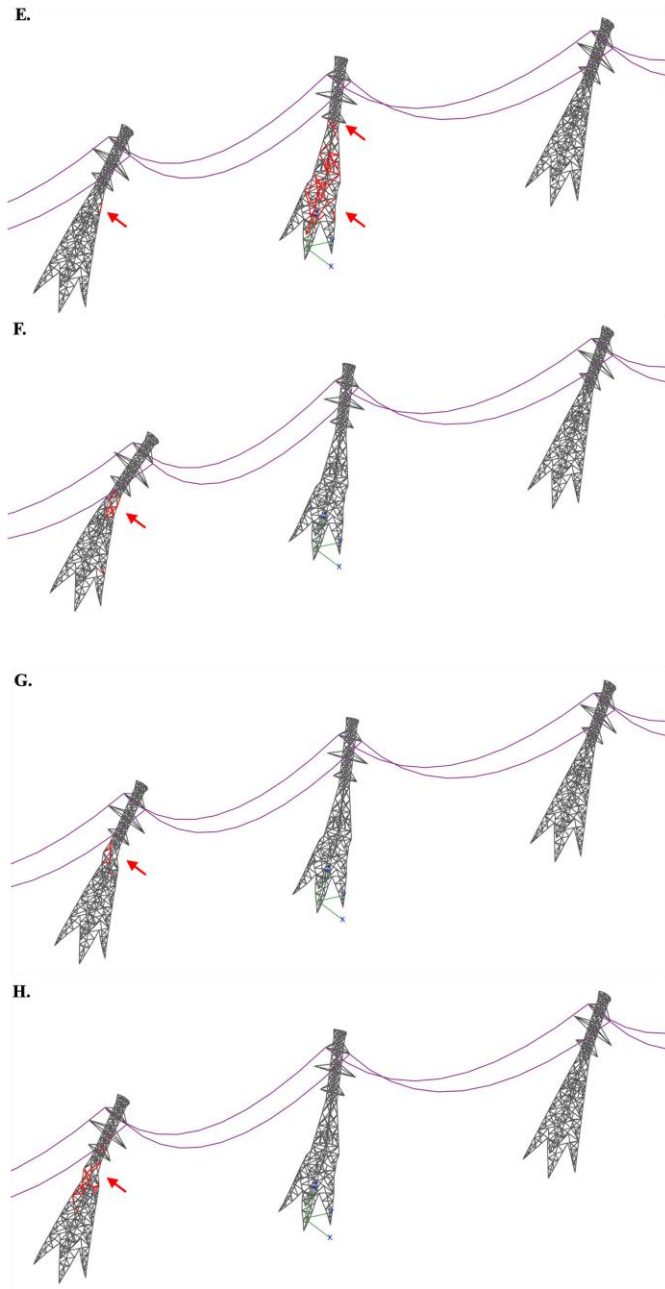


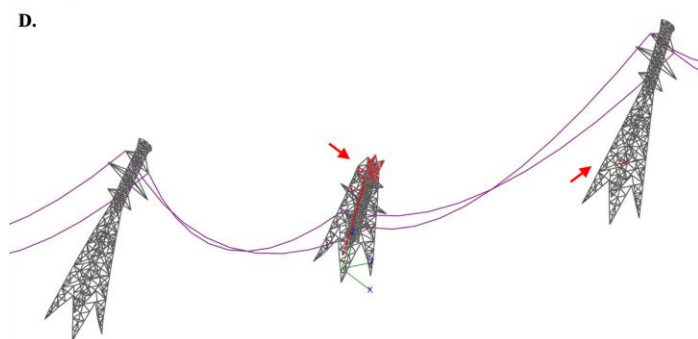
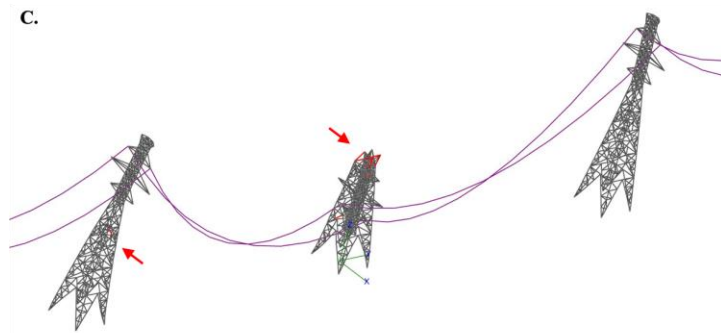
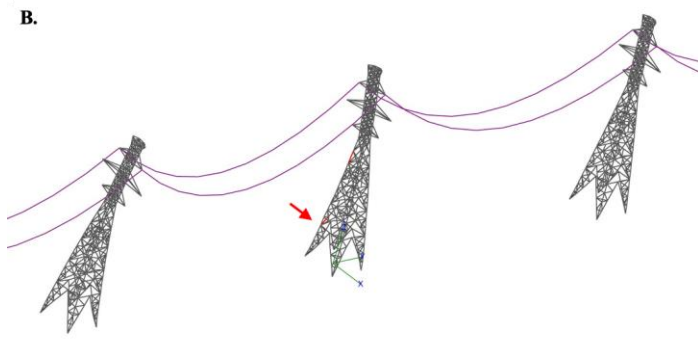
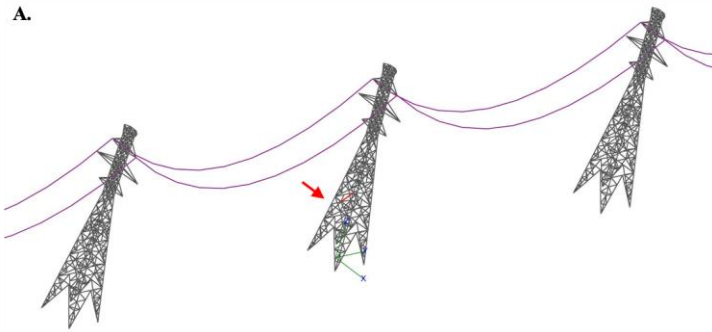
Figure 3-18: S2L third failure mode. (A) 10%; (B) 40%; (C) 42.5%; (D) 45%; (E) 47.5%; (F) 50%; (G) 52.5%; and (H) 55%.

3.4.2.2.4 The fourth failure scenario for S2 under Hangan's tornado wind field

The fourth critical tornado configuration is at $R = 120$ m and $\theta = 285^\circ$ with an associated demand-to-capacity ratio, $\lambda = 9.4$. Figure 3-19 shows the propagation of failure within the structural members of the TL towers in the transmission line. The first member to collapse within tower 1 is a diagonal member that fails at 10% of the full F2 tornado load (Figure 3-19A). The progression of failure continues through tower 1 until the formation of a plastic hinge at a height of 30.1 m at 40% of the full F2 tornado load. Tower 1 fails at 42.5% of the full F2 tornado load at a wind speed of 45.7 m/s, which represents 65.2% of the maximum resultant wind speed of the full F2 tornado.

The combination of the tornado loads and the conductors' forces on tower 3 cause the formation of a plastic hinge in tower 3 at 60% of the full F2 tornado load. Tower 3 ultimately fails at 67.5% of the full F2 tornado load at a wind speed of 57.7 m/s, which represents 85% of the maximum resultant wind speed of the full F2 tornado.

The global tower failures within the line occur only within the towers near the tornado location (towers 1 and 3), despite that some local failures are experienced in the adjacent towers 2, 4, and 5.



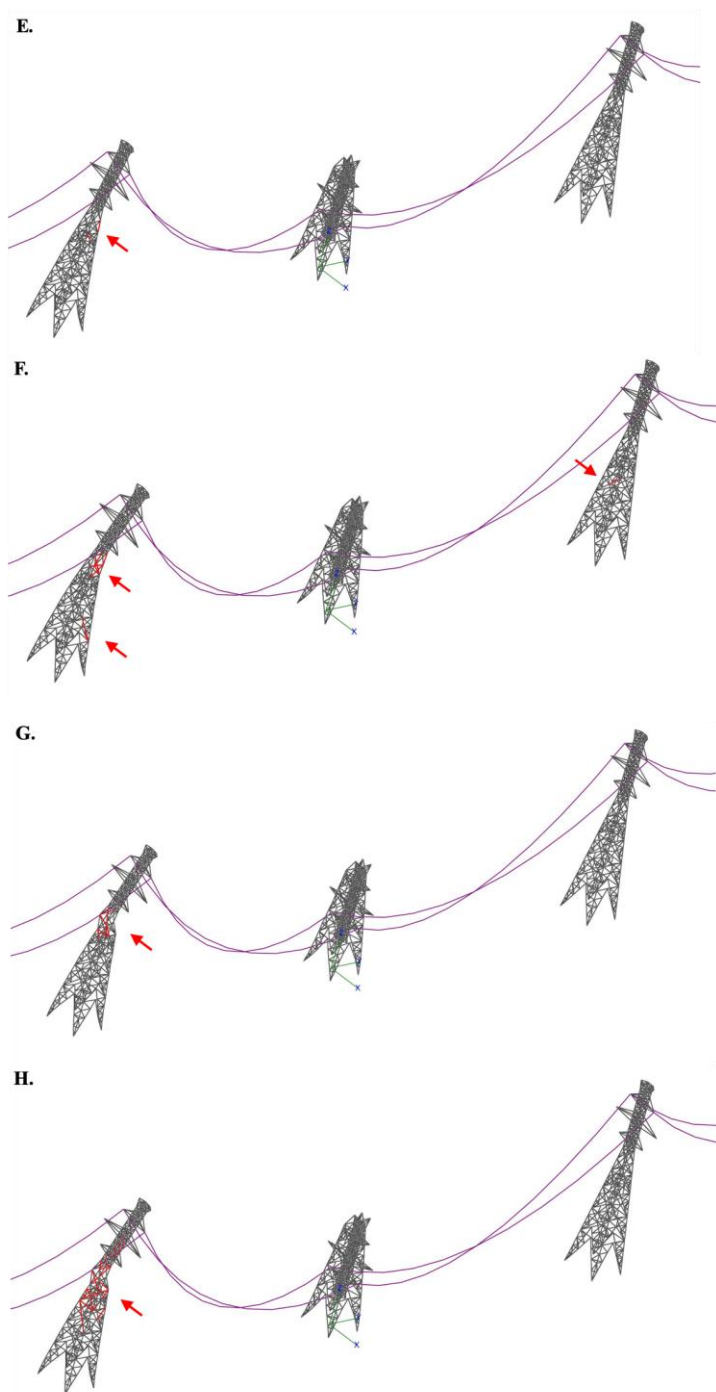
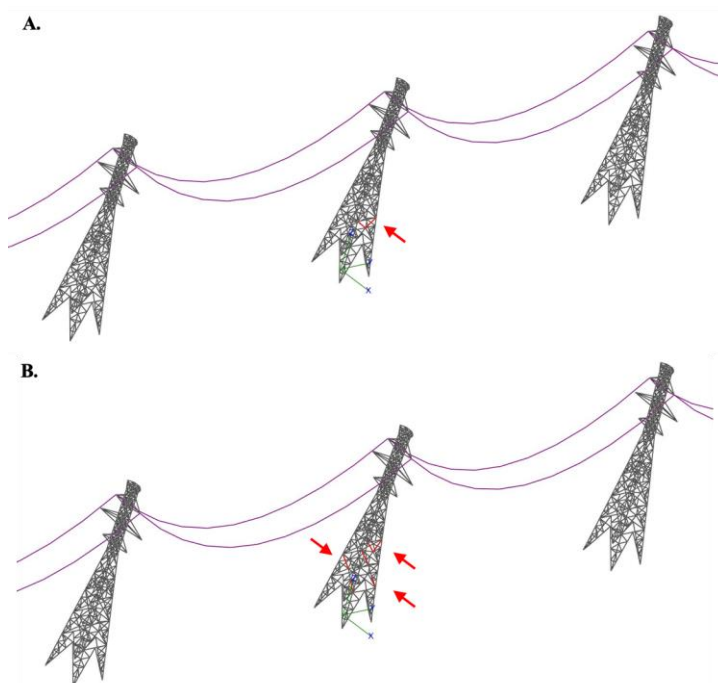


Figure 3-19: S2L fourth failure mode. (A) 10%; (B) 40%; (C) 42.5%; (D) 45%; (E) 60%; (F) 62.5%; (G) 65%; and (H) 67.5%.

3.4.2.2.5 The fifth failure scenario for S2 under Hangan's tornado wind field
The fifth critical tornado configuration is at $R = 160$ m and $\theta = 75^\circ$ with an associated demand-to-capacity ratio, $\lambda = 9.3$. Figure 3-20 shows the propagation of failure within the structural members of the TL towers in the transmission line. The first two members to collapse within tower 1 are diagonal bracing members that fail at 10% of the full F2 tornado load (Figure 3-20A). The progression of failure continues through tower 1 until the formation of a plastic hinge at a height of 30.1 m at 40% of the full F2 tornado load. Tower 1 fails at 42.5% of the full F2 tornado load at a wind speed of 45.7 m/s, which represents 65.2% of the maximum resultant wind speed of the full F2 tornado.

The combination of the tornado loads and the conductors' forces on tower 2 cause the formation of a plastic hinge in tower 2 at 40% of the full F2 tornado load. Tower 2 ultimately fails at 47.5% of the full F2 tornado load at a wind speed of 48.4 m/s, which represents 69% of the maximum resultant wind speed of the full F2 tornado.

The global tower failures within the line occur only within the towers near the tornado location (towers 1 and 2), despite that some local failures are experienced in the adjacent towers 3,4, and 5.



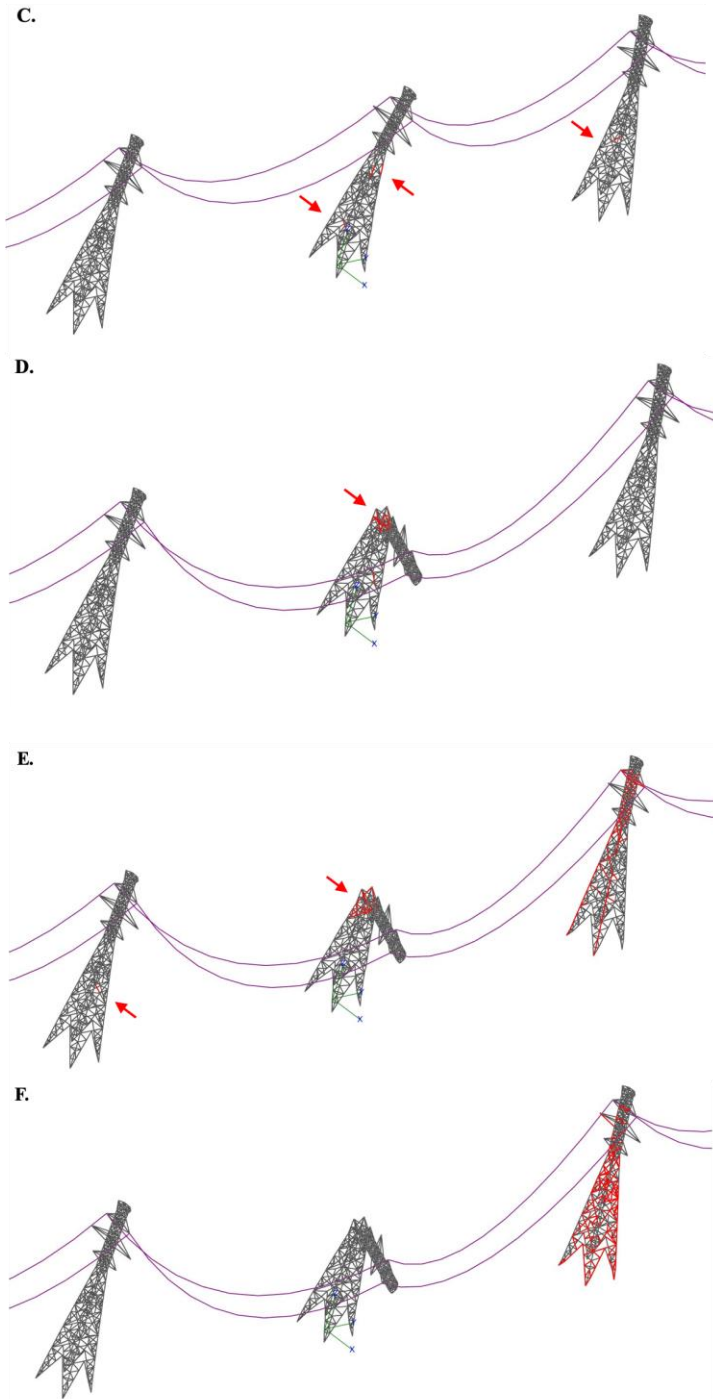


Figure 3-20: S2L fifth failure mode. (A) 10%; (B) 12.5%; (C) 40%; (D) 42.5%; (E) 45%; and (F) 47.5%.

3.4.2.3 Summary of the Progressive Failure Analysis Results

Table 3-6 and Table 3-7 summarize the results of the progressive failure analysis presented in sections 3.4.2.1 - 3.1.1.1 for S2 TL. For each of the five most critical configurations, the highlights of the failure progression under Stockton [24] and Hangan's [2] tornado wind fields are presented. These highlights include the progression of failure through towers 1, 2, and 3 by reporting: i) the load at which the members start to collapse (failure initiation); ii) the load at which the plastic hinge is formed; iii) the failure load; iv) failure wind speed; v) location of the failed segment of the tower by reporting Z_{ph} (m), θ_F (° in degrees), and θ_D (° in degrees). θ_F is an angle in the vertical plane perpendicular to the TL. θ_F is measured between the projection of the collapsed segment of the tower on the plane and the centerline of the tower. On the other hand, θ_D is an angle in the horizontal plane that is measured between the projection of the collapsed segment of the tower on the plane and the centerline of the tower.

As shown in Table 3-6 and Table 3-7, all the collapsed towers fail at smaller failure loads under Stockton tornado compared to the failure loads under Hangan's tornado. This indicates that the Stockton tornado wind field is more critical than Hangan's tornado even though both tornado wind fields are scaled so that they have the same resultant horizontal wind speeds. The results also indicate that only the tower of interest and an adjacent tower collapse within the entire TL under any of the tornado configurations. It can also be concluded that the critical configuration parameters (R , θ) vary between the two tornado wind fields. This proves that the critical configurations are dependent on the tornado wind field characteristics such as the tornado path width.

Table 3-6: Summary of the progressive failure analysis results for S2 TL under the Stockton 2005 tornado wind field.

	Critical tornado configuration (R, θ, λ)	Scenario 1 (200 m, 30°, 11)			Scenario 2 (260 m, 75°, 10.5)			Scenario 3 (200 m, 210°, 10.3)			Scenario 4 (240 m, 75°, 9.9)			Scenario 5 (180 m, 75°, 9.3)		
	Tower	T1	T2	T3	T1	T2	T3	T1	T2	T3	T1	T2	T3	T1	T2	T3
Stockton 2005 tornado [24]	Failure initiation (% of F2 tornado load)	10	17.5	17.5	10	10	25	12.5	17.5	17.5	10	10	25	10	10	20
	Load at plastic hinge formation (% of F2 tornado load)	32.5	67.5	-	32.5	37.5	-	32.5	-	62.5	32.5	37.5	-	34	37.5	-
	Failure load (% of F2 tornado load)	40	72.5	-	37.5	40	-	40	-	70	37.5	42.5	-	40	45	-
	Failure wind speed (m/s)	44.4	59.8	-	43	44.4	-	44.4	-	58.7	43	45.7	-	44.4	47	-
	Failure wind speed (% of F2 tornado wind speed)	63	85	-	61	63	-	63	-	84	61	65	-	63	67	-
	Z_{ph} (m)	30.1	30.1	-	30.1	17.7	-	30.1	-	30.1	30.1	30.1	-	30.1	30.1	-
	θ_F (°)	10	10	-	105	10	-	10	-	10	35	10	-	20	10	-
	θ_D (°)	188	167	-	256	162	-	27	-	350	253	148	-	237	157	-

Table 3-7: Summary of the progressive failure analysis results for S2 TL under Hangan’s tornado wind field.

	Critical tornado configuration (R, θ , λ)	Scenario 1 (120 m, 225°, 11)			Scenario 2 (120 m, 45°, 10.8)			Scenario 3 (120 m, 240°, 9.8)			Scenario 4 (120 m, 285°, 9.4)			Scenario 5 (160 m, 75°, 9.3)		
		T1	T2	T3	T1	T2	T3	T1	T2	T3	T1	T2	T3	T1	T2	T3
Hangan’s tornado wind field [2]	Tower															
	Failure initiation (% of F2 tornado load)	10	27.5	20	10	25	27.5	10	32.5	17.5	10	37.5	15	10	15	35
	Load at plastic hinge formation (% of F2 tornado load)	40	-	92.5	40	-	-	40	-	47.5	40	-	60	40	40	-
	Failure load (% of F2 tornado load)	45	-	97.5	45	-	-	47.5	-	55	42.5	-	67.5	42.5	47.5	-
	Failure wind speed (m/s)	47.1	-	69.3	47.1	-	-	48.4	-	52	45.7	-	57.7	45.7	48.4	-
	Failure wind speed (% of F2 tornado wind speed)	67	-	98.7	67	-	-	69	-	74	65.2	-	85	65.2	69	-
	Z_{ph} (m)	30.1	-	30.1	30.1	-	-	19.8	-	30.1	30.1	-	30.1	30.1	2.3	-
	θ_F (°)	10	-	10	10	-	-	20	-	10	180	-	15	105	5	-
θ_D (°)	42	-	335	203	-	-	69	-	356	93	-	316	256	170	-	

3.5 Effect of insulator length on the propagation of failure within the TL system

As the numerical tool can successfully examine the progressive failure in the TL line as a unit, it can be used to investigate the effect of different components in the TL on the progression of failure within the line. Specifically, the effect of changing the insulator length is examined by conducting progressive failure analysis of S2 TL with different insulator lengths varying from 0.1 – 5 m under Hangan’s F2 tornado wind field [2]. Figure 3-21 summarizes the results of the study by looking into the variation of the failure load, as a percentage of the full F2 tornado load. The failure load is reported for towers 1 and 3 in the two tornado critical configurations $R = 120$ m, $\theta = 225^\circ$ and $R = 120$ m, $\theta = 285^\circ$. Figure 3-21 demonstrates that the insulator length greatly affects the failure load of the adjacent towers. Increasing the insulator length from 0.1 to 2.438 m, which is the insulator length used in the design of the tower, increases the resilience of the line where tower 3 sustains 100% of the F2 tornado load instead of 40% under tornado critical configuration $R = 120$ m, $\theta = 225^\circ$. In the case of $R = 120$ m, $\theta = 285^\circ$, increasing the insulator length from 1 m to 5 m increases the resilience of the line where tower 3 sustains 75% of the full F2 tornado load instead of 50%. However, the results show that tower 1 is not greatly affected by the change in insulator length, which can be interpreted by the fact that the reported critical configurations are the most critical configurations for tower 1 where the tornado is at a closer distance to tower 1. Hence, the straining actions caused by the tornado wind field directly on the tower members have a bigger impact compared to conductors’ reactions.

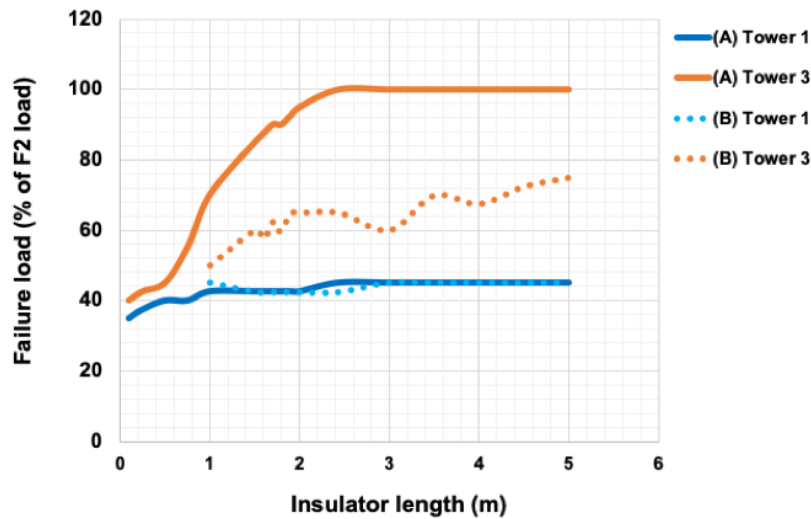


Figure 3-21: Effect of insulator length on the failure load of the transmission line. [(A) Critical scenario: $R = 120$ m, $\theta = 225^\circ$; (B) Critical scenario: $R = 120$ m, $\theta = 285^\circ$].

To summarize, the insulator length is an important component that can be used to control the propagation of failure under tornadoes within one tower among the line preventing the domino effect failure of TL towers.

Moreover, Figure 3-22 shows the effect of insulator length on the demand-to-capacity ratio, λ , for tower 1 under the two tornado critical configurations $R = 120$ m, $\theta = 225^\circ$ and $R = 120$ m, $\theta = 285^\circ$ associated with Hangan's F2 tornado wind field. The insignificant change, ranging between 5 – 15%, can be interpreted by the fact that the reported critical configurations are the most critical configurations for tower 1 where the tornado is at a closer distance to tower 1. Hence, the straining actions caused by the tornado wind field directly on the tower members have a bigger impact compared to conductors' reactions. It also shows that the effect of the insulator length is dependent on the location of the tornado relative to the tower.

To conclude, the parametric study shows the decreasing trend in the peak demand-to-capacity ratio as the insulator length increase. However, the percentage of decrease is relatively low.

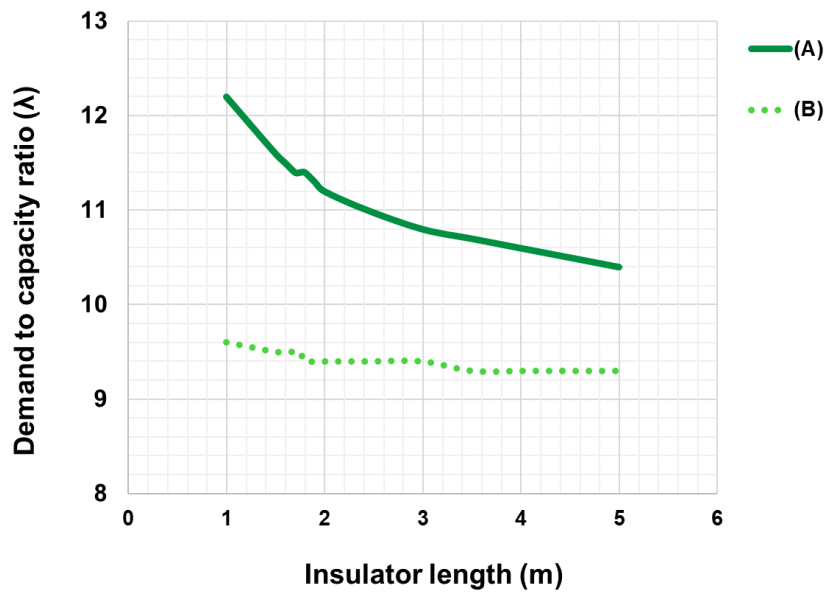


Figure 3-22: Effect of insulator length on the peak capacity ratio, λ , of the transmission line. [(A) Critical scenario: $R = 120$ m, $\theta = 225^\circ$; (B) Critical scenario: $R = 120$ m, $\theta = 285^\circ$].

3.6 Effect of Span length on the propagation of failure within the TL system

An extensive parametric study is conducted using the software to investigate the effect of changing the span on the progression of failure of TL towers within the S2 TL under Hangan’s F2 tornado wind field [2]. The parametric study is covering a range of spans from 300 – 600 m with an increment of 25 m. This range of spans covers the most common spans used in the industry. While changing the span, the percentage of sag: span ratio is kept constant at 0.03 and 0.04 for the ground wires and the conductors, respectively.

Table 3-8: Ground wires and conductors’ sag used in the parametric study.

Span (m)	Ground wires sag (m)	Conductors sag (m)
300.00	9.33	12.67
325.00	10.11	13.72
350.00	10.89	14.78
375.00	11.67	15.83
400.00	12.44	16.89
425.00	13.22	17.94
450.00	14.00	19.00
475.00	14.78	20.06
500.00	15.56	21.11
525.00	16.33	22.17
550.00	17.11	23.22
575.00	17.89	24.28
600.00	18.67	25.33

Figure 3-23 and Figure 3-24 show the effect of changing the span length on the failure load and wind speed of the TL towers within the TL. The results demonstrate that by increasing the span, the failure load and wind speed of the adjacent tower (Tower 3 in Scenario 1 (Figure 3-23A); Tower 2 in Scenario 2 (Figure 3-23B)) near the tornado location are significantly changed. However, the failure load of tower 1 is unaffected and the tower far

from the tornado does not fail. This can be interpreted by the fact that the distance between the adjacent towers and the tornado increase. Hence, the loads transferred to the adjacent tower members directly from the tornado are reduced.

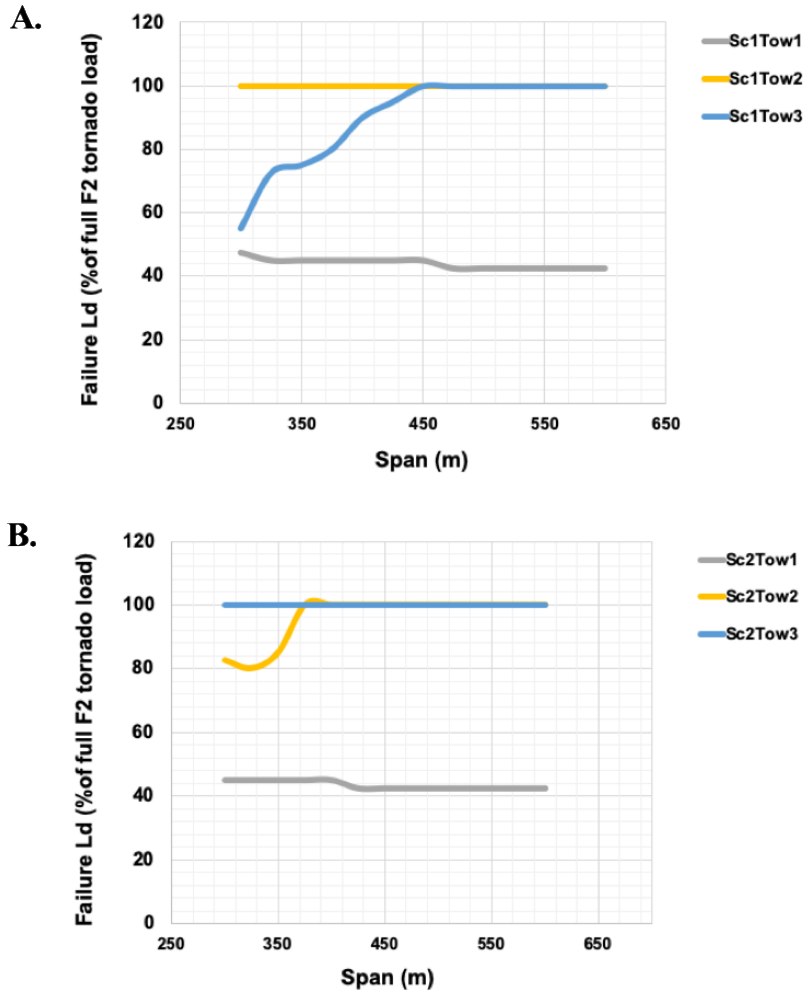


Figure 3-23: Effect of span on the failure load of the transmission line. (A) Critical scenario: $R = 120$ m, $\theta = 225^\circ$; (B) Critical scenario: $R = 120$ m, $\theta = 45^\circ$. [*Sc* = Scenario; *Tow* = Tower].

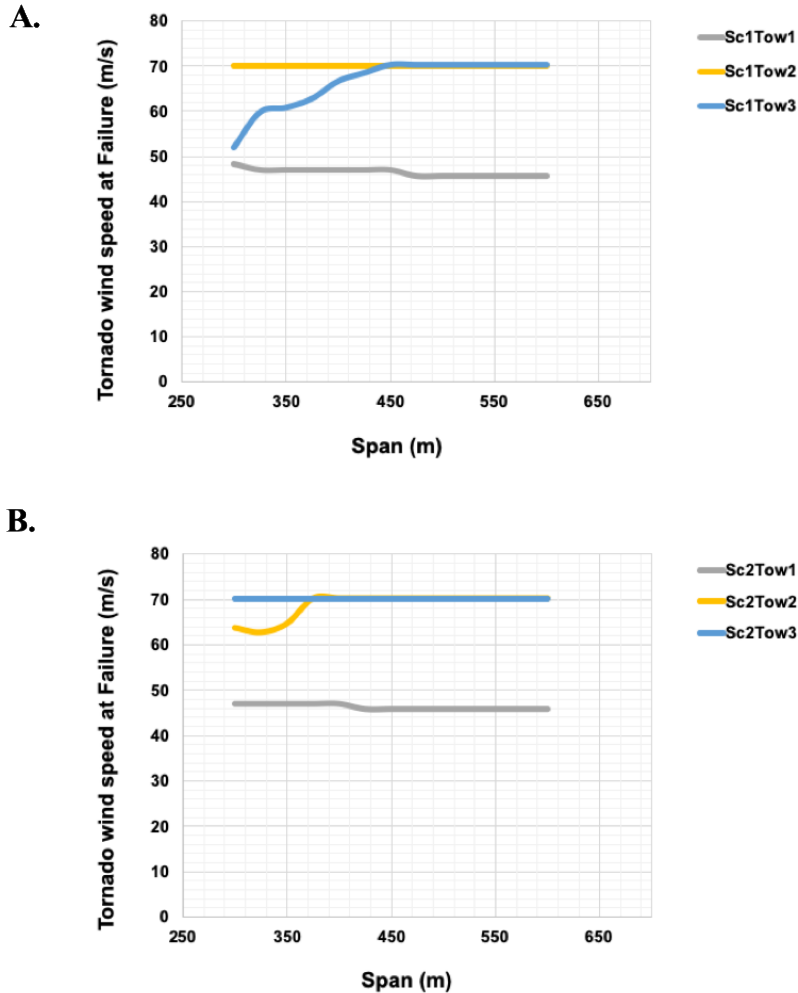


Figure 3-24: Effect of span on the tornado wind speed at failure of the transmission line towers. (A) Critical scenario: $R = 120$ m, $\theta = 225^\circ$; (B) Critical scenario: $R = 120$ m, $\theta = 45^\circ$. [*Sc* = Scenario; *Tow* = Tower].

Figure 3-25 shows the increasing trend in the demand-to-capacity ratio of the tower of interest by increasing the span. However, the results also demonstrate that λ is not significantly changed by changing the span, which can be interpreted by the fact that the reported critical configurations are the most critical configurations for tower 1 where the tornado is at a closer distance to tower 1. Hence, the straining actions caused by the tornado wind field directly on the tower members have a bigger impact compared to conductors'

reactions. The study also concludes that the change in the span length doesn't affect the post-failure geometry of the subject tower.

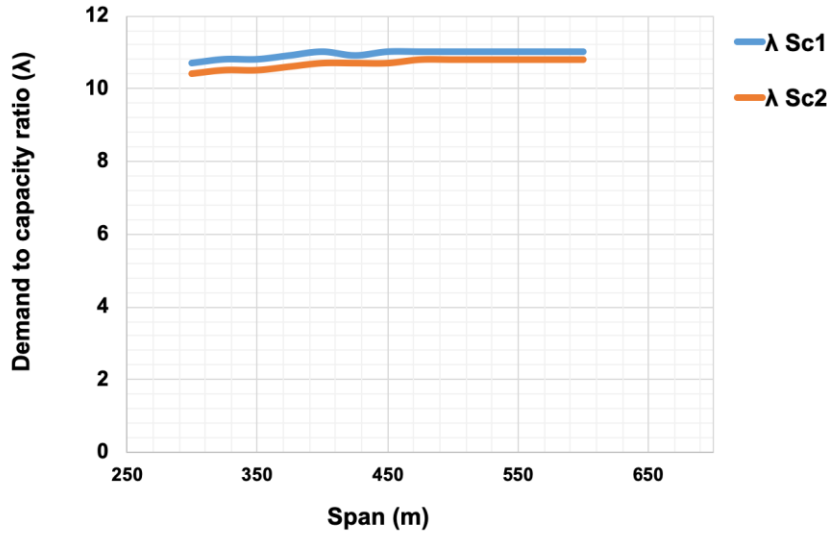


Figure 3-25: Effect of insulator length on the peak capacity ratio, λ , of the transmission line under two critical scenarios: $R = 120$ m, $\theta = 225^\circ$ (Sc1) and $R = 120$ m, $\theta = 45^\circ$ (Sc2). [*Sc* = Scenario].

To conclude, the change in the span length mainly affects the failure of the adjacent towers more than the subject tower.

3.7 Conclusion

A non-linear finite element analysis integrated with CFD models has been utilized in the current study to investigate the progressive failure of multiple self-supported TL towers within a TL system under two different tornado wind fields.

An extensive parametric study is conducted to identify the critical tornado configurations by varying the location of the tornado relative to the studied tower. Considering the identified critical configurations, progressive failure analysis is conducted for a TL system composed of eight spans and seven towers designed and constructed following current code provisions to resist synoptic normal wind loading.

The results of the parametric study, as well as the progressive failure analysis, are reported for each tower. The results include the critical configuration of the tornado with respect to the structure, associated failure load, and a description of the failure mode. The study is then repeated to investigate the difference in the progression of failure in the TL towers under a different tornado wind field. The study demonstrates that none of the investigated towers can sustain the full load produced by the various F2 tornado wind fields. However, the failure is contained within the subject tower and the next two adjacent towers.

Moreover, the effect of the insulator's length on the progression of failure of the towers within the line is investigated. The study concludes that the length of the insulators significantly affects the failure load of the adjacent towers. It can be used to control the propagation of failure under tornadoes within one tower among the line. The results of the case study presented in this paper show that increasing the insulator length from 0.1 to 2.438 m, which is the insulator length used in the design of the investigated tower, increases the resilience of the line where the adjacent tower sustains 100% of the F2 tornado load instead of 40% under tornado critical configuration $R = 120$ m, $\theta = 225^\circ$. In the case of $R = 120$ m, $\theta = 285^\circ$, increasing the insulator length from 1 m to 5 m increases the resilience of the line where the adjacent tower sustains 75% of the full F2 tornado load instead of 50%.

Lastly, a parametric study is conducted to investigate the effect of changing the span on the progressive failure of the TL towers within the line. The parametric study includes the

range of spans within 300 m – 600 m. The effect of changing the span on the failure load, peak demand-to-capacity ratio, and the post-failure geometry is reported. The results of the parametric studies under the investigated critical tornado configurations show that the change in the span length mainly affects the failure of the adjacent towers more than the subject tower. The study also concludes that the change in the span length doesn't affect the post-failure geometry of the subject tower. The parametric study results show that designing TLs with larger spans increases the resilience of the TL under the studied cases as it increases the failure load of the adjacent towers.

3.8 References

- [1] H. B. Ishac, M.F.; White, “Effect of tornado loads on transmission lines,” in *IEEE Transactions on Power Delivery*, 1995, p. Volume: 10; Issue: 1; pages: 445-451.
- [2] H. Hangan and J. D. Kim, “Swirl ratio effects on tornado vortices in relation to the Fujita scale,” *Wind Struct.*, vol. 11, pp. 291–302, Aug. 2008, doi: 10.12989/was.2008.11.4.291.
- [3] E. O. of the President, “White House 2013 - Grid Resiliency and Economic Benefit,” 2013.
- [4] T. T. Fujita, “Tornadoes and Downbursts in the Context of Generalized Planetary Scales,” *Journal of the Atmospheric Sciences*, vol. 38, no. 8. pp. 1511–1534, 1981, doi: 10.1175/1520-0469(1981)038<1511:TADITC>2.0.CO;2.
- [5] T. T. Fujita, “Proposed Characterization of Tornadoes and Hurricanes by Area and Intensity,” *SMRP, Univ. Chicago*, vol. 91, p. 42, 1971.
- [6] Fujita and D. Pearson, “Results of FPP classification of 1971 and 1972 tornadoes,” *Am. Meteorol. Soc.*, pp. 142–145, 1973.
- [7] M. J. Newark, “Canadian tornadoes, 1950–1979,” *Atmos. - Ocean*, vol. 22, no. 3, pp. 343–353, 1984, doi: 10.1080/07055900.1984.9649203.
- [8] J. Sarkar, P., Haan, F., Gallus, Jr., W., Le, K. and Wurman, “Velocity measurements in a laboratory tornado simulator and their comparison with numerical and full-scale data,” in *37th Joint Meeting Panel on Wind and Seismic Effects*.
- [9] W. C. Lee and J. Wurman, “Diagnosed three-dimensional axisymmetric structure of the Mulhall tornado on 3 May 1999,” *J. Atmos. Sci.*, vol. 62, no. 7 II, pp. 2373–2393, 2005, doi: 10.1175/JAS3489.1.
- [10] C. A. Wan and C. C. Chang, “Measurement of the Velocity Field in a Simulated Tornado-Like Vortex Using a Three-Dimensional Velocity Probe,” *Journal of the Atmospheric Sciences*, vol. 29, no. 1. pp. 116–127, 1972, doi: 10.1175/1520-0469(1972)029<0116:motvfi>2.0.co;2.

- [11] N. B. Ward, “The exploration of certain features of tornado dynamics using a laboratory model,” *J. Atmos. Sci.*, vol. 29, pp. 1194–1204, 1972.
- [12] R. P. Davies-Jones, “The Dependence of Core Radius on Swirl Ratio in a Tornado Simulator,” *Journal of the Atmospheric Sciences*, vol. 30, no. 7, pp. 1427–1430, 1973, doi: 10.1175/1520-0469(1973)030<1427:tdocro>2.0.co;2.
- [13] C. R. Church, J. T. Snow, and E. M. Agee, “Tornado Vortex Simulation at Purdue University,” *Bull. Am. Meteorol. Soc.*, vol. 58, no. 9, pp. 900–908, 1977, doi: 10.1175/1520-0477(1977)058<0900:tvsapu>2.0.co;2.
- [14] E. M. Church, C. R., Snow, J. T., Baker, G. L. and Agee, “Characteristics of tornado-like vortices as a function of swirl ratio: A laboratory investigation,” *J. Atmos. Sci.*, vol. 36, pp. 1755–1776, 1979.
- [15] G. L. Baker and C. R. Church, “Measurements of the core radii and peak velocities in modeled atmospheric vortices,” *J. Atmos. Sci.*, vol. 36, no. 12, Dec. 1979, pp. 2413–2424, 1979.
- [16] R. Rotunno, “A study in tornado like vortex dynamics,” *J. Atmos. Sci.*, vol. 36, no. 1, Jan. 1979, pp. 140–155, 1979.
- [17] W. S. Lewellen, “A solution for three-dimensional vortex flows with strong circulation,” *J. Fluid Mech.*, vol. 14, no. 3, pp. 420–432, 1962, doi: 10.1017/S0022112062001330.
- [18] W. S. Lewellen, D. C. Lewellen, and R. I. Sykes, “Large-Eddy simulation of a tornado’s interaction with the surface,” *J. Atmos. Sci.*, vol. 54, no. 5, pp. 581–605, 1997, doi: 10.1175/1520-0469(1997)054<0581:LESOAT>2.0.CO;2.
- [19] D. C. Lewellen, W. S. Lewellen, and J. Xia, “The influence of a local swirl ratio on tornado intensification near the surface,” *J. Atmos. Sci.*, vol. 57, no. 4, pp. 527–544, 2000, doi: 10.1175/1520-0469(2000)057<0527:TIOALS>2.0.CO;2.
- [20] D. C. Lewellen and W. S. Lewellen, “Near-surface intensification of tornado vortices,” *J. Atmos. Sci.*, vol. 64, no. 7, pp. 2176–2194, 2007, doi: 10.1175/JAS3965.1.

- [21] J. Xia, W. S. Lewellen, and D. C. Lewellen, “Influence of Mach number on Tornado corner flow dynamics,” *J. Atmos. Sci.*, vol. 60, no. 22, pp. 2820–2825, 2003, doi: 10.1175/1520-0469(2003)060<2820:IOMNOT>2.0.CO;2.
- [22] R. P. Selvam and P. C. Millett, “Computer modeling of tornado forces on buildings,” *Wind Struct. An Int. J.*, vol. 6, no. 3, pp. 209–220, 2003, doi: 10.12989/was.2003.6.3.209.
- [23] A. Gairola and G. Bitsuamlak, “Numerical tornado modeling for common interpretation of experimental simulators,” *J. Wind Eng. Ind. Aerodyn.*, vol. 186, no. November 2017, pp. 32–48, 2019, doi: 10.1016/j.jweia.2018.12.013.
- [24] A. El Damatty, N. Ezami, and A. Hamada, “Case Study for Behaviour of Transmission Line Structures under Full-Scale Flow Field of Stockton, Kansas, 2005 Tornado,” in *Electrical Transmission and Substation Structures 2018*, 2018, pp. 257–268.
- [25] E. Savory, G. A. R. Parke, M. Zeinoddini, N. Toy, and P. Disney, “Modeling of tornado and microburst induced wind loading and failure of a lattice transmission tower,” vol. 23, pp. 365–375, 2001.
- [26] A. Y. Shehata, A. A. El Damatty, and E. Savory, “Finite element modeling of transmission line under downburst wind loading,” *Finite Elem. Anal. Des.*, vol. 42, no. 1, pp. 71–89, 2005, doi: 10.1016/j.finel.2005.05.005.
- [27] A. Y. Shehata and A. El Damatty, “Behaviour of guyed transmission line structures under downburst wind loading,” *Wind Struct.*, vol. 10, pp. 249–268, Jun. 2007, doi: 10.12989/was.2007.10.3.249.
- [28] A. Y. Shehata and A. El Damatty, “Failure analysis of a transmission tower during a microburst,” *Wind Struct.*, vol. 11, Jun. 2008, doi: 10.12989/was.2008.11.3.193.
- [29] A. Hamada, A. A. E. Damatty, H. Hangan, and A. Y. Shehata, “Finite element modelling of transmission line structures under tornado wind loading,” *Wind Struct. An Int. J.*, vol. 13, no. 5, pp. 451–469, 2010, doi: 10.12989/was.2010.13.5.451.

- [30] A. Hamada and A. A. El Damatty, "Behaviour of guyed transmission line structures under tornado wind loading," *Comput. Struct.*, vol. 89, no. 11–12, pp. 986–1003, 2011, doi: 10.1016/j.compstruc.2011.01.015.
- [31] A. Hamada and A. El Damatty, "Failure analysis of guyed transmission lines during F2 tornado event," *Eng. Struct.*, vol. 85, Feb. 2015, doi: 10.1016/j.engstruct.2014.11.045.
- [32] A. Shehata and A. El Damatty, "Nonlinear Analysis of Transmission Lines under Downbursts," in *The 15th International Conference on Wind Engineering (ICWE15)*, 2019.
- [33] A. Shehata and A. El Damatty, "Extensible Catenary Approach in Analyzing Transmission Line 's Conductors under Downbursts .," *Manuscr. Prep.*
- [34] F. Inc., "FLUENT 6.2 User's Guide." Lebanon, NH, 2005.
- [35] A. A. El Damatty and A. Hamada, "F2 tornado velocity profiles critical for transmission line structures," *Eng. Struct.*, vol. 106, pp. 436–449, 2016, doi: 10.1016/j.engstruct.2015.10.020.
- [36] A. 74, *ASCE - 74*, Third ed., no. 74. Reston, Virginia: American Society of Civil Engineers, 2009.
- [37] H. Aboshosha and A. El Damatty, "Effective technique to analyze transmission line conductors under high intensity winds," *Wind Struct. An Int. J.*, vol. 18, no. 3, pp. 235–252, 2014, doi: 10.12989/was.2014.18.3.235.
- [38] *Design of Latticed Steel Transmission Structures (10-15)*. American Society of Civil Engineers, 2015.

Chapter 4

4 Conclusions and Future Work

4.1 Conclusions

The thesis presents research that investigates the progressive failure analysis of single and multiple Transmission Line (TL) towers considering two different types of towers, guyed and self-supported, under the effect of two different F2 tornado wind fields. In order to do such an investigation, the following procedure is performed:

- i) Two tornado wind fields numerically simulated by Hangan and Kim, and El Damatty et al. using Computational Fluid Dynamics (CFD) simulations are incorporated into a non-linear finite element analysis software developed at Western University;
- ii) The numerical model is verified by comparing the results to the findings of previous investigations conducted by Hamada and El Damatty;
- iii) Non-linear progressive failure analysis is performed for two guyed and two self-supported towers under the most critical tornado configurations identified from extensive parametric studies;
- iv) Strengthening for the guyed and self-supported towers is investigated to provide and insight into the cost associated with designing TLs that can sustain F2 tornadoes;
- v) The progression of failure within multiple self-supported TL towers under different F2 tornado wind fields is investigated;
- vi) The effect of changing the insulator length and the span of the line on the propagation of failure within self-supported TLs are then investigated.

As mentioned in Chapter 1, this procedure and its results are presented in the second and the third chapter of this thesis. The drawn conclusions from the second chapter, titled “Progressive Failure of a Single Transmission Line Tower under Different Tornado Wind Fields” can be summarized as shown below:

- i) Considering the critical configurations identified from the extensive parametric study, progressive failure analysis is conducted for four different towers that are designed and constructed following code provisions;
- ii) The results of the progressive failure analysis for each tower under the different tornado wind fields are presented. The results include the failure load and a description of the failure mode;
- iii) The results for each tower under each tornado wind field are then compared to each other. This allows identifying the difference in the progression of failure in the TL towers under different tornado wind fields. The towers fail at a smaller loading increment under Stockton's tornado compared to Hangan's tornado. This shows that Stockton's tornado is more critical to the TL towers even though both tornado wind fields are scaled to match the same maximum wind speed;
- iv) All the investigated towers fail under the F2 tornado loading resulting from each of the tornado wind fields;
- v) Strengthening of guyed and self-supported TL towers is investigated. A sample of one guyed and one self-supported TL tower is used in the study. The iterative procedure shows that the guyed tower requires an additional 5.6% of its own weight to sustain the F2 tornado wind load, while the self-supported tower requires 65% additional weight;
- vi) The investigated guyed towers designed as per current code provisions, to resist synoptic wind loads, are more resilient than the investigated self-supported towers that are designed to resist a higher wind speed.

The conclusions drawn from the third chapter titled "Progressive Failure of Self-supported Transmission Line Towers under Different Tornado Wind Fields" can be summarized as follows:

- i) The tornado wind fields are incorporated in an extended version of the fluid-structure software. The extended version of the software predicts the post-failure geometry of a TL tower and use it to calculate the conductors' forces that will be transmitted to the adjacent towers. The progressive failure of the adjacent towers

is then investigated. The analysis is conducted under the different tornado wind fields;

- ii) The study shows that the failure occurs within only three towers of the modelled TL. The height of the plastic hinge and the failure mode for each of the collapsed towers are reported;
- iii) Stockton tornado wind field is found to be more critical compared to Hangan's tornado wind field despite that both tornado wind fields are scaled to have equal horizontal resultant wind speed;
- iv) The effect of changing the insulator length on the propagation of failure within the TL towers under tornadoes is then investigated. The results show that the insulator length is of great importance in mitigating the propagation of failure within TL towers (domino effect) under tornadoes. In the shown case study, the number of failed towers due to tornado loading can vary from three towers to one tower by using an insulator length to be of 2.5m or more. The investigation also indicates that reducing the insulator length results in increasing the peak demand-to-capacity ratio in the tower of interest;
- v) An extensive parametric study is conducted to investigate the effect of changing the TL span, within the range of 300 m to 600 m, on the progression of failure within the TL towers. The span of the TL is found to be of significant effect on the failure load of the adjacent towers. The presented case study shows that increasing the span between the investigated towers to 450 m reduces the risk of losing multiple towers within the TL.

4.2 Main contributions

This study is the first to compare the progression of failure with the TL systems under different tornado wind fields. It is also the first study to investigate the effect of changing the insulator length on the propagation of failure within the TL systems. Additionally, it is the first study to examine the effect of changing the span on the propagation of failure within the TL systems. The study explores beyond the traditional, costly strengthening techniques for increasing the resilience of TLs under tornadoes. It investigates novel techniques, such as increasing the insulator length and increasing the span of the TL systems, to increase the resilience of TLs. Specifically, the investigated case studies show that increasing the insulator length or increasing the span mitigate the number of failed towers within the TL under tornadoes. The findings from the study highlight that there are alternative cost-efficient techniques to increase the resilience of TL systems aside from strengthening individual towers.

4.3 Recommendations for future work

The outcomes of the research presented in this thesis can be extended towards the following:

- i) Assessing the progressive failure of angled turn TL towers under tornado wind fields.
- ii) Conducting progressive failure analysis for TL towers carrying unsymmetrical conductors.
- iii) Conducting progressive failure analysis under the combination of tornado wind loading and ice loading
- iv) Investigating the effect of the terrain type on the progression of failure.
- v) Navigating different strengthening techniques that might be more efficient. This includes strengthening the lower zones of the tower to increase the height of the plastic hinge. Hence, the risk of losing multiple towers is mitigated.
- vi) Investigating the effect of various components within the TL on the propagation of failure within the TL towers.
- vii) Extending the numerical model to incorporate different towers within the same line. This would allow modelling an entire TL system that includes the end towers.
- viii) Using Large Eddy Simulation (LES) instead of RANS to conduct the CFD simulations.
- ix) Using Monte Carlo simulations to conduct probabilistic analysis study that investigates different variables such as tornado size, tornado wind speed, location of the tornado relative to the tower, and different paths for tornadoes.

Curriculum Vitae

Name: Wesam Abdelhamid Mohamed

Post-secondary The University of Western Ontario

Education and London, Ontario, Canada

Degrees: 2017-2020 M.E.Sc.

Ain Shams University

Cairo, Egypt

2010-2015 B.Sc.

Honours and Graduate Teaching Assistant Excellence Award

Awards: 2018

Department of Civil and Environmental Engineering

The University of Western Ontario

London, Ontario, Canada

Related Work Graduate Teaching Assistant

Experience The University of Western Ontario

2017-2019

Publications:

Abdelhamid Mohamed W., El Ansary A.M., El Damatty A.A., Progressive Failure of Transmission Line Towers under Different Tornadoes, Accepted to present at the Western Research Forum 2020, Western University, London, ON, Canada. March 2020

El Damatty A.A., **Abdelhamid Mohamed, W.**, Wind and Structural Engineering, Framework and Challenges, 15th International Conference on Structural and Geotechnical Engineering, Cairo, Egypt. December 2018.